Manuscript No.: acp-2022-654

Title: Measurement report: Aerosol vertical profiles over the Western North Atlantic Ocean during the North Atlantic Aerosols and Marine Ecosystems Study (NAAMES)

Responses to Anonymous Referee #1

Comment: The measurement report by Gallo et al. analyzed in-situ measurements during three NAAMES field campaigns in winter, spring, and summer, respectively. The results are interesting and well discussed, and I only have a few concerns.

Response: We thank Anonymous Referee #1 for his/her support of our work. We have revised the manuscript according to your suggestions. All the alterations to the manuscript are shown in the track changes revised version of the manuscript included within this document. Please find our point-by-point responses below - the original Referee #1 comments are highlighted in italic black and our responses follow in blue. (blue).

Detailed Comments:

1. Sect 3.2: *During NAAMES 1, why only BC show the MBL peaks on 12th, 2015 and Nov. 14th, 2015? If it was the continental origins, the CO should also be higher. Has the authors considered the possibility of ship emissions?*

Response: We thank Anonymous Referee #1 for this suggestion. We have conducted further analysis to constrain the possible origin of enhanced BC levels in the MBL on November 12th and 14th, 2015. First, we have assessed 5-days Hysplit frequency backtrajectory (Fig. a, b - below) and we evaluated the potential presence of wildfires along the air masses transport path using NASA Worlview FIRMS VIIRS Fire and Thermal Anomalies product (Fig. c below). The images below show that air masses originated over the Artic and did not intercept wildfires prior the arrival to the NAAMES domain. The influence of high levels of pollution along the air mass trajectories from the Artic to the Western North Atlantic is also unlikely.
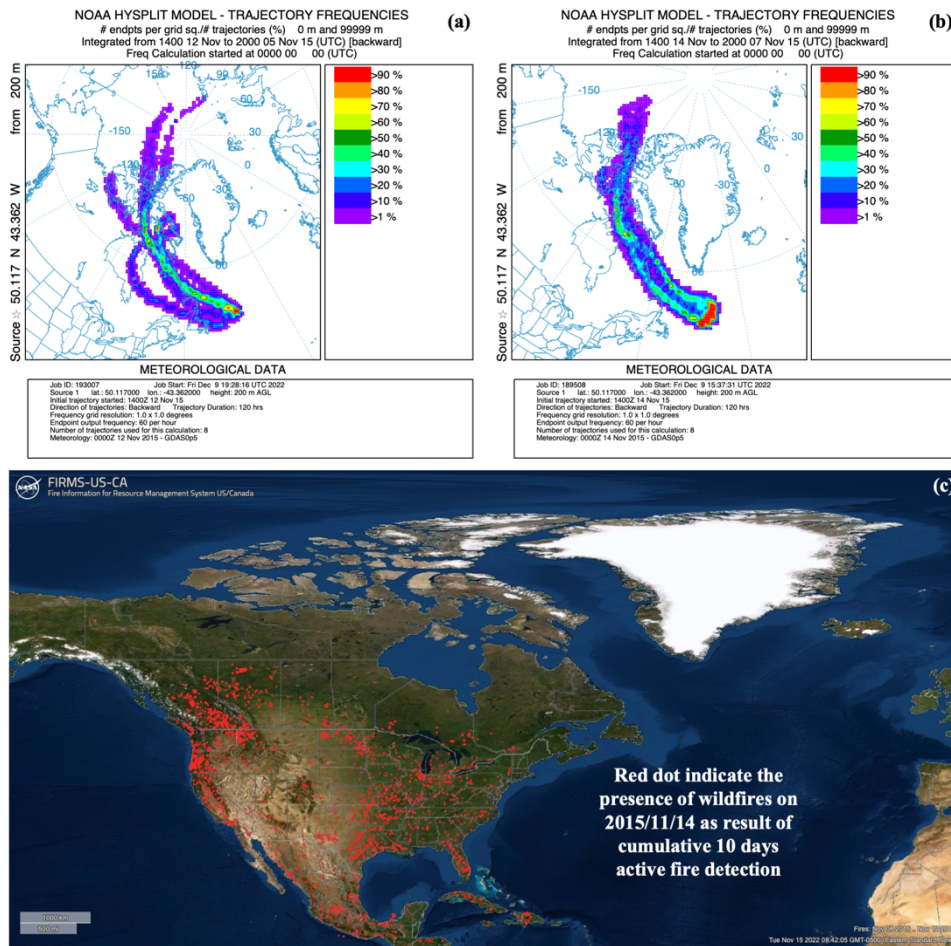
We compare our results to the BC measurements simultaneously collected on the research vessel *R/V Atlantis* through a Single Particle Soot Photometer, and we find elevated concentrations of BC (> 500 ng m^{-3}) at the surface ocean on November 12th and 14th, 2015. These analysis and the low level of CO previously observed, confirm Referee#1's hypothesis that possibility attribute the BC peaks in the MBL to ship emissions. Therefore, we have revised the manuscript (**page 6, line 38** of the track changes revised version of the manuscript) and added the figure in the supplemental materials (**Fig. SI.2** of the track changes revised version of the manuscript):

During NAAMES-1, we observe a mean CO concentration = 87.2 ± 6.6 ppbv and no significant variations within days. CO vertical profiles show similar concentrations at all the altitudes sampled, being only slightly higher in the MBL (mean = 90.1 ± 3.3 ppbv) than in the FT (mean = 86.1 ± 7.2 ppbv) ~~(Fig. 3a, Fig. SI.1.a, and Fig. SI.2.a)~~ (Table 3, Fig. 3a, Fig. 4a, and Fig. SI.1.a). BC concentrations are also generally low ~~(mean of 6.2 ± 11.2 ng m^{-3})~~ ~~(mean of 8.3 ± 21 ng m^{-3} in the MBL, and 5.1 ± 4.8 ng m^{-3} in the FT)~~, characteristic of unpolluted conditions observed during the winter (Table 3, Fig. 3b, Fig. 4b, and Fig. 6a). The only exceptions are Nov. 12th, 2015 and Nov. 14th, 2015 when BC exhibits peaks in the MBL up to 101.4 ng m^{-3} and 106.2 ng m^{-3} respectively, at altitudes < 1500 m ~~(Fig. 3b, and Fig. SI.2.a.1-3)~~ (Fig. 4b, and Fig. SI.2.a.1-3). The enhanced BC levels might be the result of ship-traffic emissions. Analysis of 5-days Hysplit frequency backtrajectory indicate the arrival of air masses from the Artic suggesting clean maritime influence (Fig. SI.2.a-b). Furthermore, Worlview FIRMS VIIRS Fire and Thermal Anomalies products show absence of wildfires on the air mass transport path prior the arrival to the NAAMES-1 domain, therefore excluding the contributions from biomass burning to the BC level observed (Fig. SI.2.c). After removing the BC measurements affected by ship-traffic emissions (data discarded altitude < 1500 m on Nov. 12th, 2015, and altitude < 1050 m on Nov. 14th, 2015) we found mean BC concentrations in the MBL of 1.8 ± 0.9 ng m^{-3} and lower than in the FT. ~~the intrusion of polluted air masses from continental origins due to wintertime low-altitude long-range transport.~~

Field studies conducted in several locations over the North Atlantic ocean region have shown background concentrations of BC ranging between 10 and 40 ng m⁻³ under unperturbed marine conditions (O'Dowd et al., 2004; Shank et al., 2012; Pohl et al., 2014; Cavalli et al., 2016), while BC concentration up to 600 ng m⁻³ have been reported during periods of time affected by intense continental emission plumes (Corrigan et al., 2008). Non-refractory aerosol chemical composition analysis also reveals low concentrations of sulfate (0.05 ± 0.03, 0.03 ± 0.03, and 0.07 ± 0.03 µg std m⁻³ respectively at the surface ocean, in the MBL, and in the FT) (Fig. 4a, Fig. 5b, and Fig. SI.2.a) (Fig. 3c, Fig. 5a, and Fig. 6b), and organic (0.1 ± 0.07, 0.05 ± 0.08, and 0.08 ± 0.06 at the surface ocean, in the MBL, and in the FT, respectively) aerosol mass (Fig. 4b, and Fig. SI.1.b, and Fig. SI.2.a).

2. Fig. 6a-c: *The correlations between CO, Sulfate, Organics and BC during NAAMES 1 are strongly biased by the BC outliers. How would the correlations be like if any BC > ~20 ng/m3 are excluded, and what's the explanations? That would be more representative of the pristine marine environment in winter. ?*

Response: We evaluate the concentrations of BC on November 12th and 14th, 2015 during the periods in which measurements were likely affected by ship emissions and we found BC being > 18 ng m⁻³. We agree with Referee #1 that the BC measurements affected are not representative of the pristine marine environment in the winter and strongly biased the correlations between BC and CO, sulfate, and organics. Therefore, we removed the affected datapoints from November 12th and 14th, 2015 spirals and re-evaluated the correlations abovementioned. Next based on the new results, we have corrected the discussion in section 3.2 as following (**Page 7, Line 17** of the track changes revised version of the manuscript):

No correlations between CO and BC, BC and sulfate, and BC and organics are found during NAAMES-1 (the linear regression R² values are 0.04, 0.25, and 0.20, respectively) (Fig. 6a, b, and c) indicating a predominantly low aerosol environment with minor influence of anthropogenic pollution and ocean emissions. No correlations between CO and BC, BC and sulfate, and BC and organics are found in the MBL (Fig. 7a, b, and c). Similarly, despite higher level of BC in the FT, we could not find correlations between FT BC and FT CO (linear regression R² values is 0.01) (Fig. 7d). On the other hand, the correlations between BC and sulfate, and BC and organics in the FT is moderate (the linear regression R² values are 0.64, and 0.40, respectively) (Fig. 7e, and f). These results indicate that, although the predominantly low aerosol environment with only reduced ocean emissions, the WNAO in the winter is subjected to minor episodes of anthropogenic pollution, such as ship-traffic in the MBL and transport of continental polluted air masses in the FT) that influence the atmospheric vertical column.

Fig. 6a, b, and c, in the revised manuscript **Fig. 7a, b, c, d, e, f** have been modified and are copied below.
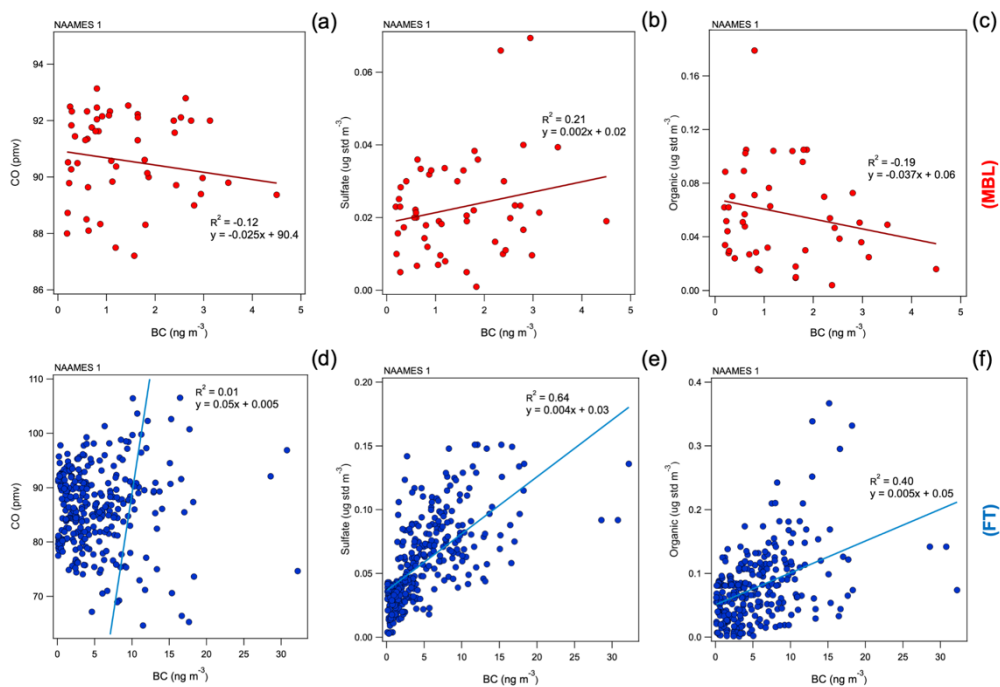
Figure 6. Correlation between BC and CO (a, d), BC and sulfate (b, e), and BC and organics (c, f) in the MBL (red) and FT (blue) during NAAMES-1

3. Minor corrections: *page 10, line 24: should be "3.3.2"; line 27: duplicate "%". ?*

Response: We thank Referee #1 for noticing this discrepancy in the text, "3.3.1 CCN seasonal variations" is incorrect and the number of the section has been changed as following (**Page 12, Line 10** of the track changes revised version of the manuscript):

"3.3.2 CCN seasonal variations"

The duplicate "%" page 10, line 27 has been removed.

Measurement report: Aerosol vertical profiles over the Western North Atlantic Ocean during the North Atlantic Aerosols and Marine Ecosystems Study (NAAMES)

Francesca Gallo[1,2], Kevin J. Sanchez[1], Bruce E. Anderson[1], Ryan Bennett[3], Matthew D. Brown[1,4], Ewan C. Crosbie[1,4], Chris Hostetler[1], Carolyn Jordan[1,5], Melissa Yang Martin[1], Claire E. Robinson[1,4], Lynn M. Russell[6], Taylor J. Shingler[1], Michael A. Shook[1], Kenneth L. Thornhill[1,4], Elizabeth B. Wiggins[1], Edward L. Winstead[1,4], Armin Wisthaler[7,8], Luke D. Ziemba[1], and Richard H. Moore[1]

[1]NASA Langley Research Center, Hampton, VA
[2]NASA Postdoctoral Program, Oak Ridge Associated Universities, Oak Ridge, TN
[3]Bay Area Environmental Research Institute, Moffett Field, CA, USA
[4]Science Systems and Applications, Inc., Hampton, VA
[5]National Institute of Aerospace, Hampton, VA
[6]Scripps Institution of Oceanography, San Diego, CA
[7]Institute for Ion Physics and Applied Physics, University of Innsbruck, Technikerstrasse 25, 6020 Innsbruck, Austria
[8]Department of Chemistry, University of Oslo, P.O. 1033 – Blindern, 0315 Oslo, Norway

Correspondence to: Richard H. Moore (richard.h.moore@nasa.gov), Francesca Gallo (francesca.gallo@nasa.gov)

Abstract.

The NASA North Atlantic Aerosols and Marine Ecosystems Study (NAAMES) ship and aircraft field campaign deployed to the western subarctic Atlantic between the years 2015 and 2018. One of the primary goals of NAAMES is to improve the understanding of aerosol-cloud interactions (ACI) over the Atlantic Ocean under different seasonal regimes. ACI currently represent the largest source of uncertainty in global climate models. During three NAAMES field campaigns (NAAMES-1 in November 2015, NAAMES-2 in May 2016, and NAAMES-3 in September 2017) multiple 10-hour science flights were conducted using the NASA C-130 aircraft to measure marine boundary layer aerosol and cloud properties. The standard flight pattern includes vertical spirals where the C-130 transitioned from high altitude to low-latitude (and vice versa) collecting in-situ measurements of aerosols, trace gases, clouds, and meteorological parameters as a function of altitude. We examine the data collected from 37 spirals during the three NAAMES field campaigns, and we present a comprehensive characterization of the vertical profiles of aerosol properties under different synoptic conditions and aerosol regimes. The vertical distribution of submicron aerosol particles exhibited strong seasonal variation, as well as elevated intra-seasonal variability depending on emission sources and aerosol processes in the atmospheric column. Pristine marine conditions and new particle formation were prevalent in the wintertime (NAAMES-1) due to low biogenic emissions from the surface ocean and reduced continental influence. Higher concentrations of submicron aerosol particles were observed in the spring (NAAMES-2) due to strong phytoplankton activity and the arrival of long-range-transported continental plumes in the free troposphere with subsequent entrainment into the marine boundary layer. Biomass burning from boreal wildfires was the main source of aerosol particles in the region during the late summer (NAAMES-3) in both the marine boundary layer and free troposphere.

1 Introduction

Atmospheric aerosols act as cloud condensation nuclei and significantly affect cloud microphysical properties and formation pathways. Subtropical marine low clouds are the most impacted by perturbations in aerosol properties and are highly sensitive to changes in cloud condensation nuclei (CCN) concentrations (Twomey, 1977; Warren et al., 1988; Albrecht, 1989; Moore
5 et al., 2013; Wood et al., 2017). However, at present, the complex interactions among aerosols and low-cloud systems in marine environments constitute one of the largest uncertainties in climate models (Carslaw et al., 2013; Simpkins, 2018), limiting the accuracy of future climate model predictions. One of the main reason for this uncertainty is the incomplete representation of aerosol properties and processes, and their spatial distribution under different synoptic conditions in remote marine regions, where aerosols loadings are lowest and cloud droplet sensitivities are greatest (Moore et al., 2013).

Recently, the North Atlantic Ocean has been the target of many research field campaigns, aiming to improve process-level understanding of marine aerosols in remote environments (Wood et al., 2015; Behrenfeld et al., 2019; Sorooshian et al., 2020; Wang et al., 2021). The region is characterized by pervasive low-lying clouds that often form under the presence of low aerosol concentrations of a few hundred particles cm^{-3}; although, perturbations may result from episodic continental transport and
15 synoptic weather systems (Wood et al., 2017). Through the year, aerosol concentrations and properties in the atmospheric column are impacted by different sources, including marine biogenic emissions from the surface ocean (O'Dowd et al., 2004; de Leeuw et al., 2011; Quinn et al., 2015; Sanchez et al., 2021) and the entrainment of both biogenic and anthropogenic particles from the free troposphere (FT) (Raes, 1995; Honrath, 2004; Clarke et al., 2013; Hamilton et al., 2014; Dzepina et al., 2015; García et al., 2017). Furthermore, several aerosol processes, such as new particle formation, condensational growth of
20 existing particles, and aerosol removal by coalescence scavenging, also play a key role in shaping aerosol budget and aerosol vertical distribution in the Atlantic region (Bates et al., 1998; Wood et al., 2017; Sanchez et al., 2018; Zheng et al., 2018).

The aerosol population in the marine boundary layer (MBL) is often dominated by particles of marine origin (Rinaldi et al., 2010; Lapina et al., 2011; de Leeuw et al., 2014). The emission of ocean-derived particles into the MBL follows different
25 pathways and is driven by meteorological conditions and ocean biological activity, thus exhibiting strong seasonal variations. Sea spray aerosols (SSA) which include sea salt, non-sea salt sulfate, and particulate organic matter are directly emitted in the MBL by bubble bursting and wave breaking processes at the atmosphere-ocean interface. Previous studies have shown that high wind speeds during fall and winter intensify the breaking of waves, and sea spray enriched in organics is the main contributor to the MBL aerosol mass and a strong contributor to the CCN budget (Quinn et al., 2017). Simultaneously, ocean
30 ecosystems are responsible for the emission of marine volatile organic compounds (VOCs) that oxidize in the atmosphere and condense onto existing particles, leading to new particle formation (Facchini et al., 2008; Rinaldi et al., 2010; Bates et al., 2020). The dominant ocean-derived biogenic VOC is dimethylsulfide (DMS), which is formed from a metabolite produced by marine phytoplankton called dimethylsulfoniopropionate (DMSP) (de Leeuw et al., 2011; Quinn et al., 2015). Once released in the atmosphere, DMS oxidizes to sulphuric acid and methanesulfonic acid (MSA), and can cause the condensational growth
35 of existing particles (Pandis et al., 1994; Hodshire et al., 2019; Lv et al., 2019; Sanchez et al., 2021). Several studies have found correlations between MBL sulfate concentrations and the phytoplankton seasonal cycle (Pandis et al., 1994; Bates et al., 1998; Quinn et al., 2014; Andreae et al., 2003), and/or chlorophyll a (Chl-a) levels in the ocean (that is sometimes used as a rough proxy for marine biomass concentration) (Bates et al., 1992; O'Dowd et al., 1997, 2004; Ovadnevaite et al., 2014; Saliba et al., 2020), while DMS-produced sulfate has been suggested as the largest source of CCN in the remote marine MBL
40 (Charlson et al., 1987; Pandis et al., 1994; O'Dowd et al., 1999; Korhonen et al., 2008; Sanchez et al., 2018).

Although regional ocean sources play a substantial role in controlling the aerosol budget over the North Atlantic, earlier studies suggested that long-range-transported particles of continental origins are the major sources of aerosols in the FT over mid-latitude oceans (Raes, 1995; Honrath, 2004; Pio et al., 2008; Dzepina et al., 2015; Wang et al., 2021). Aerosol particles originating in the North American continental boundary layer can be transported in the FT for several days and subsequently entrain into the MBL. The presence of North American pollution outflow and biomass burning particles from North American and Canadian boreal forest in the North Atlantic region have been previously reported (Zhao et al., 2012; Parrington et al., 2012; García et al., 2017; Zheng et al., 2018) and have been associated with high CCN concentration events (Wood et al., 2015).

In this context, a quantitative understanding of aerosol properties and processes, as well as the competing influences of long-range transport versus local boundary layer aerosols is crucial to assess the near-cloud aerosol burden under different atmospheric air mass types and constrain the CCN budget over the North Atlantic region. Motivated by this need, NASA conducted the North Atlantic Aerosols and Marine Ecosystems Study (NAAMES) field campaigns in the Western North Atlantic Ocean (WNAO) region between 2015 and 2018. NAAMES targets specific phases of the annual phytoplankton cycle, namely:

- NAAMES-1 (November 2015), winter transition - Chl-a concentrations (< 1 mg m^{-3}), high wind and sea states;
- NAAMES-2 (May - June 2016), bloom climax transition - increasing Chl-a levels (> 1 mg m^{-3}), relatively calm sea state and wind conditions;
- NAAMES-3 (August - September 2017), declining phase – lower phytoplankton activity (Chl-a concentrations < 0.7 mg m^{-3}); and
- NAAMES-4 (March - April 2018), accumulation phase - elevated and variable Chl-a concentrations (ranging from 0.5 to 3.5 mg m^{-3})

A detailed description of the project and each deployment is given by (Behrenfeld et al., 2019). During the campaigns, simultaneous ship- and aircraft-based observations of aerosols, trace gases, and clouds were collected in order to improve understanding of the aerosol and CCN budget sand their controlling processes over the WNAO.

This study leverages aircraft and ship-based in-situ measurements of aerosol, trace gases, and meteorological parameters collected during the NAAMES field campaigns. We examine and discuss the vertical profiles of aerosol properties under different aerosol and meteorological regimes in relation to diverse emission sources, sink mechanisms, and thermodynamic structure of the atmospheric column. With this work, we aim to achieve a quantitative understanding of aerosol seasonal variations over the WNAO and provide a framework for improving process-level understanding of marine aerosol-cloud interactions (ACI), which are critical to adequately link observations and climate modelling. This paper should be of interest to those seeking to understand the vertically-resolved, seasonal climatology of the remote marine atmosphere. In addition, we provide key observational constraints for evaluating aerosol-cloud interactions in models.

2 Measurements and methodology

2.1 NAAMES C-130 flights overview

The NAAMES field campaigns took place in the Western North Atlantic Ocean region (38-65°N, 34-50°W). The NASA C-130 aircraft flew during the first three campaigns (C-130 measurements are not available for NAAMES-4) to provide vertical observations of the MBL and lower FT structure. Standard flight patterns were performed during each 10-hour flight to investigate the atmospheric composition and meteorology below-, in- and above- clouds. Vertical spirals were conducted where

the C-130 descended from high altitude to low-latitude (and vice versa) collecting measurements as a function of altitude. This study focuses on the measurements collected during the discrete aircraft spirals, which were the periods when the C-130 sampled the same area in a relatively short time at different altitudes. Here, we analyze and discuss aerosols, trace gases, clouds, and meteorology data from a total of 37 spirals (7, 14, and 16 spirals respectively from NAAMES-1, -2, and -3). Data were collected at 1 Hz between altitudes of ∼ 7500 m and ∼ 80 m. To allow a direct comparison between spirals, the data were averaged to 100-m altitude intervals. The list of the spirals analyzed in this study is shown in Table 1, and includes UTC interval times, minimum and maximum altitude ranges, and geographical coordinates. Additionally, we analyze the ship-based aerosol measurements collected on the research vessel (R/V) *Atlantis*, heretofore referred as "at surface ocean measurements", during C-130 spirals times to link aerosol properties observations from the vertical column and surface ocean.

All the instruments deployed aboard the C-130 aircraft sampled through a low turbulence isokinetic inlet. A list of C-130 and *R/V Atlantis* measurements and instruments examined in this study is given here and summarized in Table 2. Measurements of submicron particle number concentration on the aircraft were reported at 1 Hz and standard temperature and pressure (STP 273.15K and 1031.25 hPa) from two Condensation Particle Counters (CPC): the CPC Model 3025, with a nominal lower cut-off diameter of 3 nm (TSI Inc., St. Paul, MN), and the CPC Model 3772, with lower cut-off diameter of 10 nm (TSI Inc., St. Paul, MN). On the ship, aerosol number concentrations with lower cut-off diameter of 10 nm were made using the CPC Model 3010 (TSI Inc., St. Paul, MN) and are reported at ambient, surface conditions. The total number concentration (N_{CN}) reported in the text refers to the measurements of submicron particle number concentration with $D_p > 10$ nm and obtained through the CPC Models 3772 (C-130) and 3010 (*R/V Atlantis*) unless they are stated as otherwise. On the C-130, the particle number size distributions with diameters (D_p) between 100 and 3500 nm were measured with a Laser Aerosol Spectrometer (LAS) (Model 3340, TSI, St. Paul, MN). In this study, we combine the measurements from the CPC 3025, the CPC 3772, and the LAS to describe the submicron size distribution by dividing the data into three rough size modes:

1) newly-formed particles (NP) consisting of sizes between $D_p = 3$ to 10 nm,

2) Aitken (At) mode aerosols between $D_p = 10$ to 100 nm, and

3) Accumulation (Ac) mode aerosols between $D_p = 100$ nm to 1 μm.

The number concentration of NP (N_{NP}) is the difference between the submicron number concentrations of particles with $D_p > 3$ nm (as measured by CPC 3025) and $D_p > 10$ nm (as measured by CPC 3772). Similarly, we calculate the number of At mode particles (N_{At}) as the difference between the number concentrations measured by the CPC 3772 and the LAS. The N_{Ac} mode number concentrations were directly measured by the LAS and defined as the corresponding number concentration. The total number concentration and the number of particles in the NP, At, and Ac modes are reported in the text as geometric means and geometric standard deviations, unless stated otherwise. The relative contribution of each aerosol mode to the total particle concentration was calculated as the ratio of NP, At, and Ac number concentrations to N_{CN}. A Cloud Condensation Nuclei (CCN) Counter (Droplet Measurement Technologies, DMT) measured the concentration of aerosol particles that act as cloud condensation nuclei (Roberts and Nenes, 2005; Rose et al., 2008) at a fixed water vapor supersaturation (s) of 0.21% at 1 Hz and STP on the aircraft, and water vapor supersaturation level of 0.2% and ambient temperature and pressure on the ship. In order to avoid artifacts due to C-130 inlet shattering impacting the CPCs, LAS and CCN measurements, spiral portions affected by the presence of cloud droplets were removed and, when possible, were integrated with measurements collected during the C-130 above-clouds legs subsequent to the spirals. Aerosol composition was investigated using an Aerodyne Research High-Resolution Aerosol Mass Spectrometer (HR-ToF-AMS; DeCarlo et al., 2006) on both the aircraft and ship. The AMS provides single particle composition measurements of the mass concentrations of non-refractory organic, sulfate, nitrate, and ammonium at 30 second intervals on the ship and 1 Hz on the aircraft.

We assess the contribution of anthropogenic sources using a Single Particle Soot Photometer at 0.1 Hz (SP2, DMT, Boulder,

CO) which measures refractory black carbon particle (BC) mass as well as a Los Gatos Research (LGR) CO/CO$_2$ gas analyser to measure carbon monoxide (CO) mixing ratios. To identify ocean biological emissions, dimethylsulfide (DMS) mixing ratio measurements were conducted with a Proton Transfer Reaction Time of Flight Mass Spectrometer (PTR-ToF-MS) at 1 Hz (Müller et al., 2014) (NAAMES-1 data not available available as gas-phase concentrations were generally below detection limits). A Cloud Droplet Probe (CDP, DMT, Boulder, CO) measured the number concentrations of cloud droplets for droplets size ranging between 2 and 50 μm in diameter on the aircraft. CDP measurements made below 300 m are excluded from the analysis due to the potential presence of fog layers and sea spray (Sinclair et al., 2019).

Potential temperature (θ) and relative humidity (RH) were measured through meteorological sensor packages. H$_2$O mixing ratio (w) measurements on the aircraft were made using the H$_2$O channel of the LGR CO/CO$_2$ gas analyser described above. In this study, we use the vertical profiles of potential temperatures and H$_2$O mixing ratio to determine the heights of the MBL, defined as the level of the maximum gradient of thermal inversion and H$_2$O mixing ratio profiles (Chan and Wood, 2013; Wang and Wang, 2014; Dong et al., 2015). Furthermore, MBL potential temperature and H$_2$O mixing ratio gradients are used to identify when the upper portion of the sub-cloud layer is coupled or decoupled to the ocean surface layer.

3 Results and discussion

3.1 Vertical structure of the atmospheric column

Vertical gradients of potential temperature, H$_2$O mixing ratio, and relative humidity play important roles in shaping the structure of the vertical column (Dong 2015). Here, we evaluate θ, w, and RH vertical profiles to assess the thermodynamic structure of the atmospheric vertical column during the three NAAMES campaigns. Figure 1a shows that potential temperature vertical distributions are relatively similar within the three NAAMES campaigns with mean vertical column θ slightly higher during the summer (mean θ = 294 ± 11, 297 ± 12, and 310 ± 12 K, respectively during NAAMES-1, -2, and -3) and cold air breaks occasionally affecting the column thermodynamics. H$_2$O mixing ratio is higher for the spring campaign and exhibits variability within days during all the seasons, with at least one day per campaign showing values < 4000 ppmv and another day > 12000 ppmv (Fig. 1b). RH levels are higher in the winter and spring than in the summer (especially in the MBL where they show higher frequency of RH values above 74%), and inter-day variability is observed across all seasons (Fig. 1c). A comprehensive summary statistic of MBL and FT θ, w, and RH variations during the three NAAMES field campaigns is provided in Table 3.

Marine boundary layer heights show strong seasonal variability. Mean MBL heights are higher in the winter and spring (1776 ± 313 m and 1657 ± 445 m, respectively) during NAAMES-1 and -2 and decrease in the summer (mean value of 1144 ± 311 m). Furthermore, in most of the cases analyzed, within the upper part of the MBL we observe the presence of a residual layer, a zone of transition between the surface mixed layer and FT that has a strong gradient in thermodynamic properties and influence FT-MBL exchange (Lenschow et al., 2000; Katzwinkel et al., 2012; Dadashazar et al., 2018). A similar seasonal trend has been previously observed in the Eastern North Atlantic (Wang et al., 2021) and is likely related to different seasonal synoptic conditions, namely: 1) a strong gradient of surface pressure between the Icelandic low and the Azores high and enhanced convective activities in the winter that cause the MBL to deepen, and 2) strengthening of the high pressure system over the North Atlantic in the summer and fall that leads to a stronger and lower inversion altitude (Rémillard et al., 2012; Wood et al., 2015). Furthermore, we found that in winter and spring the MBL is more often decoupled in two separate layers (a surface mixed layer at the surface ocean, and an upper decoupled layer) than in the summer (MBL decoupled occurrence in 58%, 64%, and 37% of the cases analysed respectively during NAAMES-1, -2, and -3) (Fig. 2). Indeed, in winter and spring,

when the MBL is deeper, the turbulent motions from the surface heating become separated from the radiative turbulence in the cloud layer and the MBL organizes in two separated layers with their own circulation (Albrecht, 1989; Jones et al., 2011; Dong et al., 2015). On the contrary, in the summer shallower MBLs and strong MBL inversions favour more effective vertical mixing over the entire depth of the boundary and the development of single stratocumulus layer clouds whose top well correlates with the inversion (Rémillard et al., 2012; Ho et al., 2015). The height of the marine boundary layer has a role in the degree of MBL decoupling with the surface ocean and, therefore, in regulating MBL cloud development and coverage (Wood and Bretherton, 2006; Wood, 2012).

The number concentrations of cloud droplets (N_d) measured by the CDP also vary annually with a maximum in spring and minima during the winter and summer, in accordance with previous studies conducted in the Western and Eastern North Atlantic ocean (Sinclair et al., 2020; Wang et al., 2021) (Fig. 2). In-cloud geometric mean and geometric standard deviation N_d values are 43 ∗ 7, 52 ∗ 3.6, and 32 ∗ 4.3 cm^{-3}, respectively for NAAMES-1, -2, and -3 and lower N_d are associated with decoupled MBL conditions. However, it is worth noting that the mean N_d value during NAAMES-1 was affected by particularly high droplet concentrations (ranging between 71 and 109 cm^{-3}) occurring on Nov. 12th 2015 and it would have been significantly lower (14 ∗ 2.1 cm^{-3} with maximum N_d = 37 cm^{-3}) excluding that case. Furthermore, while spring exhibits thicker clouds (bases ~ 1000 m extending up to 3000 m) and persistent multilayers clouds, during the summer we observe higher frequency in single thin layers (maximum thickness 500 m) of clouds at lower altitudes. The seasonal variability in N_d and cloud vertical distribution between the three campaigns is driven by different meteorological processes (including MBL decoupling degree) and changes in cloud condensation nuclei (CCN) concentrations. Indeed, stratocumulus clouds can form within both deep and shallow MBL (Rémillard et al., 2012), however under decoupling conditions, as observed in the winter, the stratocumulus in the upper decoupled layer might not experience the same aerosol conditions as at the surface ocean. Furthermore, being separated from the ocean moisture supply and often exposed to the entrainment of warm and dry FT air, stratocumulus bases tend to rise and cloud droplets evaporate (Nicholls and Turton, 1986; Gerber, 1996), while cumulus clouds can form at the top of the surface mixed layer originating a new dynamical organization of the MBL (Bretherton and Wyant, 1997).

3.2 Regional marine environments versus continental periods

We assess the seasonal and spatial variations of CO, black carbon, and DMS concentrations as well as the non-refractory aerosol chemical composition to disentangle competing contributions of air masses from continental origins versus regional emissions. A number of previous studies have shown that CO and BC, mainly produced from incomplete combustion of fossil fuel and biomass burning, are good tracers of non-marine aerosols, and thus good tracers to investigate events of long-range transport of continental air masses in remote regions (Parrish et al., 1998; Stohl et al., 2002; Duncan, 2004; Shank et al., 2012). Measurements of non-refractory aerosol chemical composition such as sulfate, organics, nitrate, and ammonium also provide an important insight into aerosol sources in the WNAO. In a recent work, Corral et al. (2021) found that BC, sulfate, and organic aerosols in WNAO are mainly the result of continental emissions from the eastern U.S. Meanwhile, DMS is an indicator of local ocean biological activity (Andreae et al., 1985; Charlson et al., 1987; Bates et al., 1992).

During NAAMES-1, we observe a mean CO concentration = 87.2 ± 6.6 ppbv and no significant variations within days. CO vertical profiles show similar concentrations at all the altitudes sampled, being only slightly higher in the MBL (mean = 90.1 ± 3.3 ppbv) than in the FT (mean = 86.1 ± 7.2 ppbv) (Table 3, Fig. 3a, Fig. 4a, Fig. SI.1.a, and Fig. SI.21.a). BC concentrations are also generally low (mean of 8.3 ± 21 ng m^{-3} in the MBL, and 5.1 ± 4.8 ng m^{-3}6.2 ± 11.2 ng m^{-3}in the FT), characteristic of unpolluted conditions observed during the winter (Table 3, Fig. 3b, Fig. 4a4b, and Fig. 6aand Fig. SI.2.a). The only exceptions

are Nov. 12th, 2015 and Nov. 14th, 2015 when BC exhibits peaks in the MBL up to 101.4 ng m-3 and 106.2 ng m-3 respectively, at altitudes < 1500 m (Fig. ~~3b~~4b, and Fig. SI.~~2~~3.a.1-3). The enhanced BC levels might be the result of ship-traffic emissions. Analysis of 5-days Hysplit frequency backtrajectory indicate the arrival of air masses from the Artic suggesting clean maritime influence (Fig. SI.2.a-b). Furthermore, Worlview FIRMS VIIRS Fire and Thermal Anomalies products show absence of wildfires on the air mass transport path prior the arrival to the NAAMES-1 domain, therefore excluding the contributions from biomass burning to the BC level observed (Fig. SI.2.c). After removing the BC measurements affected by ship-traffic emissions (data discarded altitude < 1500 m on Nov. 12th, 2015, and altitude < 1050 m on Nov. 14th, 2015) we found mean BC concentrations in the MBL of 1.8 ± 0.9 ng m-3 and lower than in the FT. ~~the intrusion of polluted air masses from continental origins due to wintertime low-altitude long-range transport. Field studies conducted in several locations over the North Atlantic ocean region have shown background concentrations of BC ranging between 10 and 40 ng m-3 under unperturbed marine conditions (O'Dowd et al., 2004; Shank et al., 2012; Pohl et al., 2014; Cavalli et al., 2016), while BC concentration up to 600 ng m-3 have been reported during periods of time affected by intense continental emission plumes (Corrigan et al., 2008).~~ Non-refractory aerosol chemical composition analysis also reveals low concentrations of sulfate (0.05 ± 0.03, 0.03 ± 0.03, and 0.07 ± 0.03 µg std m-3 respectively at the surface ocean, in the MBL, and in the FT) (Fig. 3c, Fig. ~~4a~~5a, and Fig. ~~5b~~6b, ~~and Fig. SI.2.a~~), and organic (0.1 ± 0.07, 0.05 ± 0.08, and 0.08 ± 0.06 at the surface ocean, in the MBL, and in the FT, respectively~~-~~) aerosol mass (Fig. 3d, ~~4b~~5b, and Fig. SI.1.b~~, and Fig. SI.2.a~~). No correlations between CO and BC, BC and sulfate, and BC and organics are found in the MBL (Fig. 7a, b, and c). Similarly, despite higher level of BC in the FT, we could not find correlations between FT BC and FT CO (linear regression R^2 values is 0.01) (Fig. 7d). On the other hand, the correlations between BC and sulfate, and BC and organics in the FT is moderate (~~are found during NAAMES-1 (~~the linear regression R^2 values are ~~0.04~~0.64, and 0.40~~0.25, and 0.20, ~~respectively) (Fig. ~~6a~~7e, ~~b, ~~and ~~c~~f). These results~~,~~ indicate that, although the predominantly low aerosol environment with only reduced ocean emissions, the WNAO in the winter is subjected to minor episodes of anthropogenic pollution, such as ship-traffic in the MBL and transport of continental polluted air masses in the FT) that influence the atmospheric vertical column. ~~ing a predominantly low aerosol environment with minor influence of anthropogenic pollution and ocean emissions.~~

The highest mean CO and BC values are observed during NAAMES-2, being respectively 107.9 ± 15.7 ppbv and 24.8 ± 32.1 ng m-3. Maximum CO and BC concentrations in the springtime have been previously reported over the North Atlantic and are related to more frequent contributions from North American continental outflow which is lofted into the FT and transported over the ocean by westerly frontal passages and convection that occasionally mix emissions down into the MBL (Zhao et al., 2012; Wood et al., 2015; Zheng et al., 2018). Namely, field studies conducted in several locations over the North Atlantic ocean region have shown background concentrations of BC ranging between 10 and 40 ng m-3 under unperturbed marine conditions (O'Dowd et al., 2004; Shank et al., 2012; Pohl et al., 2014; Cavalli et al., 2016), while BC concentration up to 600 ng m-3 have been reported during periods of time affected by intense continental emission plumes (Corrigan et al., 2008). Along the vertical column, mean CO levels remain almost constant (mean MBL CO = 104.4 ± 8.5 ppbv, and mean FT CO = 109 ± 18.8 ppbv) (Table 3, Fig. 3a, Fig. 4a, ~~Fig. SI.1.a, ~~and Fig. SI.~~2~~1.~~b~~a), while in the case of BC, we observe a well-defined vertical trend with 3-fold lower concentrations in the MBL (mean MBL BC = 9.4 ± 8 ng m-3) than in the FT (mean FT BC = 30.7 ± 35 ng m-3) (Table 3, Fig. 3b, Fig. ~~4a~~4b, and Fig. ~~SI.2.b~~6a). It is important noting that BC concentrations in the FT also have a statistically relevant higher variability due to the occurrence of high-concentration BC events (BC > 30 ng m-3) during some of the flights analyzed, namely on May 20th, 28th, 29th and 30th, 2016 (Fig. 3b). Excluding the above-mentioned events, BC concentrations are still higher than what observed during NAAMES-1, suggesting minor but persistent contributions from continental polluted emissions over the entire period. Overall~~MBL~~, BC is not well correlated with CO (linear regression R^2 = 0.29, and R^2 = 0.28, respectively in the MBL and FT)~~,~~ but the correlation improves in the FT when BC concentrations are > 30 ng m-3 (linear regression R^2 = 0.79) (Fig.~~6d~~8a, and d). Possible explanations for this are different CO and BC lifetimes and

removal mechanisms ~~in the MBL and FT~~. Indeed, while CO has an atmospheric lifetime of months and its concentration is mainly driven by hydroxyl radical (OH) oxidation (Novelli et al., 1998; Seinfeld and Pandis, 2016), BC lifetime is shorter and it is removed through cloud and precipitation scavenging processes (Cape et al., 2012; Bond et al., 2013). Sulfate loadings are ~~and organic mean loadings~~ are ~~respectively~~ 0.2 ± 0.08, ~~and 0.4 ± 0.15~~ µg std m^{-3} at the surface ocean, 0.2 ± 0.16, ~~and 0.25 ±~~ ~~0.18~~ µg std m^{-3} in the MBL, and 0.18 ± 0.11 ~~, and 0.77 ± 1.21 µg std m^{-3} respectively~~ in the FT, ~~.~~ (Table 3, Fig. 3c, Fig. ~~4a~~5a, and Fig. ~~5b~~ 6b ~~ sulfate, Fig. 4b, and Fig. SI.1.b ~~ organic, and Fig. SI.2.b~~), and the mixing ratio of DMS in the MBL ~~D~~during ~~the~~ NAAMES-2 ~~field campaign, we find~~ the highest ~~mixing ratio of DMS in the MBL~~id the highest observed during the three field campaign (values up to 0.325 ppbv) consistent with other works conducted in the North Atlantic region (Yoon et al., 2007; Quinn et al., 2019; Saliba et al., 2020; Sanchez et al., 2021) (Fig. ~~3~~4c, ~~and Fig. SI.2.b~~). The organic mean loadings and associated standard deviations follow a different trend being lower in the MBL (0.4 ± 0.15 µg std m^{-3} at the surface ocean, and 0.25 ± 0.18 µg std m^{-3} in the MBL) and more elevated in the FT (0.77 ± 1.21 µg std m^{-3}) (Table 3, Fig. 3d, Fig. 5b, Fig. SI.1.b). ~~. The~~ In the MBL the correlation between BC and sulfate is moderate (R^2 = 0.69) suggesting that part of the sulfate has marine origin (Fig. 7b). Simultaneously, in the FT we found linear regression R^2 = 0.27 when BC concentrations are < 30 ng m^{-3} and R^2 = 0.67 and for BC > 30 ng m^{-3} ~~and similar in MBL and FT~~ (Fig. ~~6e~~7f). The weak correlation between sulfate and BC when BC is < 30 ng m^{-3}~~,~~ is driven by the measurements collected on May 19th and 26th, 2016. Excluding those spirals, the linear regression would generate an R^2 = 0.61, in agreement to what observed in the MBL and in the FT for BC > 30 ng m^{-3}. This result might indicate sulfate mass production from DMS oxidation in the FT occurring after the loft of DMS from the MBL. ~~while a s~~Similar results were observed for the correlation between BC and organic being the linear regression R^2 values 0.64 in the MBL, and 0.42 and 0.91 in the FT respectively for BC < 30 ng m^{-3} and BC > 30 ng m^{-3}. Again, the modest correlation found in the MBL provide evidence of an additional source of organic particles not related to long-range transport of continental air masses. In a recent field study conducted in the Arctic, Mungall et al. (2017) showed that the sea surface microlayer at the ocean-atmosphere interface is enriched by dissolved organic carbon content (e.g. surfactants and plankton exudates) and can be an important source of oxygenated volatile organic compounds in the MBL which can be lofted to the FT and , possibly contribut~~ing~~ to the total sub-micron non-refractory mass along the vertical column. Simultaneously, in the FT, the stronger correlation between BC and organic when BC > 30 ng m^{-3} is accompanied by mean organic mass ~4-fold higher during periods when BC < 30 ng m^{-3} indicating the contributions from anthropogenic sources of continental origins with high organic components. ~~tronger correlation is observed between BC and organics (R^2 = 0.91) (Fig. 6f), especially in the FT. In accordance with the results of (Sanchez et al., 2018), the above results indicate contributions from anthropogenic sources of continental origins, especially in the case of the organic components for which we observed mean organic mass ~ 4-fold higher when BC concentrations > 40 ng m^{-3}. However, the lower correlation between BC and sulfate also suggest that part of the sulfate has marine origin. Similarly, if considering only the MBL, the R^2 obtained comparing BC and organics is lower (0.64), suggesting an additional source not related to long-range transport of particles. In a recent field study conducted in the Arctic, Mungall et al. (2017) showed that the sea surface microlayer at the ocean-atmosphere interface is enriched by dissolved organic carbon content (e.g. surfactants and plankton exudates) and can be an important source of oxygenated volatile organic compounds in the MBL, possibly contributing to the total sub-micron non-refractory mass. During the NAAMES-2 field campaign, we find the highest mixing ratio of DMS in the MBL (values up to 0.325 ppbv) consistent with other works conducted in the North Atlantic region (Yoon et al., 2007; Quinn et al., 2019; Saliba et al., 2020; Sanchez et al., 2021) (Fig. 3c, and Fig. SI.2.b).~~

During NAAMES-3, CO and BC concentrations vary significantly within flights (Fig. 3a, Fig. 4a, Fig. SI.1.a - CO, and Fig. 3b, Fig. ~~4a~~ 4b, Fig. 6a - BC). The lowest mean CO and BC concentrations are observed on Sept. 08th and 09th (CO mean of 83.5 ± 6.5 ppbv, BC mean 3.9 ± 3.4 ng m^{-3}) and remain relatively constant throughout the vertical column (Fig. SI.~~2~~3.c.27-31). Minimum CO levels in the summer have been reported by several studies (Honrath, 2004; Wood et al., 2015; Zheng et

al., 2018) and are found to be associated with photolytic destruction due to high summertime OH levels (Novelli et al., 1998). However, the analysis conducted on the data collected on the other days of the NAAMES-3 field campaign show higher mean and standard deviation CO and BC values of respectively 124.7 ± 27.3 ppbv and BC of 22.3 ± 32.5 ng m⁻³ and a. hHigh concentrations of CO and BC have been related to the long-range transport of continental biomass burning plumes over the

5   WNAO due to the North American and Canadian wildfire season (Honrath et al., 2004; Val Martín et al., 2006). , non-uniform distribution along the vertical columns characterized by ~ 800 to 2000 m height layers with CO levels > 200 ppbv and BC concentrations > 100 ng m⁻³. Low-level altitude (below ~3000 m) transport of CO from North America to the Atlantic Ocean has been observed in summer by earlier studies (Li et al., 2005; Owen et al., 2006), and while Zheng et al. (2020) reported upper troposphere transport of biomass burning particles from western Canadian wildfire over the Eastern North Atlantic in

10   late August 2017. The distributions of CO and BC along the vertical columns are non-uniform characterized by ~ 800 to 2000 m height layers with CO levels > 200 ppbv and BC concentrations > 100 ng m⁻³ at different altitudes depending on the day, or even on the time of the day. Here we observe the highest concentration of CO and BC and diverse multi-layer structures on September 4th, 6th, and 12th 2017. Namely, on Sept. 4th we found CO > 200 ppmv and BC > 30 ng m⁻³ at altitudes > 4.2 Km and in the residual layer (1. 2 to 1.8 Km), which entrained into the MBL in the late afternoon (spiral 2 at 16:07 UTC). Similar

15   enhanced CO and BC concentrations were also observed on Sept 6th between 1.9 and 3 Km and in the MBL, and on Sept. 12th in the FT at altitudes > 4 Km (Fig. 4a, and b). high concentrations of CO and BC have been related to the long-range transport of continental biomass burning plumes over the WNAO due to the North American and Canadian wildfire season (Honrath et al., 2004; Val Martín et al., 2006). The linear regression obtained comparingCorrelation between BC and CO is moderate and slightly lower in the MBL ($R^2 = 0.47$ for BC < 30 ng m⁻³ and $R^2 = 0.41$ for BC > 30 ng m⁻³) than in the FT ($R^2 = 0.52$ for BC

20   < 30 ng m⁻³ and $R^2 = 0.57$ for BC > 30 ng m⁻³) and CO generate an $R^2 = 0.54$ (Fig. 6g9a, and d). Our result is consistent with Val Martín et al. (2006) who observed higher variability in BC than CO at Pico Mountain (in the Eastern North Atlantic) due to different fire emission rates and wet scavenging during the transport to the site. Mean mass concentrations of non-refractory sulfate and organic are , respectively, 0.12 ± 0.13 and 0.49 ± 0.42 µg std m⁻³ at the surface ocean, 0.25 ± 0.16, and 1.03 ± 1.12 µg std m⁻³ in the MBL, and 0.14 ± 0.07, and 1.03 ± 1.12 µg std m⁻³ respectively in the FT (Table 3, Fig. 3c, Fig. 4a5a, and Fig.

25   5b 6b sulfate, Fig. 4b, and Fig. SI.1.b organic, and Fig. SI.2.e). Compared to NAAMES-2 sulfate mass in the MBL is higher, and During NAAMES-3, mixing ratio of DMS wereis lower than in the spring being up to 0.11 ppbv in the MBL (Fig. 34cd). These results are likely related to the combination of likely due to the decline of phytoplankton abundance and reduced productivity reduction at the end of the summer / beginning of fall which cause DMS levels to decline (Lana et al., 2011), and (Lana et al., 2011). Iincreased sunlight in summertime and enhanced concentrations of OH may alsowhich lead to have caused

30   quicker DMS oxidation sulfate mass production (Zawadowicz et al., 2020). than in spring led by enhanced concentrations of OH.. Supporting our hypothesis, highest concentrations of sulfate in the MBL are associated to the lowest level of DMS on Sept. 6th, 8th, and 9th, while we observed the opposite trend on Sept. 4th, 16th, and 17th, 2017 (Fig. 4c, and Fig. 5a). In the FT, sulfate concentrations are lower than during NAAMES-2. Accordingly, No the correlation is found between BC and sulfate is weak and only slightly improves in the FT when BC concentration are > 30 ng m⁻³ ($R^2 = 0.38$ for BC < 30 ng m⁻³ and $R^2 =$

35   0.11 for BC > 30 ng m⁻³ in the MBL, and $R^2 = 0.09$ for BC < 30 ng m⁻³ and $R^2 = 0.51$ for BC > 30 ng m⁻³ in the FT)($R^2 = 0.21$) (Fig. 6hbc, and e), and sulfate concentrations in the FT are lower than during NAAMES-2 therefore excluding the presence of a dominant strong anthropogenic source of sulfate. Instead, enhanced sulfate mass concentrations over the Atlantic Ocean in summertime have been previously attributed to DMS production and high oxidant levels at the surface ocean (Zawadowicz et al., 2020). Mean mass concentrations of non-refractory organic are 0.49 ± 0.42 µg std m⁻³ at the surface ocean, 1.03 ± 1.12 µg

40   std m⁻³ in the MBL, and 1.03 ± 1.12 µg std m⁻³ respectively in the FT (Table 3, Fig. 3d, Fig. 5b and Fig. SI.3.b), and Conversely, organic aerosol loadings are higher than what was observed during the other two NAAMES field campaigns. The correlation between BC and organic is moderate and $R^2 \sim 0.5$ in both MBL and FT ($R^2 = 0.54$ for BC < 30 ng m⁻³ and $R^2 = 0.59$ for BC > 30 ng m⁻³ in the MBL, and $R^2 = 0.56$ for BC < 30 ng m⁻³ in the FT), have $R^2 = 0.89$ (Fig. 6i9c, and f), however when BC > 30

ng m^{-3} and mean organic mass ~~were~~ are ~6-fold higher and the linear regression between BC and organic generate an R^2 = 0.5. for~~when BC concentrations were > 40 ng m^{-3}~~. Our obersevations are supported by ~~P~~previous work ~~has~~ show~~ing~~n that in biomass burning plumes, aerosol composition is typically dominated by organic~~s~~ which can cover BC particles with a thick coating (Ditas et al., 2018), while concentrations of sulfate are lower and increase with aging (Schlosser et al., 2017). ~~During NAAMES-3, mixing ratio of DMS were lower than in the spring being up to 0.11 ppbv in the MBL (Fig. 3d) likely due to the decline of phytoplankton abundance and reduced productivity at the end of the summer / beginning of fall (Lana et al., 2011). Increased sunlight in summertime may also have caused quicker DMS oxidation than in spring led by enhanced concentrations of OH.~~

3.3 Aerosol properties and processes in the Western North Atlantic region

3.3.1 Seasonal variations of submicron aerosol particle concentrations and size distribution

The concentration and vertical distribution of submicron aerosol particles over the WNAO vary through the year as a function of emission sources and aerosol processes. In this section, we discuss how a combination of NAAMES measurements constrain the concentration and size distribution of aerosol particles in the atmospheric column and their seasonal variations. In figure ~~7a~~10a, 3e we show the vertical distribution of N_{CN} during the three NAAMES campaigns. N_{CN} exhibits strong seasonal variations and marked vertical gradients with lower geometric mean concentrations in the winter and higher in spring and summer. During NAAMES-1, geometric mean aerosol number concentrations are 94.3 ∗ 3.5 cm^{-3}, 96.9 ∗ 2.6 cm^{-3}, and 286 ∗ 1.9 cm^{-3} at the surface ocean, in the MBL, and in the FT respectively (Table 3, and Fig. SI.1.c). These low values are likely due to a combination of minimal contributions from phytoplankton activities and continental anthropogenic sources, and particle loss by in-cloud precipitation and coalescence scavenging during NAAMES-1 (Quinn et al., 2019). Similar results were also observed by Pennypacker and Wood (2017) in an earlier study conducted in the Eastern North Atlantic region. The aerosol number concentration in both MBL and FT is dominated by particles with D_p < 100 nm. Geometric mean N_{NP} are 32 ∗ 3.1 cm^{-3} and 24 ∗ 2.2 cm^{-3} in the MBL and the FT, respectively, and the average fraction of the NP mode particles is higher than in the other seasons in both MBL and FT, both being roughly a third of N_{CN} (Fig. ~~7b~~10b). However, it is worth to note that the absolute number concentration of particles in the NP remains low due to low level of VOC precursors. New particle formation events have been widely reported in environments characterized by low aerosol surface area, cold air temperature, and high actinic fluxes (Clarke, 1993; Hoppel et al., 1994; Raes et al., 1997; Russell et al., 1998; Petters et al., 2006; Seinfeld and Pandis, 2016; Sanchez et al., 2018), and occurring after convective mixing between FT and MBL from the passage of cold front (Hoppel et al., 1994; Bates et al., 1998; Clarke et al., 1998; Pirjola et al., 2000). However, new particle formation occurs regularly also in the upper part of the MBL when aerosol surface area and air temperature are low such as observed in the WNAO during the wintertime (Kolstad et al., 2009; Zheng et al., 2021). Therefore, the occurrence of recently formed particles in the MBL observed during NAAMES-1 is likely associated with nucleation processes in the MBL, rather than entrainment from the FT, because of reduced aerosol surface area and low temperature during NAAMES-1. Once formed, new particles have the potential to contribute to the Aitken mode by condensational growth and coagulation (Kerminen et al., 2018). During the NAAMES-1 field campaign, the geometric mean concentration of particles in the Aitken mode are 57 ∗ 2.6 cm^{-3} in the MBL and 231 ∗ 2.1 cm^{-3} in the FT, accounting for 50-60% of N_{CN} (Fig. ~~7c~~10c). Entrainment from the FT has been recognized as the major source of Aitken mode particles in the MBL, while in the FT the relative contribution from growth of NP and long-range transported particles is still unclear (Clarke et al., 1998; Andreae et al., 2018). The concentration of larger particles with D_p > 100 nm is generally low with geometric mean MBL N_{Ac} = 7 ∗ 2.2 cm^{-3} and FT N_{Ac} = 14 ∗ 2.2 cm^{-3}, representing only a small percentage of N_{CN} (~ 6% in the MBL and ~ 3% in the FT) (Fig. ~~7d~~10d). In the North Atlantic region, controlling

processes of the accumulation mode in the MBL include the entrainment of accumulation mode particles from the FT, condensational growth of Aitken mode aerosols, and sea spray aerosol production, while the major source of accumulation mode particles in the FT is the long-range transport of anthropogenic particles (Zheng et al., 2018). Reduced transport of particles from continental regions in the winter, might explain the low FT N_{Ac} observed here and low contribution from FT

5 entrainment to MBL N_{Ac}. Similarly, the condensational growth of Aitken mode particles in the MBL is expected to be a weak source of N_{Ac} in the winter due to low MSA and sulfate oceanic emissions. The major source of accumulation mode particles in the MBL during winter is the production of sea spray aerosols due to high wind speed, surpassing the contribution from the condensational growth (Zheng et al., 2018).

10 High geometric mean N_{CN} values are found in both spring and summer, consistent with previous studies conducted in the North Atlantic ocean region (Wood et al., 2015; Zheng et al., 2018; Quinn et al., 2019). Overall, the concentrations of particles in the MBL are 1.4 to 4-fold lower than in the FT and showed high variability within flights (Table 3, and Fig. SI.1.c). Geometric mean N_{CN} are 243.6 $*$ 2 cm^{-3}, 345.3 $*$ 2 cm^{-3} and 553.5 $*$ 2 cm^{-3}, respectively at the surface ocean, in the MBL and in the FT (Fig. 7a10a). Geometric mean N_{NP} during NAAMES-2 are 82 $*$ 3.5 cm^{-3} in the MBL and 180 $*$ 3 cm^{-3} and in the FT, and the

15 nucleation mode accounted for roughly a quarter of the total number of particles (Fig. 7b10b). Interestingly, we find that higher N_{CN} are associated with enhanced concentration of particles in the nucleation mode. Indeed, when N_{CN} is > 1000 cm^{-3}, nucleation particle concentrations are > 354 cm^{-3} and the nucleation mode contributes to > 43% and up to 84% of the total particle concentration, becoming predominant over the Aitken and accumulation modes. The passage of cold fronts associated with higher biogenic precursors in the spring over the WNAO might be the cause of the elevated N_{CN} observed. Geometric

20 mean concentrations of particles in the Aitken mode are 218 $*$ 1.8 cm^{-3} in the MBL and 394 $*$ 1.9 cm^{-3} in the FT, accounting for just over half of N_{CN} (Fig. 7e10c), while the geometric means of accumulation mode particle concentration is 40 $*$ 2.3 cm^{-3} in the MBL (11% of N_{CN}) and 44 $*$ 3.5 cm^{-3} in the FT (7% of N_{CN}) (Fig. 7e10c). Stronger ocean emissions and high DMS levels in the spring favour the growth of nucleation particles into Aitken and accumulation mode through condensation and coagulation (O'Dowd et al., 1997; Andreae et al., 2003). Here, we find substantially higher concentrations of accumulation

25 particle modes (133 $*$ 2.5 cm^{-3}) when BC levels are higher than the threshold values of 40 ng m^{-3} (Pohl et al., 2014; Cavalli et al., 2016) indicate a further contribution to to N_{At} and N_{Ac} from long-range transport of particles from polluted continental areas (Zhao et al., 2012; Wood et al., 2015).

The highest concentrations of submicron aerosol particles are observed during NAAMES-3 in both MBL and FT. Elevated

30 N_{CN} over the North Atlantic ocean during summer have been reported by previous studies (Wood et al., 2015; Zheng et al., 2020) and are likely related to the transport of biomass burning plumes from boreal wildfires (Honrath et al., 2004; Val Martín et al., 2006; Dzepina et al., 2015; Zhang et al., 2017; Mardi et al., 2021). Summer 2017 was an extreme wildfire season in the north-western United States and western Canada (Kloss et al., 2019). The intense heating generated above the fires led to the development of fire-trigged pyrocumulonimbus releasing smoke particles into the lower extratropical stratosphere which were

35 then transported over the Atlantic Ocean (Khaykin et al., 2018; Peterson et al., 2018). Here, we find geometric mean N_{CN} to be 220.3 $*$ 1.8 cm^{-3}, 441.8 $*$ 1.9 cm^{-3} and 860.15 $*$ 1.6 cm^{-3} respectively at the surface ocean, in the MBL, and in the FT (Table 3, Fig. 7a10a, and Fig. SI.1.c). Furthermore, we observe a change in aerosol population characterized by a shift towards larger particles, as expected in presence of aged biomass burning aerosols (Niemi et al., 2005; Petzold et al., 2007). The concentration of particles in the nucleation mode are 52 $*$ 2.5 cm^{-3} and 160 $*$ 2.4 cm^{-3} respectively in the MBL and in the FT, and the

40 contribution to the total particle concentration is lower than in other seasons representing 11% of MBL N_{CN} and 18% of FT N_{CN} (Fig. 7b10b). Simultaneously, the Aitken mode contribution to N_{CN} remains similar to the other seasons being 58% in the MBL (N_{At} = 268 $*$ 1.9 cm^{-3}) and 60% of N_{CN} in the FT (N_{At} = 526 $*$ 1.9 cm^{-3}) (Fig. 7e10c), while the concentrations of particles in the accumulation mode are higher than during NAAMES-1 and -2, being 76 $*$ 3.6 cm^{-3} and 62 $*$ 3.3 cm^{-3} respectively in the

MBL and in the FT, and contributing to 17% of MBL N_{CN} and 14% of FT N_{CN} (Fig. ~~7d~~10d). Interestingly, we find that enhanced concentrations of accumulation mode particles are associated with increased levels of sulfate in the MBL, and elevated concentrations of CO, BC, and organics in the FT. These observations suggest that in addition to the large contribution from biomass burning plumes, the condensational growth of Aitken mode particles due to biogenic emissions from ocean surface also represent an important source of accumulation mode aerosols. Mungall et al. (2017) found that the formation of secondary organic aerosol from oxygenated gas-phase organic compounds due to photochemistry and/or oxidation at the surface layer might contribute to the growth of Aitken mode particles during periods of low biological activity, which is consistent with our observations.

3.3.~~1~~2 CCN seasonal variations

Seasonal changes in total aerosol number concentration, size distribution and chemical composition influence the ability of the particles to act as cloud condensation nuclei (CCN). Here, we assess the concentration of CCN (N_{CCN}) during the three NAAMES field campaigns at water vapour super saturation (SS) of 0.21~~%,~~%, which is a reasonable estimate for the maximum supersaturation in marine boundary layer clouds where CCN activation occurs (Korolev and Mazin, 2003; Clarke and Kapustin, 2010; Wood, 2012) (Fig ~~8a~~11a). Furthermore, we calculate the CCN activation fractions (AF) defined as the ratio of N_{CCN} at the determined super-saturation SS of 0.21% to the total submicron aerosol number (Fig. ~~8b~~11b).

Overall, N_{CCN} is lower during the winter than in the spring, and significantly increase in the summer, while the vertical distribution of CCN in the atmospheric column is different between seasons. During NAAMES-1 cloud condensation nuclei concentrations in the MBL are lower than in the FT, being the geometric means N_{CCN} 15 $*$ 2.3 cm^{-3} and 41 $*$ 2.4 cm^{-3} respectively in the MBL and FT (Table 3, Fig. 3f, Fig. ~~8a~~11a, and Fig. SI.~~2~~3.d). Similarly, the potential activation fraction exhibits higher mean values in the MBL (mean potential AF = 27%) than in the FT (mean potential AF = 16%) (Fig. ~~8b~~11b). The low concentration of CCN in the MBL are likely related to reduced marine biological activity, and therefore low phytoplankton DMS and VOC contributions. However, the higher MBL activation fraction observed in the MBL suggests that particles in the marine boundary layer are more CCN active than FT aerosols. In this context, wind-generated sea spray aerosols at the surface ocean might play an important role in CCN formation (Quinn and Bates, 2011). Supporting this hypothesis, Sanchez et al. (2018) report that during NAAMES-1 sea spray particles contribute > 50% to the CCN budget. Furthermore, frequent precipitation in the winter might also contribute to lower CCN concentration in the MBL through coalescence scavenging (Sharon et al., 2006; Pennypacker and Wood, 2017). Simultaneously, the prevailing nucleation particle mode associated with low occurrence of continental plumes in the wintertime constrained the CCN budget in the FT.

During NAAMES-2, we found geometric means N_{CCN} being 72 $*$ 2.2 cm^{-3} in the MBL and 89 $*$ 3.3 cm^{-3} in the FT (Table , Fig. 3f, Fig. ~~8a~~11a, and Fig. SI.~~2~~3.d), with potential activation fractions of 34% and 29%, respectively (Fig. ~~8b~~11b). CCN budget over the WNAO in spring is the result of a combination of elevated biogenic emissions in the MBL and the arrival of aerosol particles of continental origins in the FT. Supporting the attribution of high springtime CCN to biogenic in MBL and continental in FT, we found that elevated N_{CCN} and potential activation fraction (>60%) values in the MBL are associated with the presence of particles in the accumulation mode and sulfate mass, thus suggesting the contribution to CCN from hygroscopic phytoplankton-derived aerosols to CCN concentrations (Sanchez et al., 2018; Quinn et al., 2019). Simultaneously, enhanced CCN concentrations and AF values in the FT are associated with BC levels > 60 ng m^{-3}, and organic and sulfate aerosol masses respectively > 1.3 µg std m^{-3} and > 0.26 µg std m^{-3} likely indicating the influence of long-range transported pollution on the CCN budget at high altitudes. The similar MBL and FT N_{CCN} mean values observed here suggest that the entrainment of CCN from the FT does not serve as direct source of CCN particles in the MBL. Instead, FT particles of continental origins can enter

the MBL, grow through condensation and subsequently, thus contributing to the CCN concentrations in the MBL during the springtime.

Mean cloud condensation nuclei values in the summer are similar to spring being 79 ∗ 3.5 cm⁻³ in the MBL and 61 ∗ 3.4 cm⁻³ in the FT (Table 3, Fig. 3f, Fig. 8a11a, and Fig. SI.23.d), with mean potential activation fractions of 26% and 13% in the MBL and FT, respectively (Fig. 8b11b). However, CCN concentrations during NAAMES-3 vary significantly within flights and N_{CCN} values > 300 cm⁻³ in the FT are accompanied by CO levels ~ 190 ppbv, BC concentrations > 90 ng m⁻³, and organic aerosol mass > 4.8 µg std m⁻³, consistent with the arrival of transported continental particles discussed in Section 3.3.1. and the subsequent entrainment of FT particles in the MBL due to favourable meteorological conditions. In the MBL, we observe elevated concentrations of CCN and enhanced potential activation fraction values (N_{CCN} values > 120 cm⁻³, AF > 37%) associated with sulfate aerosol mass > 0.72 µg std m⁻³ suggesting that the CCN budget is, to a large degree, also related to biological activities at the surface ocean. Indeed the final phase of the phytoplankton bloom and microbial activities are responsible for the emissions leading to elevated concentrations of sulfate that enhance the concentrations of CCN in the MBL (Saliba et al., 2020).

4 Conclusions

In this study, we analyze in-situ measurements of aerosol, trace gases, and meteorological parameters collected during three NAAMES field campaigns. We find that, the properties and vertical distribution of aerosol particles over the Western North Atlantic Ocean exhibit strong seasonal variability due to diverse aerosol controlling processes and synoptic meteorological conditions. Here, we provide a characterization of the aerosol vertical profiles under different aerosol and meteorological regimes during NAAMES-1, -2, and -3 field campaigns, occurring respectively in winter, spring, and summer. Pristine marine conditions of low aerosol concentrations and trace gas mixing ratios were observed during the winter and were to a large degree related to minor influences of long-range transported continental plumes and reduced biological activity at the surface ocean. The occurrence of recently formed particle is prevalent in both MBL and FT due to low aerosol surface area caused by wet scavenging occurring during cold front passages, although particle concentrations remain in a very low number regime. The concentration of larger particles with D_p > 100 nm is generally low and consistent with the reduced contribution from continental sources and higher occurrence of precipitation. Higher concentrations of aerosol particles were found in the spring and summer. Springtime vertical profiles of CO, BC, DMS, and mass-concentration of non-refractory particles suggest there is influence of long-range transported anthropogenic particles in the FT and biogenic oceanic emissions strongly contribute to the MBL on N_{CN} and CCN budgets. In the summer, we found biomass burning from boreal wildfires to largely contribute to aerosol concentrations and impact aerosol population. Particularly, enhanced concentration of large particles (D_p > 100 nm) and cloud condensation nuclei were observed along with elevated concentrations of CO, BC, and organics in the FT. This result highlights the importance that long-range transported continental aerosol particles have in shaping aerosol properties over the North Atlantic Ocean.

With our findings we aim to inform future studies for evaluating key aerosol processes over remote midlatitude oceans, including the role of aerosols on cloud microphysics and control on precipitation. Ultimately, this analysis could provide new knowledge to constrain the parametrization of aerosol-cloud interactions in climate models.

Data availability: data are available from http://doi.org/10.5067/Suborbital/NAAMES/DATA001.

FG and RM conceptualized the analysis. FG led the analyses and wrote the manuscript with additional input from KS and RM. RM was the project administrator. All authors were involved in helpful discussions and contributed to the manuscript.

Competing interest: The authors declare that they have no conflicts of interest.

Acknowledgements: We thank Michael Behrenfeld (the NAAMES PI) and the pilots and crew of the NASA C-130 and WHOI/UNOLS R/V Atlantis. FG was supported by a NASA Postdoctoral Program (NPP) fellowship. PTR-ToF-MS measurements of DMS during NAAMES were supported by the Austrian Federal Ministry for Transport, Innovation and Technology (bmvit) through the Austrian Space Applications Programme (ASAP; grants #833451, #840086, #847967) of the

10   Austrian Research Promotion Agency (FFG) and by the Tiroler Wissenschaftsförderung (TWF, grant # UNI-0404/1895). Support from the PTR-TOF-MS instrument team (Phillip Eichler, Tomas Mikoviny, Markus Müller, Felix Piel, Sven Arne Schiller) and from IONICON Analytik is gratefully acknowledged.

References

Albrecht, B. A.: Aerosols, Cloud Microphysics, and Fractional Cloudiness, Science, 245, 1227–1230, https://doi.org/10.1126/science.245.4923.1227, 1989.

5 Andreae, M. O., Ferek, R. J., Bermond, F., Byrd, K. P., Engstrom, R. T., Hardin, S., Houmere, P. D., LeMarrec, F., Raemdonck, H., and Chatfield, R. B.: Dimethyl sulfide in the marine atmosphere, J. Geophys. Res., 90, 12891, https://doi.org/10.1029/JD090iD07p12891, 1985.

Andreae, M. O., Andreae, T. W., Meyerdierks, D., and Thiel, C.: Marine sulfur cycling and the atmospheric aerosol over the springtime North Atlantic, Chemosphere, 52, 1321–1343, https://doi.org/10.1016/S0045-6535(03)00366-7, 2003.

10 Andreae, M. O., Afchine, A., Albrecht, R., Holanda, B. A., Artaxo, P., Barbosa, H. M. J., Borrmann, S., Cecchini, M. A., Costa, A., Dollner, M., Fütterer, D., Järvinen, E., Jurkat, T., Klimach, T., Konemann, T., Knote, C., Krämer, M., Krisna, T., Machado, L. A. T., Mertes, S., Minikin, A., Pöhlker, C., Pöhlker, M. L., Pöschl, U., Rosenfeld, D., Sauer, D., Schlager, H., Schnaiter, M., Schneider, J., Schulz, C., Spanu, A., Sperling, V. B., Voigt, C., Walser, A., Wang, J., Weinzierl, B., Wendisch, M., and Ziereis, H.: Aerosol characteristics and particle production in the upper troposphere over the Amazon Basin, Atmos. Chem. Phys., 18, 921–961, https://doi.org/10.5194/acp-18-921-2018, 2018.

15 Bates, T. S., Lamb, B. K., Guenther, A., Dignon, J., and Stoiber, R. E.: Sulfur emissions to the atmosphere from natural sources, J Atmos Chem, 14, 315–337, https://doi.org/10.1007/BF00115242, 1992.

Bates, T. S., Kapustin, V. N., Quinn, P. K., Covert, D. S., Coffman, D. J., Mari, C., Durkee, P. A., De Bruyn, W. J., and Saltzman, E. S.: Processes controlling the distribution of aerosol particles in the lower marine boundary layer during the First Aerosol Characterization Experiment (ACE 1), J. Geophys. Res., 103, 16369–16383, https://doi.org/10.1029/97JD03720, 20 1998.

Bates, T. S., Quinn, P. K., Coffman, D. J., Johnson, J. E., Upchurch, L., Saliba, G., Lewis, S., Graff, J., Russell, L. M., and Behrenfeld, M. J.: Variability in Marine Plankton Ecosystems Are Not Observed in Freshly Emitted Sea Spray Aerosol Over the North Atlantic Ocean, Geophysical Research Letters, 47, https://doi.org/10.1029/2019GL085938, 2020.

Behrenfeld, M. J., Moore, R. H., Hostetler, C. A., Graff, J., Gaube, P., Russell, L. M., Chen, G., Doney, S. C., Giovannoni, S., 25 Liu, H., Proctor, C., Bolaños, L. M., Baetge, N., Davie-Martin, C., Westberry, T. K., Bates, T. S., Bell, T. G., Bidle, K. D., Boss, E. S., Brooks, S. D., Cairns, B., Carlson, C., Halsey, K., Harvey, E. L., Hu, C., Karp-Boss, L., Kleb, M., Menden-Deuer, S., Morison, F., Quinn, P. K., Scarino, A. J., Anderson, B., Chowdhary, J., Crosbie, E., Ferrare, R., Hair, J. W., Hu, Y., Janz, S., Redemann, J., Saltzman, E., Shook, M., Siegel, D. A., Wisthaler, A., Martin, M. Y., and Ziemba, L.: The North Atlantic Aerosol and Marine Ecosystem Study (NAAMES): Science Motive and Mission Overview, Front. Mar. Sci., 6, 122, 30 https://doi.org/10.3389/fmars.2019.00122, 2019.

Bond, T. C., Doherty, S. J., Fahey, D. W., Forster, P. M., Berntsen, T., DeAngelo, B. J., Flanner, M. G., Ghan, S., Kärcher, B., Koch, D., Kinne, S., Kondo, Y., Quinn, P. K., Sarofim, M. C., Schultz, M. G., Schulz, M., Venkataraman, C., Zhang, H., Zhang, S., Bellouin, N., Guttikunda, S. K., Hopke, P. K., Jacobson, M. Z., Kaiser, J. W., Klimont, Z., Lohmann, U., Schwarz, J. P., Shindell, D., Storelvmo, T., Warren, S. G., and Zender, C. S.: Bounding the role of black carbon in the climate system: 35 A scientific assessment: BLACK CARBON IN THE CLIMATE SYSTEM, J. Geophys. Res. Atmos., 118, 5380–5552, https://doi.org/10.1002/jgrd.50171, 2013.

Bretherton, C. S. and Wyant, M. C.: Moisture Transport, Lower-Tropospheric Stability, and Decoupling of Cloud-Topped Boundary Layers, Journal of the Atmospheric Sciences, 54, 148–167, https://doi.org/10.1175/1520-0469(1997)054<0148:MTLTSA>2.0.CO;2, 1997.

40 Cape, J. N., Coyle, M., and Dumitrean, P.: The atmospheric lifetime of black carbon, Atmospheric Environment, 59, 256–263, https://doi.org/10.1016/j.atmosenv.2012.05.030, 2012.

Carslaw, K. S., Lee, L. A., Reddington, C. L., Pringle, K. J., Rap, A., Forster, P. M., Mann, G. W., Spracklen, D. V., Woodhouse, M. T., Regayre, L. A., and Pierce, J. R.: Large contribution of natural aerosols to uncertainty in indirect forcing, Nature, 503, 67–71, https://doi.org/10.1038/nature12674, 2013.

45 Cavalli, F., Alastuey, A., Areskoug, H., Ceburnis, D., Čech, J., Genberg, J., Harrison, R. M., Jaffrezo, J. L., Kiss, G., Laj, P., Mihalopoulos, N., Perez, N., Quincey, P., Schwarz, J., Sellegri, K., Spindler, G., Swietlicki, E., Theodosi, C., Yttri, K. E., Aas, W., and Putaud, J. P.: A European aerosol phenomenology -4: Harmonized concentrations of carbonaceous aerosol at 10

regional background sites across Europe, Atmospheric Environment, 144, 133–145, https://doi.org/10.1016/j.atmosenv.2016.07.050, 2016.

Chan, K. M. and Wood, R.: The seasonal cycle of planetary boundary layer depth determined using COSMIC radio occultation data, Journal of Geophysical Research: Atmospheres, 118, 12,422-12,434, https://doi.org/10.1002/2013JD020147, 2013.

5   Charlson, R. J., Lovelock, J. E., Andreae, M. O., and Warren, S. G.: Oceanic phytoplankton, atmospheric sulphur, cloud albedo and climate, Nature, 326, 655–661, https://doi.org/10.1038/326655a0, 1987.

Clarke, A. and Kapustin, V.: Hemispheric Aerosol Vertical Profiles: Anthropogenic Impacts on Optical Depth and Cloud Nuclei, Science, 329, 1488–1492, https://doi.org/10.1126/science.1188838, 2010.

Clarke, A. D.: Atmospheric nuclei in the Pacific midtroposphere: Their nature, concentration, and evolution, J. Geophys. Res., 10   98, 20633, https://doi.org/10.1029/93JD00797, 1993.

Clarke, A. D., Varner, J. L., Eisele, F., Mauldin, R. L., Tanner, D., and Litchy, M.: Particle production in the remote marine atmosphere: Cloud outflow and subsidence during ACE 1, J. Geophys. Res., 103, 16397–16409, https://doi.org/10.1029/97JD02987, 1998.

Clarke, A. D., Freitag, S., Simpson, R. M. C., Hudson, J. G., Howell, S. G., Brekhovskikh, V. L., Campos, T., Kapustin, V. 15   N., and Zhou, J.: Free troposphere as a major source of CCN for the equatorial pacific boundary layer: long-range transport and teleconnections, Atmos. Chem. Phys., 13, 7511–7529, https://doi.org/10.5194/acp-13-7511-2013, 2013.

Corral, A. F., Braun, R. A., Cairns, B., Gorooh, V. A., Liu, H., Ma, L., Mardi, A. H., Painemal, D., Stamnes, S., van Diedenhoven, B., Wang, H., Yang, Y., Zhang, B., and Sorooshian, A.: An Overview of Atmospheric Features Over the Western North Atlantic Ocean and North American East Coast – Part 1: Analysis of Aerosols, Gases, and Wet Deposition Chemistry, 20   Geophys Res Atmos, 126, https://doi.org/10.1029/2020JD032592, 2021.

Corrigan, C. E., Roberts, G. C., Ramana, M. V., Kim, D., and Ramanathan, V.: Capturing vertical profiles of aerosols and black carbon over the Indian Ocean using autonomous unmanned aerial vehicles, Atmos. Chem. Phys., 8, 737–747, https://doi.org/10.5194/acp-8-737-2008, 2008.

Dadashazar, H., Braun, R. A., Crosbie, E., Chuang, P. Y., Woods, R. K., Jonsson, H. H., and Sorooshian, A.: Aerosol 25   characteristics in the entrainment interface layer in relation to the marine boundary layer and free troposphere, Atmos. Chem. Phys., 18, 1495–1506, https://doi.org/10.5194/acp-18-1495-2018, 2018.

DeCarlo, P. F., Kimmel, J. R., Trimborn, A., Northway, M. J., Jayne, J. T., Aiken, A. C., Gonin, M., Fuhrer, K., Horvath, T., Docherty, K. S., Worsnop, D. R., and Jimenez, J. L.: Field-Deployable, High-Resolution, Time-of-Flight Aerosol Mass Spectrometer, Anal. Chem., 78, 8281–8289, https://doi.org/10.1021/ac061249n, 2006.

30   Ditas, J., Ma, N., Zhang, Y., Assmann, D., Neumaier, M., Riede, H., Karu, E., Williams, J., Scharffe, D., Wang, Q., Saturno, J., Schwarz, J. P., Katich, J. M., McMeeking, G. R., Zahn, A., Hermann, M., Brenninkmeijer, C. A. M., Andreae, M. O., Pöschl, U., Su, H., and Cheng, Y.: Strong impact of wildfires on the abundance and aging of black carbon in the lowermost stratosphere, Proc Natl Acad Sci USA, 115, E11595–E11603, https://doi.org/10.1073/pnas.1806868115, 2018.

Dong, X., Schwantes, A. C., Xi, B., and Wu, P.: Investigation of the marine boundary layer cloud and CCN properties under 35   coupled and decoupled conditions over the Azores: MBL CLOUD AND CCN PROPERTIES, J. Geophys. Res. Atmos., 120, 6179–6191, https://doi.org/10.1002/2014JD022939, 2015.

Duncan, B. N.: A modeling study of the export pathways of pollution from Europe: Seasonal and interannual variations (1987–1997), J. Geophys. Res., 109, D08301, https://doi.org/10.1029/2003JD004079, 2004.

Dzepina, K., Mazzoleni, C., Fialho, P., China, S., Zhang, B., Owen, R. C., Helmig, D., Hueber, J., Kumar, S., Perlinger, J. A., 40   Kramer, L. J., Dziobak, M. P., Ampadu, M. T., Olsen, S., Wuebbles, D. J., and Mazzoleni, L. R.: Molecular characterization of free tropospheric aerosol collected at the Pico Mountain Observatory: a case study with a long-range transported biomass burning plume, Atmos. Chem. Phys., 15, 5047–5068, https://doi.org/10.5194/acp-15-5047-2015, 2015.

Facchini, M. C., Rinaldi, M., Decesari, S., Carbone, C., Finessi, E., Mircea, M., Fuzzi, S., Ceburnis, D., Flanagan, R., Nilsson, E. D., de Leeuw, G., Martino, M., Woeltjen, J., and O'Dowd, C. D.: Primary submicron marine aerosol dominated by insoluble 45   organic colloids and aggregates, Geophys. Res. Lett., 35, L17814, https://doi.org/10.1029/2008GL034210, 2008.

García, M. I., Rodríguez, S., and Alastuey, A.: Impact of North America on the aerosol composition in the North Atlantic free troposphere, Atmos. Chem. Phys., 17, 7387–7404, https://doi.org/10.5194/acp-17-7387-2017, 2017.

Gerber, H.: Microphysics of Marine Stratocumulus Clouds with Two Drizzle Modes, Journal of Atmospheric Sciences, 53, 1649–1662, https://doi.org/10.1175/1520-0469(1996)053<1649:MOMSCW>2.0.CO;2, 1996.

5   Hamilton, D. S., Lee, L. A., Pringle, K. J., Reddington, C. L., Spracklen, D. V., and Carslaw, K. S.: Occurrence of pristine aerosol environments on a polluted planet, Proc Natl Acad Sci USA, 111, 18466–18471, https://doi.org/10.1073/pnas.1415440111, 2014.

Ho, S., Peng, L., Anthes, R. A., Kuo, Y.-H., and Lin, H.-C.: Marine Boundary Layer Heights and Their Longitudinal, Diurnal, and Interseasonal Variability in the Southeastern Pacific Using COSMIC, CALIOP, and Radiosonde Data, Journal of Climate,
10   28, 2856–2872, https://doi.org/10.1175/JCLI-D-14-00238.1, 2015.

Hodshire, A. L., Campuzano-Jost, P., Kodros, J. K., Croft, B., Nault, B. A., Schroder, J. C., Jimenez, J. L., and Pierce, J. R.: The potential role of methanesulfonic acid (MSA) in aerosol formation and growth and the associated radiative forcings, Atmos. Chem. Phys., 19, 3137–3160, https://doi.org/10.5194/acp-19-3137-2019, 2019.

Honrath, R. E.: Regional and hemispheric impacts of anthropogenic and biomass burning emissions on summertime CO and
15   O $_3$ in the North Atlantic lower free troposphere, J. Geophys. Res., 109, D24310, https://doi.org/10.1029/2004JD005147, 2004.

Honrath, R. E., Owen, R. C., Val Martín, M., Seid, J. S., Lapina, K., Fialho, P., Dziobak, M. P., Kleissl, J., and Westphal, D. L.: Regional and hemispheric impacts of anthropogenic and biomass burning emissions on summertime CO and O $_3$ in the North Atlantic lower free troposphere, J. Geophys. Res., 109, D24310, https://doi.org/10.1029/2004JD005147, 2004.

Hoppel, W. A., Frick, G. M., Fitzgerald, J. W., and Larson, R. E.: Marine boundary layer measurements of new particle
20   formation and the effects nonprecipitating clouds have on aerosol size distribution, J. Geophys. Res., 99, 14443, https://doi.org/10.1029/94JD00797, 1994.

Jones, C. R., Bretherton, C. S., and Leon, D.: Coupled vs. decoupled boundary layers in VOCALS-REx, Atmos. Chem. Phys., 11, 7143–7153, https://doi.org/10.5194/acp-11-7143-2011, 2011.

Katzwinkel, J., Siebert, H., and Shaw, R. A.: Observation of a Self-Limiting, Shear-Induced Turbulent Inversion Layer Above
25   Marine Stratocumulus, Boundary-Layer Meteorol, 145, 131–143, https://doi.org/10.1007/s10546-011-9683-4, 2012.

Kerminen, V.-M., Chen, X., Vakkari, V., Petäjä, T., Kulmala, M., and Bianchi, F.: Atmospheric new particle formation and growth: review of field observations, Environ. Res. Lett., 13, 103003, https://doi.org/10.1088/1748-9326/aadf3c, 2018.

Khaykin, S. M., Godin-Beekmann, S., Hauchecorne, A., Pelon, J., Ravetta, F., and Keckhut, P.: Stratospheric Smoke With Unprecedentedly High Backscatter Observed by Lidars Above Southern France, Geophys. Res. Lett., 45, 1639–1646,
30   https://doi.org/10.1002/2017GL076763, 2018.

Kloss, C., Berthet, G., Sellitto, P., Ploeger, F., Bucci, S., Khaykin, S., Jégou, F., Taha, G., Thomason, L. W., Barret, B., Le Flochmoen, E., von Hobe, M., Bossolasco, A., Bègue, N., and Legras, B.: Transport of the 2017 Canadian wildfire plume to the tropics and global stratosphere via the Asian monsoon circulation, Aerosols/Remote Sensing/Stratosphere/Physics (physical properties and processes), https://doi.org/10.5194/acp-2019-204, 2019.

35   Kolstad, E. W., Bracegirdle, T. J., and Seierstad, I. A.: Marine cold-air outbreaks in the North Atlantic: temporal distribution and associations with large-scale atmospheric circulation, Clim Dyn, 33, 187–197, https://doi.org/10.1007/s00382-008-0431-5, 2009.

Korhonen, H., Carslaw, K. S., Spracklen, D. V., Mann, G. W., and Woodhouse, M. T.: Influence of oceanic dimethyl sulfide emissions on cloud condensation nuclei concentrations and seasonality over the remote Southern Hemisphere oceans: A global
40   model study, J. Geophys. Res., 113, D15204, https://doi.org/10.1029/2007JD009718, 2008.

Korolev, A. V. and Mazin, I. P.: Supersaturation of Water Vapor in Clouds, J. Atmos. Sci., 60, 2957–2974, https://doi.org/10.1175/1520-0469(2003)060<2957:SOWVIC>2.0.CO;2, 2003.

Lana, A., Bell, T. G., Simó, R., Vallina, S. M., Ballabrera-Poy, J., Kettle, A. J., Dachs, J., Bopp, L., Saltzman, E. S., Stefels, J., Johnson, J. E., and Liss, P. S.: An updated climatology of surface dimethlysulfide concentrations and emission fluxes in the

global ocean: UPDATED DMS CLIMATOLOGY, Global Biogeochem. Cycles, 25, n/a-n/a, https://doi.org/10.1029/2010GB003850, 2011.

Lapina, K., Heald, C. L., Spracklen, D. V., Arnold, S. R., Allan, J. D., Coe, H., McFiggans, G., Zorn, S. R., Drewnick, F., Bates, T. S., Hawkins, L. N., Russell, L. M., Smirnov, A., O'Dowd, C. D., and Hind, A. J.: Investigating organic aerosol loading in the remote marine environment, Atmos. Chem. Phys., 11, 8847–8860, https://doi.org/10.5194/acp-11-8847-2011, 2011.

de Leeuw, G., Andreas, E. L., Anguelova, M. D., Fairall, C. W., Lewis, E. R., O'Dowd, C., Schulz, M., and Schwartz, S. E.: Production flux of sea spray aerosol, Rev. Geophys., 49, RG2001, https://doi.org/10.1029/2010RG000349, 2011.

de Leeuw, G., Guieu, C., Arneth, A., Bellouin, N., Bopp, L., Boyd, P. W., van der Gon, H. A. C. D., Desboeufs, K. V., Dulac, F., Facchini, M. C., Gantt, B., Langmann, B., Mahowald, N. M., Marañón, E., O'Dowd, C., Olgun, N., Pulido-Villena, E., Rinaldi, M., Stephanou, E. G., and Wagener, T.: Ocean–Atmosphere Interactions of Particles, in: Ocean-Atmosphere Interactions of Gases and Particles, edited by: Liss, P. S. and Johnson, M. T., Springer Berlin Heidelberg, Berlin, Heidelberg, 171–246, https://doi.org/10.1007/978-3-642-25643-1_4, 2014.

Lenschow, D. H., Zhou, M., Zeng, X., Chen, L., and Xu, X.: Measurements Of Fine-Scale Structure At The Top Of Marine Stratocumulus, Boundary-Layer Meteorology, 97, 331–357, https://doi.org/10.1023/A:1002780019748, 2000.

Li, Q., Jacob, D. J., Park, R., Wang, Y., Heald, C. L., Hudman, R., and Yantosca, R. M.: North American pollution outflow and the trapping of convectively lifted pollution by upper-level anticyclone, J. Geophys. Res., 110, D10301, https://doi.org/10.1029/2004JD005039, 2005.

Lv, G., Zhang, C., and Sun, X.: Understanding the oxidation mechanism of methanesulfinic acid by ozone in the atmosphere, Sci Rep, 9, 322, https://doi.org/10.1038/s41598-018-36405-0, 2019.

Mardi, A. H., Dadashazar, H., Painemal, D., Shingler, T., Seaman, S. T., Fenn, M. A., Hostetler, C. A., and Sorooshian, A.: Biomass Burning Over the United States East Coast and Western North Atlantic Ocean: Implications for Clouds and Air Quality, Geophys Res Atmos, 126, https://doi.org/10.1029/2021JD034916, 2021.

Moore, R. H., Karydis, V. A., Capps, S. L., Lathem, T. L., and Nenes, A.: Droplet number uncertainties associated with CCN: an assessment using observations and a global model adjoint, Atmos. Chem. Phys., 13, 4235–4251, https://doi.org/10.5194/acp-13-4235-2013, 2013.

Müller, M., Mikoviny, T., Feil, S., Haidacher, S., Hanel, G., Hartungen, E., Jordan, A., Märk, L., Mutschlechner, P., Schottkowsky, R., Sulzer, P., Crawford, J. H., and Wisthaler, A.: A compact PTR-ToF-MS instrument for airborne measurements of volatile organic compounds at high spatiotemporal resolution, Atmos. Meas. Tech., 7, 3763–3772, https://doi.org/10.5194/amt-7-3763-2014, 2014.

Mungall, E. L., Abbatt, J. P. D., Wentzell, J. J. B., Lee, A. K. Y., Thomas, J. L., Blais, M., Gosselin, M., Miller, L. A., Papakyriakou, T., Willis, M. D., and Liggio, J.: Microlayer source of oxygenated volatile organic compounds in the summertime marine Arctic boundary layer, Proc Natl Acad Sci USA, 114, 6203–6208, https://doi.org/10.1073/pnas.1620571114, 2017.

Nicholls, S. and Turton, J. D.: An observational study of the structure of stratiform cloud sheets: Part II. Entrainment, Q.J Royal Met. Soc., 112, 461–480, https://doi.org/10.1002/qj.49711247210, 1986.

Niemi, J. V., Tervahattu, H., Vehkamäki, H., Martikainen, J., Laakso, L., Kulmala, M., Aarnio, P., Koskentalo, T., Sillanpää, M., and Makkonen, U.: Characterization of aerosol particle episodes in Finland caused by wildfires in Eastern Europe, Atmos. Chem. Phys., 5, 2299–2310, https://doi.org/10.5194/acp-5-2299-2005, 2005.

Novelli, P. C., Masarie, K. A., and Lang, P. M.: Distributions and recent changes of carbon monoxide in the lower troposphere, J. Geophys. Res., 103, 19015–19033, https://doi.org/10.1029/98JD01366, 1998.

O'Dowd, C. D., Smith, M. H., Consterdine, I. E., and Lowe, J. A.: Marine aerosol, sea-salt, and the marine sulphur cycle: a short review, Atmospheric Environment, 31, 73–80, https://doi.org/10.1016/S1352-2310(96)00106-9, 1997.

O'Dowd, C. D., Lowe, J. A., and Smith, M. H.: Observations and modelling of aerosol growth in marine stratocumulus—case study, Atmospheric Environment, 33, 3053–3062, https://doi.org/10.1016/S1352-2310(98)00213-1, 1999.

O'Dowd, C. D., Facchini, M. C., Cavalli, F., Ceburnis, D., Mircea, M., Decesari, S., Fuzzi, S., Yoon, Y. J., and Putaud, J.-P.: Biogenically driven organic contribution to marine aerosol, Nature, 431, 676–680, https://doi.org/10.1038/nature02959, 2004.

Ovadnevaite, J., Ceburnis, D., Leinert, S., Dall'Osto, M., Canagaratna, M., O'Doherty, S., Berresheim, H., and O'Dowd, C.: Submicron NE Atlantic marine aerosol chemical composition and abundance: Seasonal trends and air mass categorization: Seasonal Trends of Marine Aerosol, J. Geophys. Res. Atmos., 119, 11,850-11,863, https://doi.org/10.1002/2013JD021330, 2014.

Owen, R. C., Cooper, O. R., Stohl, A., and Honrath, R. E.: An analysis of the mechanisms of North American pollutant transport to the central North Atlantic lower free troposphere: LOWER FREE TROPOSPHERE EXPORT MECHANISMS, J. Geophys. Res., 111, https://doi.org/10.1029/2006JD007062, 2006.

Pandis, S. N., Russell, L. M., and Seinfeld, J. H.: The relationship between DMS flux and CCN concentration in remote marine regions, J. Geophys. Res., 99, 16945, https://doi.org/10.1029/94JD01119, 1994.

Parrington, M., Palmer, P. I., Henze, D. K., Tarasick, D. W., Hyer, E. J., Owen, R. C., Helmig, D., Clerbaux, C., Bowman, K. W., Deeter, M. N., Barratt, E. M., Coheur, P.-F., Hurtmans, D., Jiang, Z., George, M., and Worden, J. R.: The influence of boreal biomass burning emissions on the distribution of tropospheric ozone over North America and the North Atlantic during 2010, Atmos. Chem. Phys., 12, 2077–2098, https://doi.org/10.5194/acp-12-2077-2012, 2012.

Parrish, D. D., Trainer, M., Holloway, J. S., Yee, J. E., Warshawsky, M. S., Fehsenfeld, F. C., Forbes, G. L., and Moody, J. L.: Relationships between ozone and carbon monoxide at surface sites in the North Atlantic region, J. Geophys. Res., 103, 13357–13376, https://doi.org/10.1029/98JD00376, 1998.

Pennypacker, S. and Wood, R.: A Case Study in Low Aerosol Number Concentrations Over the Eastern North Atlantic: Implications for Pristine Conditions in the Remote Marine Boundary Layer, J. Geophys. Res. Atmos., 122, 12,393-12,415, https://doi.org/10.1002/2017JD027493, 2017.

Peterson, D. A., Campbell, J. R., Hyer, E. J., Fromm, M. D., Kablick, G. P., Cossuth, J. H., and DeLand, M. T.: Wildfire-driven thunderstorms cause a volcano-like stratospheric injection of smoke, npj Clim Atmos Sci, 1, 30, https://doi.org/10.1038/s41612-018-0039-3, 2018.

Petters, M. D., Snider, J. R., Stevens, B., Vali, G., Faloona, I., and Russell, L. M.: Accumulation mode aerosol, pockets of open cells, and particle nucleation in the remote subtropical Pacific marine boundary layer, J. Geophys. Res., 111, D02206, https://doi.org/10.1029/2004JD005694, 2006.

Petzold, A., Weinzierl, B., Huntrieser, H., Stohl, A., Real, E., Cozic, J., Fiebig, M., Hendricks, J., Lauer, A., Law, K., Roiger, A., Schlager, H., and Weingartner, E.: Perturbation of the European free troposphere aerosol by North American forest fire plumes during the ICARTT-ITOP experiment in summer 2004, Atmos. Chem. Phys., 7, 5105–5127, https://doi.org/10.5194/acp-7-5105-2007, 2007.

Pio, C. A., Legrand, M., Alves, C. A., Oliveira, T., Afonso, J., Caseiro, A., Puxbaum, H., Sanchez-Ochoa, A., and Gelencsér, A.: Chemical composition of atmospheric aerosols during the 2003 summer intense forest fire period, Atmospheric Environment, 42, 7530–7543, https://doi.org/10.1016/j.atmosenv.2008.05.032, 2008.

Pirjola, L., O'Dowd, C. D., Brooks, I. M., and Kulmala, M.: Can new particle formation occur in the clean marine boundary layer?, J. Geophys. Res., 105, 26531–26546, https://doi.org/10.1029/2000JD900310, 2000.

Pohl, K., Cantwell, M., Herckes, P., and Lohmann, R.: Black carbon concentrations and sources in the marine boundary layer of the tropical Atlantic Ocean using four methodologies, Atmos. Chem. Phys., 14, 7431–7443, https://doi.org/10.5194/acp-14-7431-2014, 2014.

Quinn, P. K. and Bates, T. S.: The case against climate regulation via oceanic phytoplankton sulphur emissions, Nature, 480, 51–56, https://doi.org/10.1038/nature10580, 2011.

Quinn, P. K., Bates, T. S., Schulz, K. S., Coffman, D. J., Frossard, A. A., Russell, L. M., Keene, W. C., and Kieber, D. J.: Contribution of sea surface carbon pool to organic matter enrichment in sea spray aerosol, Nature Geosci, 7, 228–232, https://doi.org/10.1038/ngeo2092, 2014.

Quinn, P. K., Collins, D. B., Grassian, V. H., Prather, K. A., and Bates, T. S.: Chemistry and Related Properties of Freshly Emitted Sea Spray Aerosol, Chem. Rev., 115, 4383–4399, https://doi.org/10.1021/cr500713g, 2015.

Quinn, P. K., Coffman, D. J., Johnson, J. E., Upchurch, L. M., and Bates, T. S.: Small fraction of marine cloud condensation nuclei made up of sea spray aerosol, Nature Geosci, 10, 674–679, https://doi.org/10.1038/ngeo3003, 2017.

Quinn, P. K., Bates, T. S., Coffman, D. J., Upchurch, L., Johnson, J. E., Moore, R., Ziemba, L., Bell, T. G., Saltzman, E. S., Graff, J., and Behrenfeld, M. J.: Seasonal Variations in Western North Atlantic Remote Marine Aerosol Properties, J. Geophys. Res. Atmos., 124, 14240–14261, https://doi.org/10.1029/2019JD031740, 2019.

Raes, F.: Entrainment of free tropospheric aerosols as a regulating mechanism for cloud condensation nuclei in the remote marine boundary layer, J. Geophys. Res., 100, 2893, https://doi.org/10.1029/94JD02832, 1995.

Raes, F., Van Dingenen, R., Cuevas, E., Van Velthoven, P. F. J., and Prospero, J. M.: Observations of aerosols in the free troposphere and marine boundary layer of the subtropical Northeast Atlantic: Discussion of processes determining their size distribution, J. Geophys. Res., 102, 21315–21328, https://doi.org/10.1029/97JD01122, 1997.

Rémillard, J., Kollias, P., Luke, E., and Wood, R.: Marine Boundary Layer Cloud Observations in the Azores, J. Climate, 25, 7381–7398, https://doi.org/10.1175/JCLI-D-11-00610.1, 2012.

Rinaldi, M., Decesari, S., Finessi, E., Giulianelli, L., Carbone, C., Fuzzi, S., O'Dowd, C. D., Ceburnis, D., and Facchini, M. C.: Primary and Secondary Organic Marine Aerosol and Oceanic Biological Activity: Recent Results and New Perspectives for Future Studies, Advances in Meteorology, 2010, 1–10, https://doi.org/10.1155/2010/310682, 2010.

Roberts, G. C. and Nenes, A.: A Continuous-Flow Streamwise Thermal-Gradient CCN Chamber for Atmospheric Measurements, Aerosol Science and Technology, 39, 206–221, https://doi.org/10.1080/027868290913988, 2005.

Rose, D., Gunthe, S. S., Mikhailov, E., Frank, G. P., Dusek, U., Andreae, M. O., and Pöschl, U.: Calibration and measurement uncertainties of a continuous-flow cloud condensation nuclei counter (DMT-CCNC): CCN activation of ammonium sulfate and sodium chloride aerosol particles in theory and experiment, Atmos. Chem. Phys., 8, 1153–1179, https://doi.org/10.5194/acp-8-1153-2008, 2008.

Russell, L. M., Lenschow, D. H., Laursen, K. K., Krummel, P. B., Siems, S. T., Bandy, A. R., Thornton, D. C., and Bates, T. S.: Bidirectional mixing in an ACE 1 marine boundary layer overlain by a second turbulent layer, J. Geophys. Res., 103, 16411–16432, https://doi.org/10.1029/97JD03437, 1998.

Saliba, G., Chen, C., Lewis, S., Russell, L. M., Quinn, P. K., Bates, T. S., Bell, T. G., Lawler, M. J., Saltzman, E. S., Sanchez, K. J., Moore, R., Shook, M., Rivellini, L., Lee, A., Baetge, N., Carlson, C. A., and Behrenfeld, M. J.: Seasonal Differences and Variability of Concentrations, Chemical Composition, and Cloud Condensation Nuclei of Marine Aerosol Over the North Atlantic, J. Geophys. Res. Atmos., 125, https://doi.org/10.1029/2020JD033145, 2020.

Sanchez, K. J., Chen, C.-L., Russell, L. M., Betha, R., Liu, J., Price, D. J., Massoli, P., Ziemba, L. D., Crosbie, E. C., Moore, R. H., Müller, M., Schiller, S. A., Wisthaler, A., Lee, A. K. Y., Quinn, P. K., Bates, T. S., Porter, J., Bell, T. G., Saltzman, E. S., Vaillancourt, R. D., and Behrenfeld, M. J.: Substantial Seasonal Contribution of Observed Biogenic Sulfate Particles to Cloud Condensation Nuclei, Sci Rep, 8, 3235, https://doi.org/10.1038/s41598-018-21590-9, 2018.

Sanchez, K. J., Zhang, B., Liu, H., Saliba, G., Chen, C.-L., Lewis, S. L., Russell, L. M., Shook, M. A., Crosbie, E. C., Ziemba, L. D., Brown, M. D., Shingler, T. J., Robinson, C. E., Wiggins, E. B., Thornhill, K. L., Winstead, E. L., Jordan, C., Quinn, P. K., Bates, T. S., Porter, J., Bell, T. G., Saltzman, E. S., Behrenfeld, M. J., and Moore, R. H.: Linking marine phytoplankton emissions, meteorological processes, and downwind particle properties with FLEXPART, Atmos. Chem. Phys., 21, 831–851, https://doi.org/10.5194/acp-21-831-2021, 2021.

Schlosser, J. S., Braun, R. A., Bradley, T., Dadashazar, H., MacDonald, A. B., Aldhaif, A. A., Aghdam, M. A., Mardi, A. H., Xian, P., and Sorooshian, A.: Analysis of aerosol composition data for western United States wildfires between 2005 and 2015: Dust emissions, chloride depletion, and most enhanced aerosol constituents, J. Geophys. Res. Atmos., 122, 8951–8966, https://doi.org/10.1002/2017JD026547, 2017.

Seinfeld, J. H. and Pandis, S. N.: Atmospheric chemistry and physics: from air pollution to climate change, Third edition., John Wiley & Sons, Hoboken, New Jersey, 1 pp., 2016.

Shank, L. M., Howell, S., Clarke, A. D., Freitag, S., Brekhovskikh, V., Kapustin, V., McNaughton, C., Campos, T., and Wood, R.: Organic matter and non-refractory aerosol over the remote Southeast Pacific: oceanic and combustion sources, Atmos. Chem. Phys., 12, 557–576, https://doi.org/10.5194/acp-12-557-2012, 2012.

Sharon, T. M., Albrecht, B. A., Jonsson, H. H., Minnis, P., Khaiyer, M. M., van Reken, T. M., Seinfeld, J., and Flagan, R.: Aerosol and Cloud Microphysical Characteristics of Rifts and Gradients in Maritime Stratocumulus Clouds, Journal of the Atmospheric Sciences, 63, 983–997, https://doi.org/10.1175/JAS3667.1, 2006.

Simpkins, G.: Aerosol–cloud interactions, Nature Clim Change, 8, 457–457, https://doi.org/10.1038/s41558-018-0195-9, 2018.

Sinclair, K., van Diedenhoven, B., Cairns, B., Alexandrov, M., Moore, R., Crosbie, E., and Ziemba, L.: Polarimetric retrievals of cloud droplet number concentrations, Remote Sensing of Environment, 228, 227–240, https://doi.org/10.1016/j.rse.2019.04.008, 2019.

Sinclair, K., Diedenhoven, B., Cairns, B., Alexandrov, M., Moore, R., Ziemba, L. D., and Crosbie, E.: Observations of Aerosol-Cloud Interactions During the North Atlantic Aerosol and Marine Ecosystem Study, Geophys. Res. Lett., 47, https://doi.org/10.1029/2019GL085851, 2020.

Sorooshian, A., Corral, A. F., Braun, R. A., Cairns, B., Crosbie, E., Ferrare, R., Hair, J., Kleb, M. M., Hossein Mardi, A., Maring, H., McComiskey, A., Moore, R., Painemal, D., Scarino, A. J., Schlosser, J., Shingler, T., Shook, M., Wang, H., Zeng, X., Ziemba, L., and Zuidema, P.: Atmospheric Research Over the Western North Atlantic Ocean Region and North American East Coast: A Review of Past Work and Challenges Ahead, J. Geophys. Res. Atmos., 125, https://doi.org/10.1029/2019JD031626, 2020.

Stohl, A., Eckhardt, S., Forster, C., James, P., and Spichtinger, N.: On the pathways and timescales of intercontinental air pollution transport: INTERCONTINENTAL AIR POLLUTION TRANSPORT, J.-Geophys.-Res., 107, ACH 6-1-ACH 6-17, https://doi.org/10.1029/2001JD001396, 2002.

Twomey, S.: The Influence of Pollution on the Shortwave Albedo of Clouds, Journal of Atmospheric Sciences, 34, 1149–1152, https://doi.org/10.1175/1520-0469(1977)034<1149:TIOPOT>2.0.CO;2, 1977.

Val Martín, M., Honrath, R. E., Owen, R. C., Pfister, G., Fialho, P., and Barata, F.: Significant enhancements of nitrogen oxides, black carbon, and ozone in the North Atlantic lower free troposphere resulting from North American boreal wildfires: WILDFIRE IMPACTS ON BC, NO $_x$, NO $_y$ AND O $_3$, J. Geophys. Res., 111, https://doi.org/10.1029/2006JD007530, 2006.

Wang, J., Wood, R., Jensen, M. P., Chiu, J. C., Liu, Y., Lamer, K., Desai, N., Giangrande, S. E., Knopf, D. A., Kollias, P., Laskin, A., Liu, X., Lu, C., Mechem, D., Mei, F., Starzec, M., Tomlinson, J., Wang, Y., Yum, S. S., Zheng, G., Aiken, A. C., Azevedo, E. B., Blanchard, Y., China, S., Dong, X., Gallo, F., Gao, S., Ghate, V. P., Glienke, S., Goldberger, L., Hardin, J. C., Kuang, C., Luke, E. P., Matthews, A. A., Miller, M. A., Moffet, R., Pekour, M., Schmid, B., Sedlacek, A. J., Shaw, R. A., Shilling, J. E., Sullivan, A., Suski, K., Veghte, D. P., Weber, R., Wyant, M., Yeom, J., Zawadowicz, M., and Zhang, Z.: Aerosol and Cloud Experiments in the Eastern North Atlantic (ACE-ENA), Bulletin of the American Meteorological Society, 1–51, https://doi.org/10.1175/BAMS-D-19-0220.1, 2021.

Wang, X. Y. and Wang, K. C.: Estimation of atmospheric mixing layer height from radiosonde data, Atmos. Meas. Tech., 7, 1701–1709, https://doi.org/10.5194/amt-7-1701-2014, 2014.

Warren, S. G., Hahn, C. J., London, J., Chervin, R. M., and Jenne, R. L.: Global distribution of total cloud cover and cloud type amounts over the ocean, https://doi.org/10.2172/5415329, 1988.

Wood, R.: Stratocumulus Clouds, Monthly Weather Review, 140, 2373–2423, https://doi.org/10.1175/MWR-D-11-00121.1, 2012.

Wood, R. and Bretherton, C. S.: On the Relationship between Stratiform Low Cloud Cover and Lower-Tropospheric Stability, Journal of Climate, 19, 6425–6432, https://doi.org/10.1175/JCLI3988.1, 2006.

Wood, R., Wyant, M., Bretherton, C. S., Rémillard, J., Kollias, P., Fletcher, J., Stemmler, J., Szoeke, S. de, Yuter, S., Miller, M., Mechem, D., Tselioudis, G., Chiu, J. C., Mann, J. A. L., O'Connor, E. J., Hogan, R. J., Dong, X., Miller, M., Ghate, V., Jefferson, A., Min, Q., Minnis, P., Palikonda, R., Albrecht, B., Luke, E., Hannay, C., and Lin, Y.: Clouds, Aerosols, and Precipitation in the Marine Boundary Layer: An Arm Mobile Facility Deployment, Bulletin of the American Meteorological Society, 96, 419–440, https://doi.org/10.1175/BAMS-D-13-00180.1, 2015.

Wood, R., Stemmler, J. D., Rémillard, J., and Jefferson, A.: Low-CCN concentration air masses over the eastern North Atlantic: Seasonality, meteorology, and drivers, J. Geophys. Res. Atmos., 122, 1203–1223, https://doi.org/10.1002/2016JD025557, 2017.

Yoon, Y. J., Ceburnis, D., Cavalli, F., Jourdan, O., Putaud, J. P., Facchini, M. C., Decesari, S., Fuzzi, S., Sellegri, K., Jennings, S. G., and O'Dowd, C. D.: Seasonal characteristics of the physicochemical properties of North Atlantic marine atmospheric aerosols, J. Geophys. Res., 112, D04206, https://doi.org/10.1029/2005JD007044, 2007.

5   Zawadowicz, M. A., Suski, K., Liu, J., Pekour, M., Fast, J., Mei, F., Sedlacek, A., Springston, S., Wang, Y., Zaveri, R. A., Wood, R., Wang, J., and Shilling, J. E.: Aircraft measurements of aerosol and trace gas chemistry in theEastern North Atlantic, Aerosols/Field Measurements/Troposphere/Chemistry (chemical composition and reactions), https://doi.org/10.5194/acp-2020-887, 2020.

Zhang, B., Owen, R. C., Perlinger, J. A., Helmig, D., Val Martín, M., Kramer, L., Mazzoleni, L. R., and Mazzoleni, C.: Ten-year chemical signatures associated with long-range transport observed in the free troposphere over the central North Atlantic,
10   Elementa: Science of the Anthropocene, 5, 8, https://doi.org/10.1525/elementa.194, 2017.

Zhao, T. L., Gong, S. L., Huang, P., and Lavoué, D.: Hemispheric transport and influence of meteorology on global aerosol climatology, Atmos. Chem. Phys., 12, 7609–7624, https://doi.org/10.5194/acp-12-7609-2012, 2012.

Zheng, G., Wang, Y., Aiken, A. C., Gallo, F., Jensen, M. P., Kollias, P., Kuang, C., Luke, E., Springston, S., Uin, J., Wood, R., and Wang, J.: Marine boundary layer aerosol in the eastern North Atlantic: seasonal variations and key controlling
15   processes, Atmos. Chem. Phys., 18, 17615–17635, https://doi.org/10.5194/acp-18-17615-2018, 2018.

Zheng, G., Sedlacek, A. J., Aiken, A. C., Feng, Y., Watson, T. B., Raveh-Rubin, S., Uin, J., Lewis, E. R., and Wang, J.: Long-range transported North American wildfire aerosols observed in marine boundary layer of eastern North Atlantic, Environment International, 139, 105680, https://doi.org/10.1016/j.envint.2020.105680, 2020.

Zheng, G., Wang, Y., Wood, R., Jensen, M. P., Kuang, C., McCoy, I. L., Matthews, A., Mei, F., Tomlinson, J. M., Shilling, J.
20   E., Zawadowicz, M. A., Crosbie, E., Moore, R., Ziemba, L., Andreae, M. O., and Wang, J.: New particle formation in the remote marine boundary layer, Nat Commun, 12, 527, https://doi.org/10.1038/s41467-020-20773-1, 2021.

Tables and figures

Table 1. UTC interval times, minimum and maximum altitude ranges, and geographical coordinates of the C-130 spirals analysed in this study.

	Date	Spiral	#	UTC Time		Altitude (Km)		GPS coordinates	
				Start	End	Start	End	Latitude	Longitude
NAAMES 1	12 Nov. 2015	S1	1	13:00	13:21	6.95	0.14	50.117	316.638
	14 Nov. 2015	S1	2	13:24	13:41	6.23	0.15	54.038	321.650
		S2	3	15:01	15:23	6.28	0.09	54.160	318.486
	17 Nov. 2015	S1	4	14:40	14:59	6.13	0.10	50.745	320.349
		S2	5	16:07	16:22	0.93	6.18	49.799	320.279
	18 Nov. 2015	S1	6	14:45	15:02	6.26	0.09	46.459	323.307
	23 Nov. 2015	S1	7	12:25	12:46	6.72	0.10	42.495	320.200
NAAMES 2	13 May 2016	S1	8	21:09	21:30	7.22	0.17	43.907	300.019
	18 May 2016	S1	9	11:19	11:40	6.25	0.09	44.476	315.524
	19 May2016	S1	10	13:54	14:15	6.16	0.09	42.952	317.048
	20 May2016	S1	11	14:58	15:15	0.10	5.75	42.250	317.750
	26 May2016	S1	12	14:17	14:41	0.09	6.67	38.585	321.415
		S2	13	15:44	16:08	6.71	0.08	38.766	321.234
		S3	14	18:24	18:39	0.19	6.54	45.319	314.681
	27 May2016	S1	15	12:28	12:52	6.27	0.10	45.653	314.347
	28 May2016	S1	16	13:36	13:55	6.35	0.09	44.493	315.507
	29 May2016	S1	17	12:11	12:33	6.37	0.09	44.486	315.514
		S2	18	13:44	13:56	0.10	3.36	40.713	319.287
	30 May2016	S1	19	14:46	15:07	6.44	0.12	44.675	315.325
		S2	20	17:39	17:58	6.40	0.11	43.078	316.922
	1 June 2016	S1	21	15:12	14:17	6.18	0.10	38.358	321.642
NAAMES 3	04 Sept. 2017	S1	22	13:36	13:56	6.752	0.095	43.058	316.261
		S2	23	16:07	16:21	6.791	0.095	42.020	317.589
	06 Sept. 2017	S1	24	11:35	11:58	6.857	0.086	44.157	318.224
		S2	25	13:59	14:28	0.098	7.543	44.356	316.636
		S3	26	14:57	15:11	7.523	0.093	44.384	316.264
	08 Sept. 2017	S1	27	12:34	12:54	6.842	0.106	47.658	319.421
		S2	28	14:43	15:04	0.565	6.851	47.243	319.729
		S3	29	15:32	15:45	6.836	0.209	47.454	320.813
	09 Sept. 2017	S1	30	12:25	12:41	6.838	0.122	48.453	323.646
		S2	31	14:27	14:47	6.890	0.098	48.478	321.049
	12 Sept. 2017	S1	32	17:57	18:14	6.267	0.081	51.830	319.418
		S2	33	18:44	19:03	0.075	6.036	51.718	320.429
		S3	34	19:29	19:45	6.276	0.121	51.450	321.654
	16 Sept. 2017	S1	35	11:57	12:12	6.297	0.093	54.032	321.048
		S2	36	14:24	14:38	6.489	0.133	52.739	320.015
	17 Sept. 2017	S1	37	12:29	12:44	6.268	0.106	53.377	320.571

Table 2. Measurements of aerosol and clouds properties on the C-130 used in this study.

Measurement	Symbol	Unit	Instrument
Total aerosol number concentration	N_{CN}	cm^{-3}	TSI CPC Model 3025A (D_p) > 3 nm TSI CPC Model 3772A (D_p) > 10 nm
Accumulation mode aerosol (100 nm < D_p < 1000 nm)	Ac	cm^{-3}	TSI LAS Model 3340
CCN number concentration at 0.21% SS	CCN	cm^{-3}	DMT CCN counter
Aerosol mass composition (NH_4, SO_4, Chloride, Organics)		μg sd m^{-3}	Aerodyne HR-ToF-AMS
Number concentration of cloud droplets (2 μm < D_p < 50 μm)	N_d		DMT CDP
Black carbon mass concentration	BC	ng m^{-3}	DMT SP2
CO mixing ratio	CO	ppbv	LGR CO/CO_2 gas analyzer
Dimethylsulfide mixing ratio	DMS	ppbv	PTR-MS
Potential temperature	θ	K	Meteorological sensor packages
Relative humidity	RH	%	Meteorological sensor packages
H2O mixing ratio	w	pppmv	LGR CO/CO_2 gas analyser

Table 3. Summary statistic of meteorological parameters, trace gasses, and aerosol properties measured during the three NAAMES field campaigns. The numbers are shown as mean ± standard deviation. N_{CN} and N_{CCN} values indicate geometric mean ∗ geometric standard deviation.
* MBL BC levels removing data affected by the ship-traffic events discussed in Section 3.2.

Parameters	NAAMES-1		NAAMES-2		NAAMES-3	
MBL Height	1776 ± 313		1657 ± 445		1144 ± 311	
	MBL	**FT**	**MBL**	**FT**	**MBL**	**FT**
θ (K)	279 ± 8	298 ± 8	296 ± 11	302 ± 9	292 ± 5	315 ± 9
W (ppmv)	5204 ± 2937	2001 ± 2712	5422 ± 4404	3475 ± 2640	8323 ± 1928	2008 ± 2201
RH (%)	78 ± 15	43 ± 26	55 ± 27	45 ± 23	63 ± 19	22 ± 17
CO (ppmv)	90 ± 3.3	86 ± 7.2	104 ± 8.5	109 ± 18.8	112 ± 17	107 ± 32.7
BC (ng m^{-3})	8.3 ± 21 *(1.8 ± 0.9)	5.1 ± 4.8	9.4 ± 8	30.7 ± 35	21 ± 28	15 ± 28
DMS			0.034 ± 0.03		0.014 ± 0.02	
Sulfate (ug std m^{-3})	0.03 ± 0.03	0.07 ± 0.03	0.2 ± 0.16	0.18 ± 0.11	0.25 ± 0.16	0.14 ± 0.07
Organic (ug std m^{-3})	0.07 ± 0.03	0.08 ± 0.06	0.25 ± 0.18	0.77 ± 1.21	1.03 ± 1.12	1.03 ± 1.12
N_{CN} (cm^{-3})	96 ∗ 2.6	286 ∗ 1.9	345 ∗ 2	553 ∗ 2	442 ∗ 1.9	860 ∗ 1.6
N_{CCN} (cm^{-3})	15 ∗ 2.3	41 ∗ 2.4	72 ∗ 2.2	89 ∗ 3.3	79 ∗ 3.5	61 ∗ 3.4
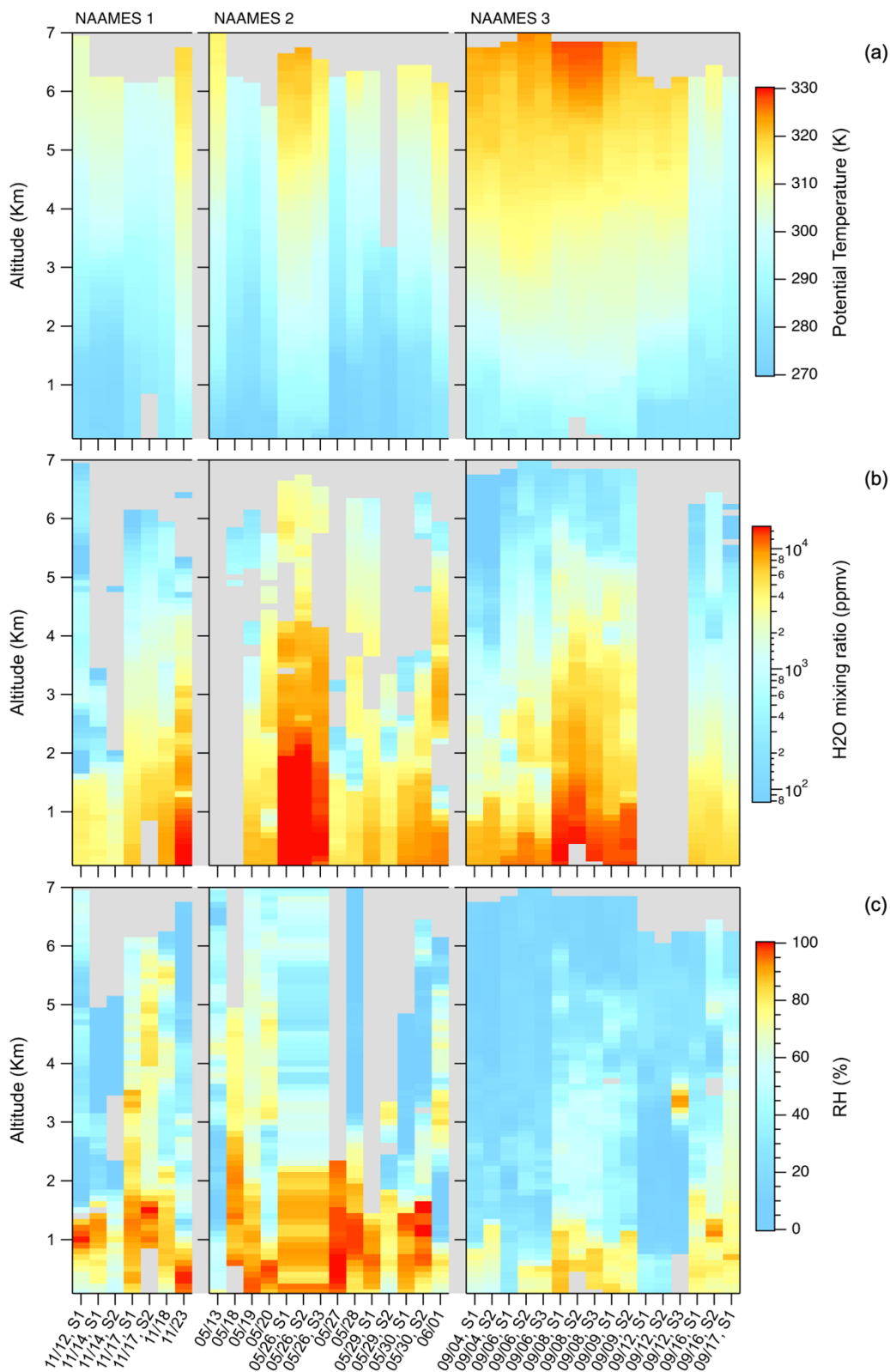
Figure 1. Vertical profiles potential temperature (a), H2O mixing ratio (b), and relative humidity (c) during NAAMES-1, -2, and -3. Relative humidity measurements from the meteorological sensor package are not available for the spirals conducted on May 26th, 2016, therefore RH measurement collected via radiosonde ship-launch on May 26th, 2016 at 2:26pm UTC time.
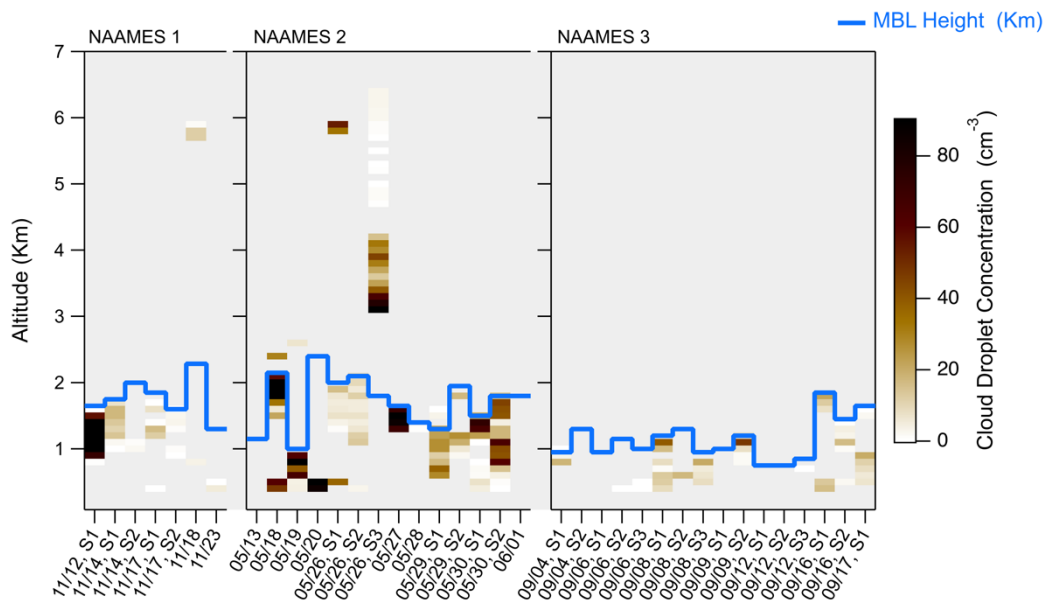
Figure 2. MBL and FT thermodynamic structure and vertical profiles of droplet concentration during NAAMES-1, -2, and -3
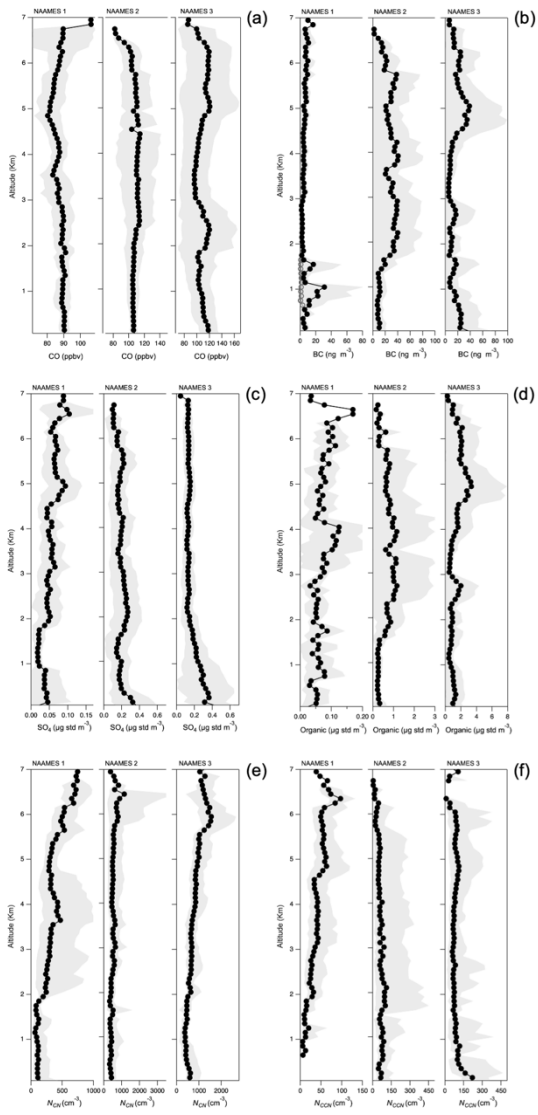
Figure 3. Vertical profiles of mean and standard deviation (grey shadow) of CO (a), BC (b), sulfate (c), organic (d), and geometric mean ∗ geometric standard deviation of N_{CN} (e), and N_{CCN} (f) during the three NAAMES field campaigns. Empty grey dots in Fig. b, represent mean of BC when data affected by the ship-traffic events discussed in Section 3.2 are removed.
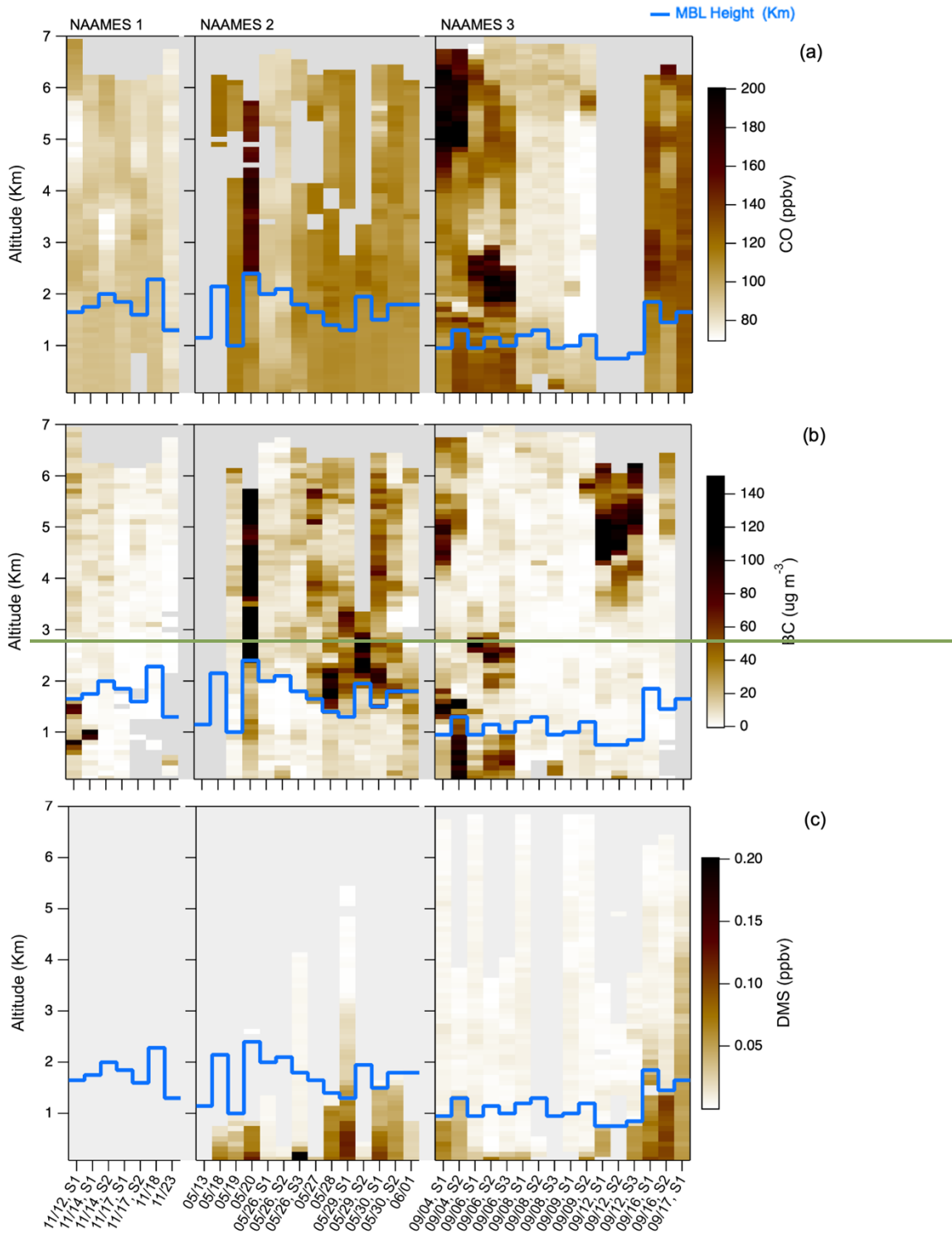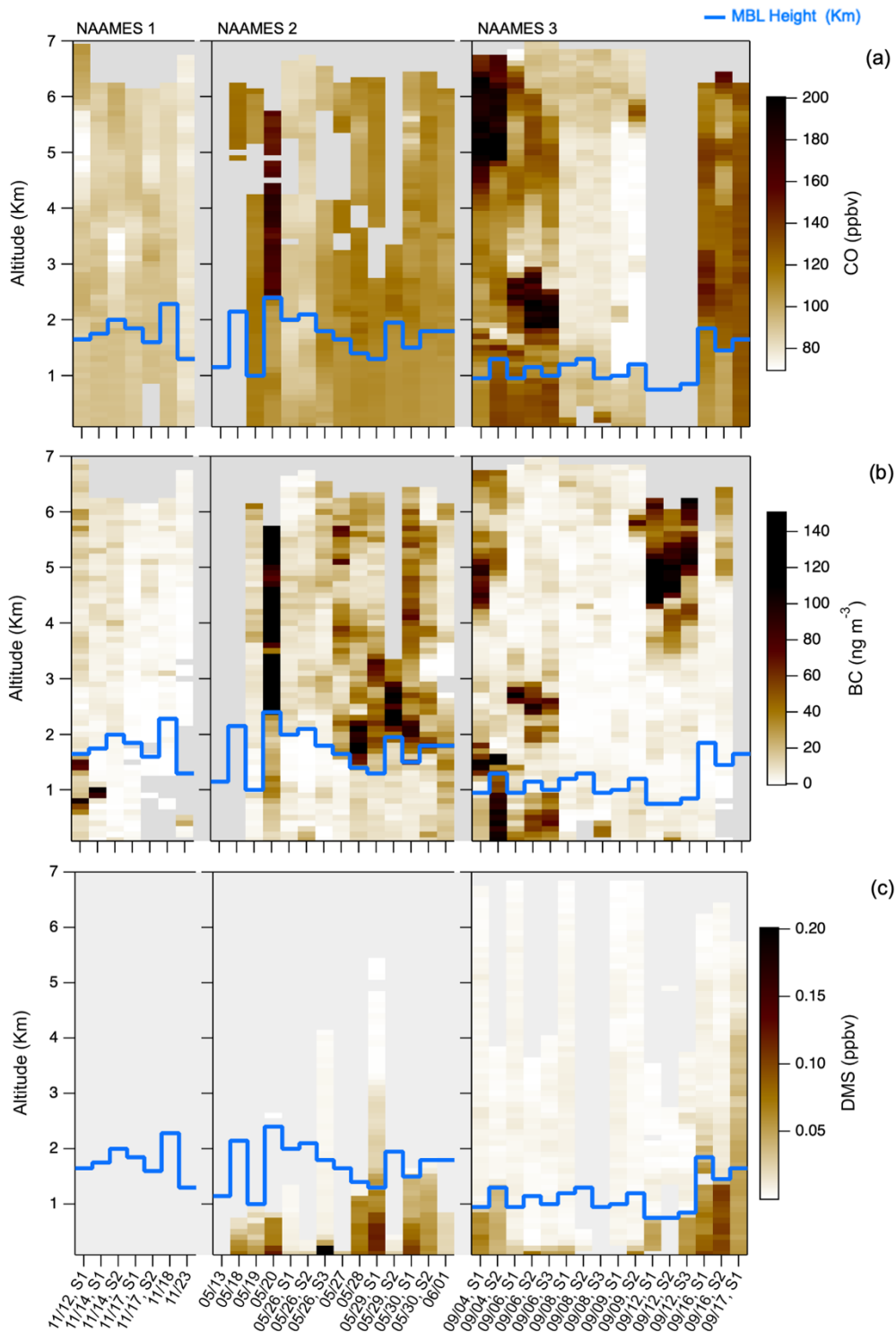
Figure 34. Vertical profile CO (a), black carbon (b), and DMS (c) during NAAMES-1, -2, and -3.
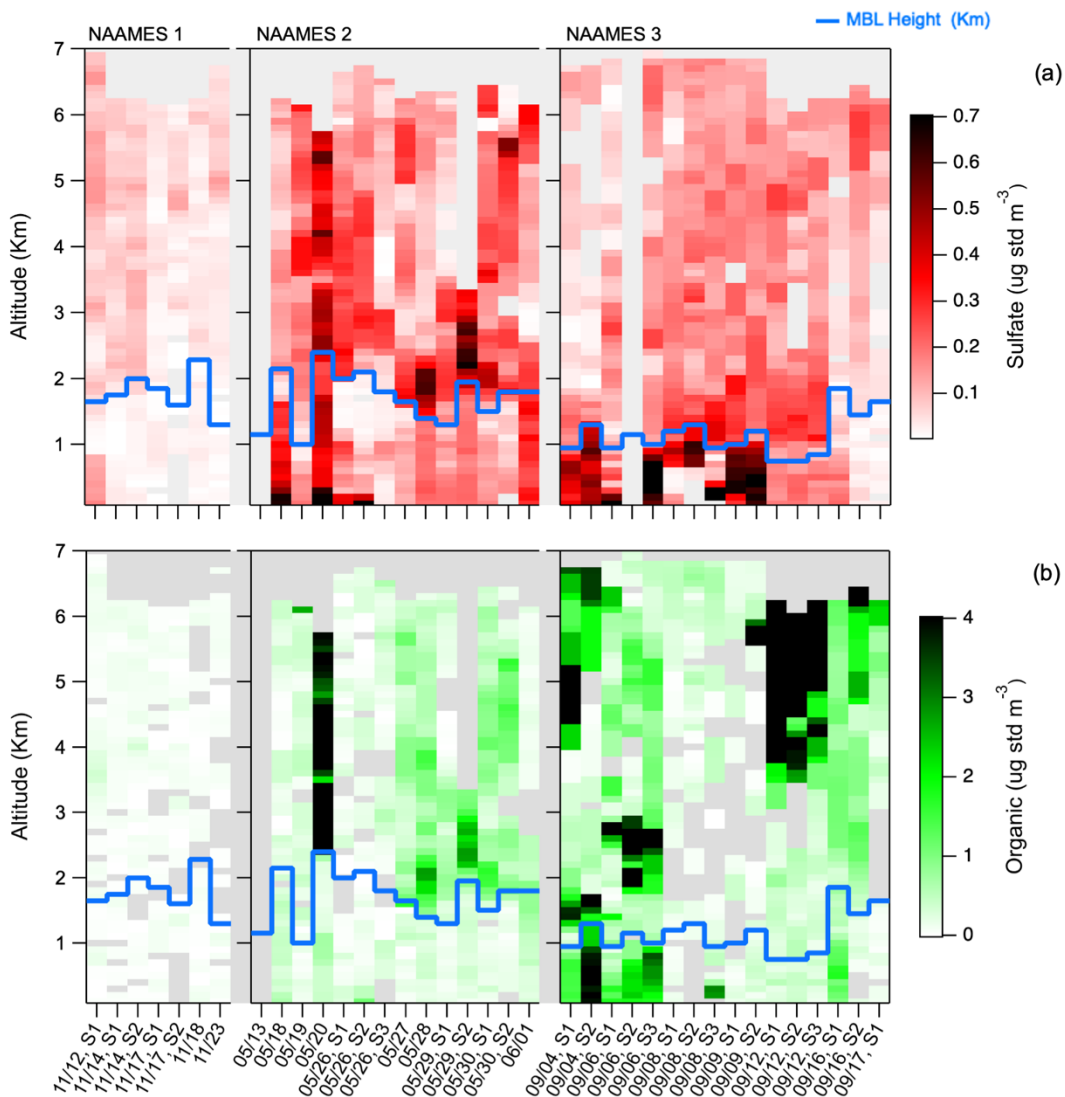
Figure 45. Vertical profile non-refractory aerosol chemical composition of aerosol particles during NAAMES-1, -2, and -3: sulfate (a), total organics (b).
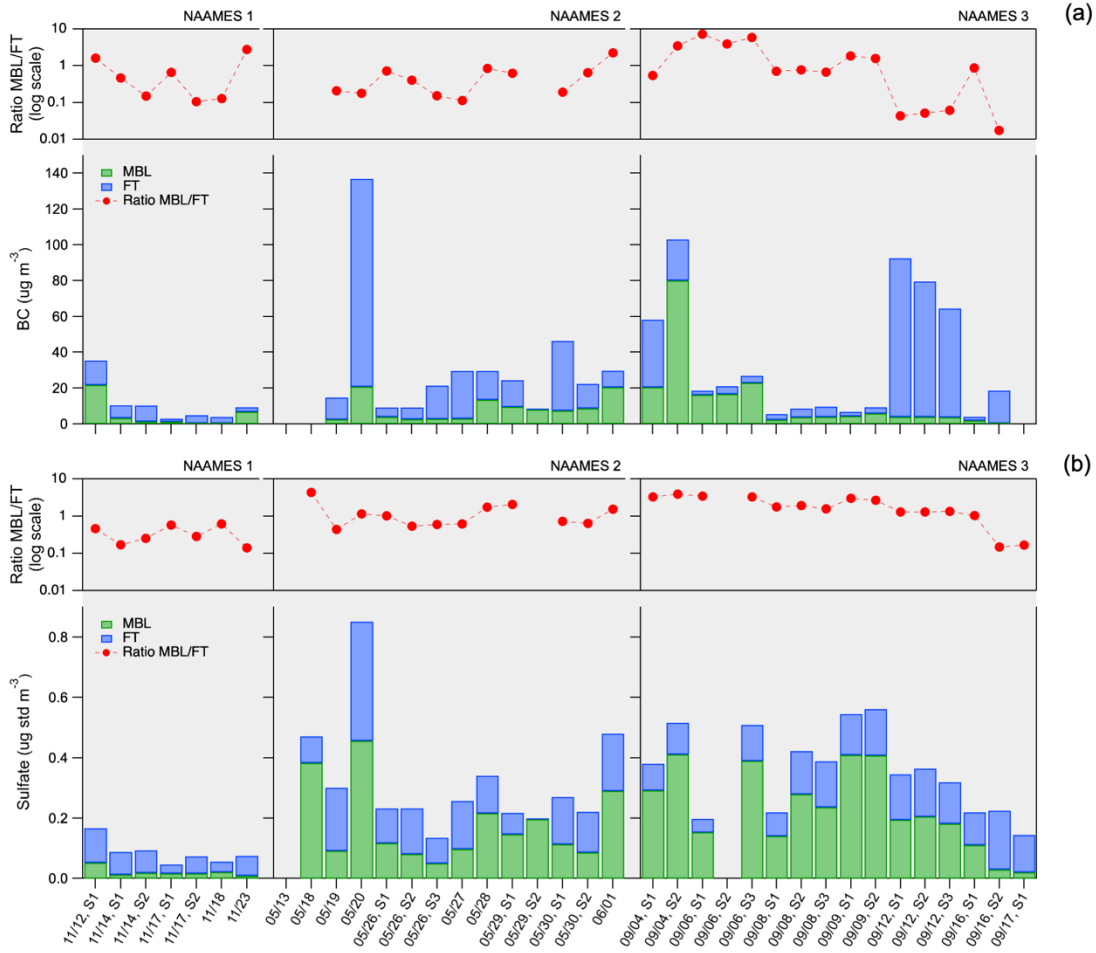
Figure 6̶5̶. MBL (green bars) and FT (blue bars) mean values of BC (a), and sulfate (b) for each C-130 spirals during NAAMES-1, -2, and -3. The red circles denote the ratio between MBL and FT mean values for the parameters considered (logarithmic scale).
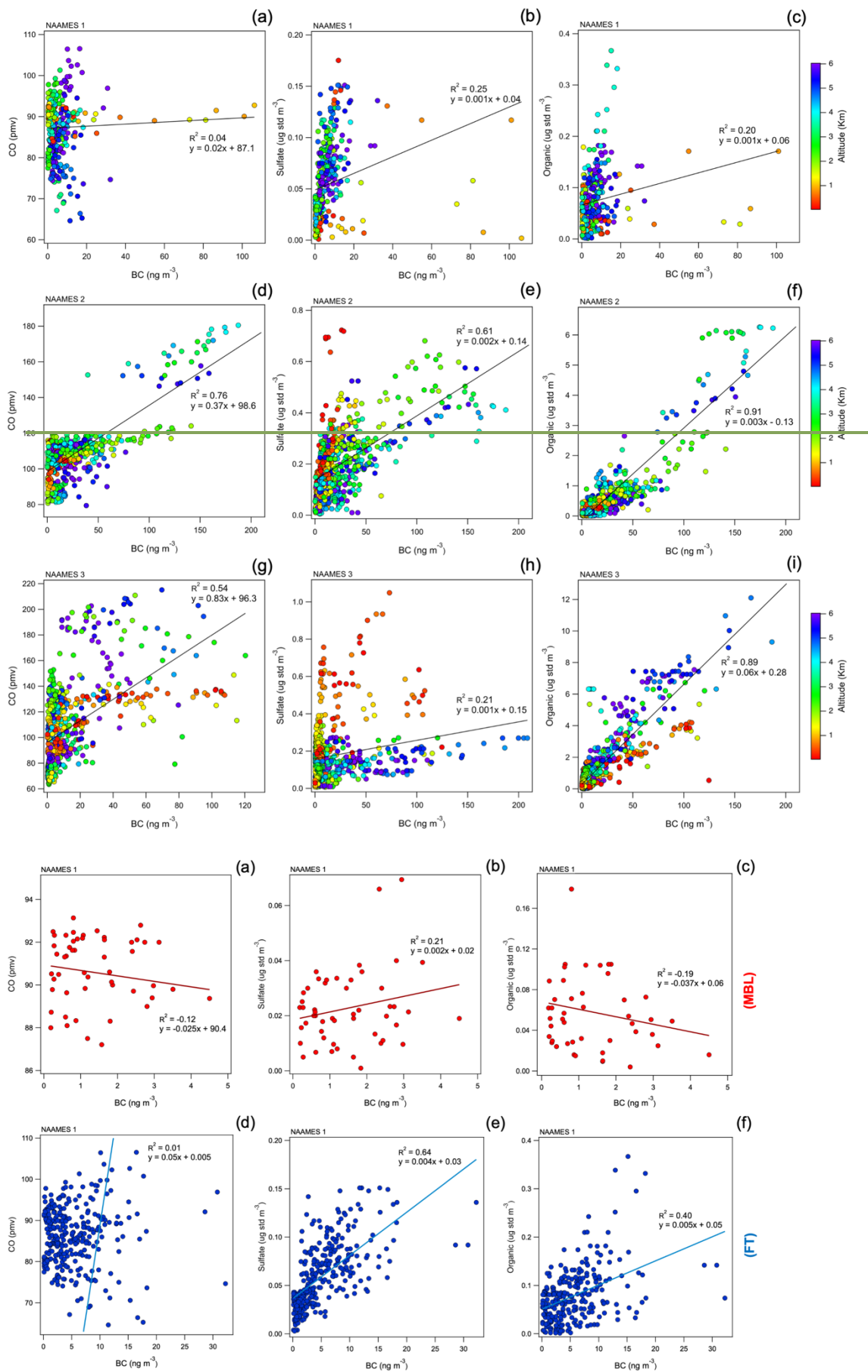
Figure 6̶7. Correlation between BC and CO (a, d,̶ g), BC and sulfate (b, e,̶ h̶), and BC and organics (c, f,̶ i̶) in the MBL (red) and FT (blue) during NAAMES-1.̶,̶ ̶2̶,̶ ̶a̶n̶d̶ ̶3̶
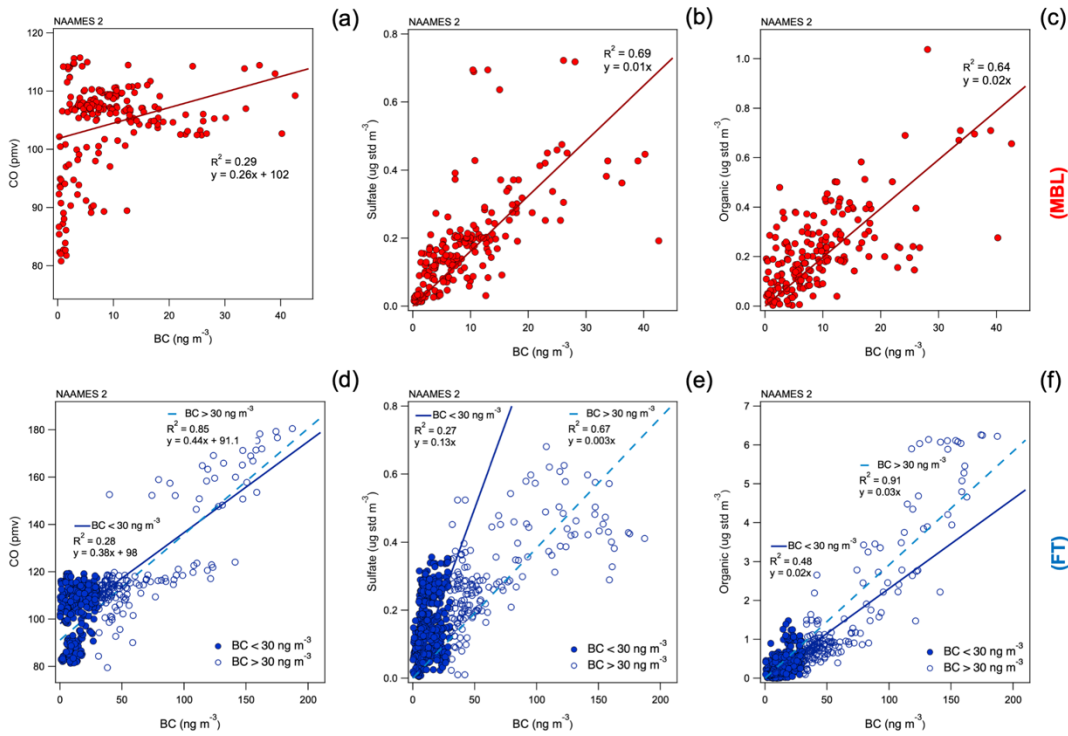
Figure 8. Correlation between BC and CO (a, d), BC and sulfate (b, e), and BC and organics (c, f) in the MBL (red) and FT (blue) during NAAMES-2.
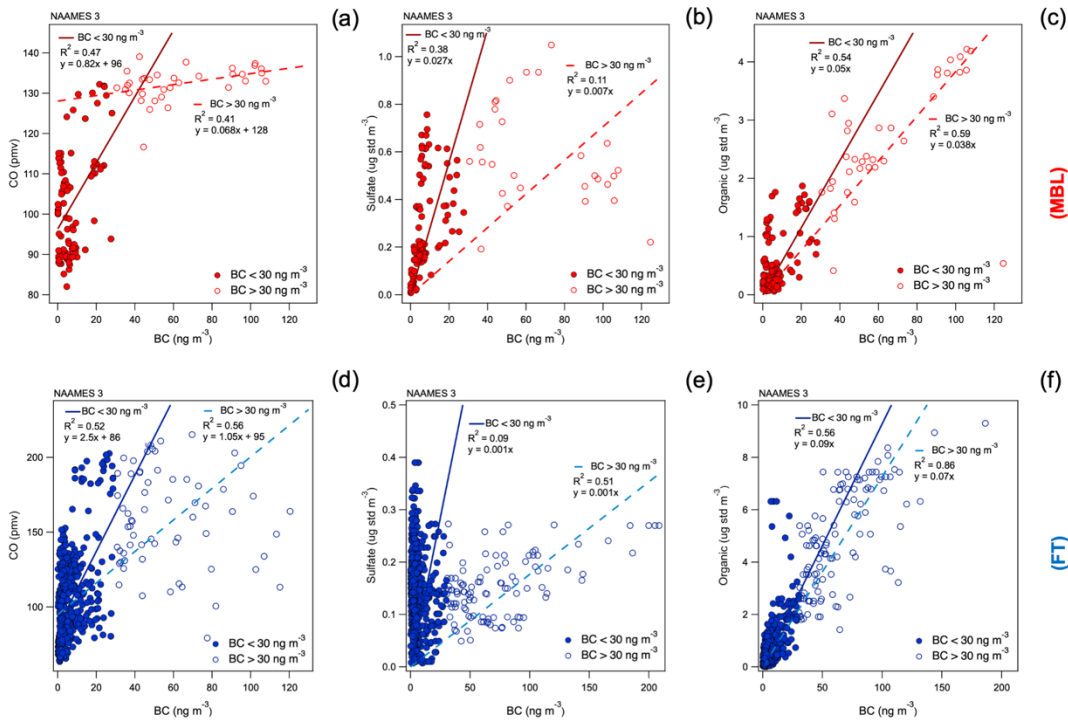
Figure 9. Correlation between BC and CO (a, d), BC and sulfate (b, e), and BC and organics (c, f) in the MBL (red) and FT (blue) during NAAMES-3.
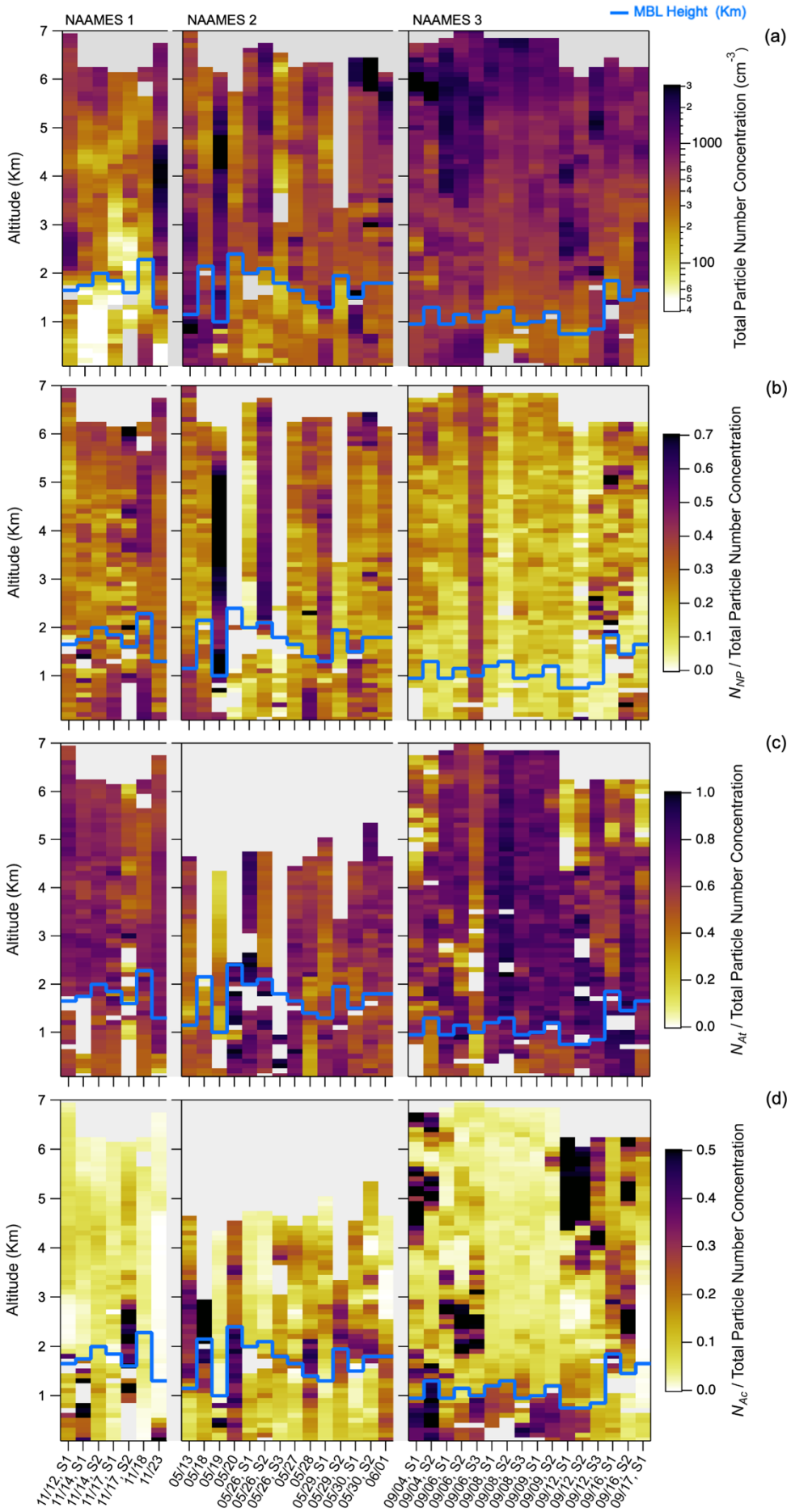
Figure ~~7~~10. Vertical profile of N_{CN} (a), N_{NP}/N_{CN} (b) N_{At}/N_{CN}(c), and N_{Ac}/N_{CN} during NAAMES-1, -2, and -3
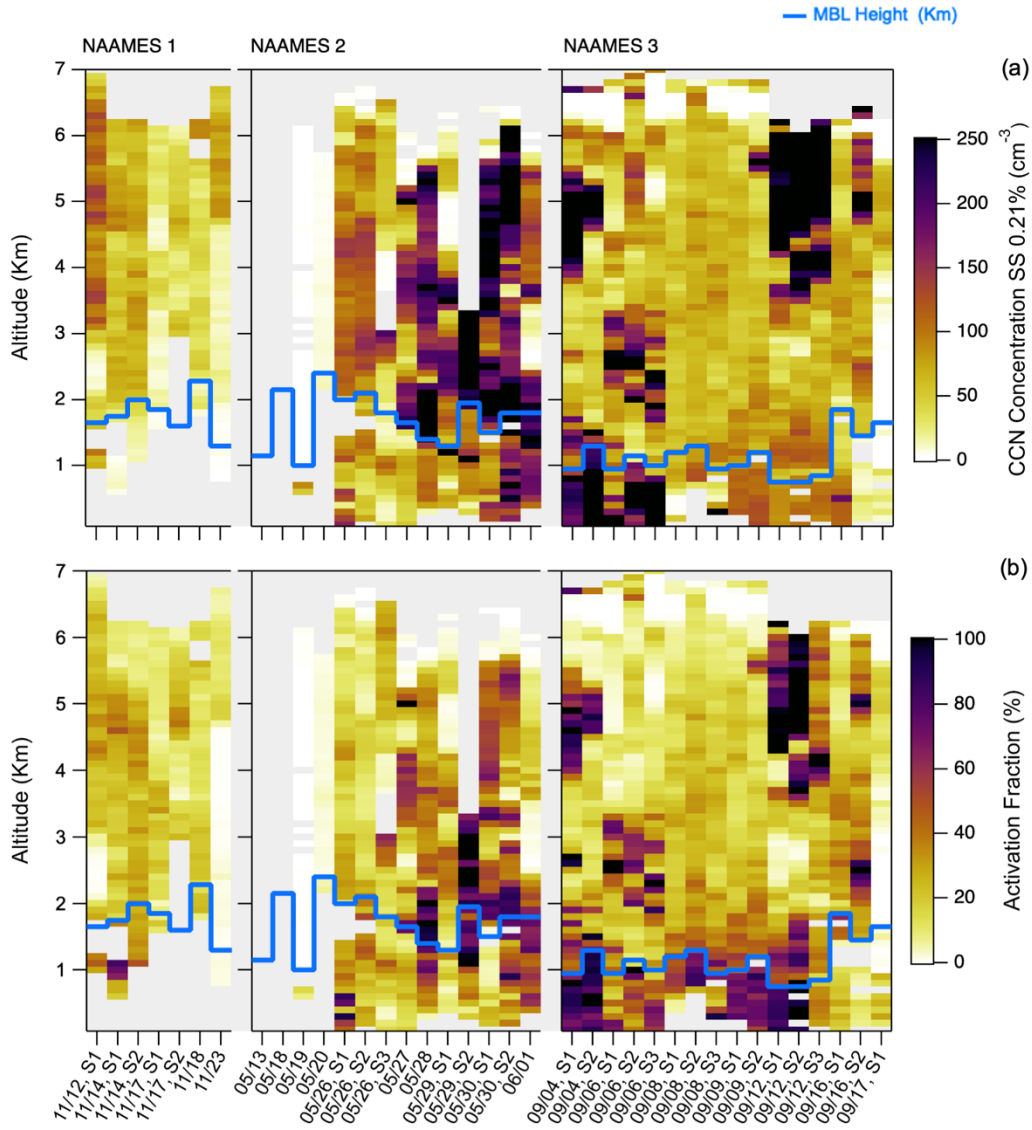
Figure 8̶11. Vertical profile N_{CCN} (a), and CCN activation fraction during NAAMES-1, -2, and -3.

Supplement information of

Measurement report: Aerosol vertical profiles over the Western North Atlantic Ocean during the North Atlantic Aerosols and Marine Ecosystems Study (NAAMES)

5 Francesca Gallo[1,2], Kevin J. Sanchez[1], Bruce E. Anderson[1], Ryan Bennett[3], Matthew D. Brown[1,4], Ewan C. Crosbie[1,4], Chris Hostetler[1], Carolyn Jordan[1,5], Melissa Yang Martin[1], Claire E. Robinson[1,4], Lynn M. Russell[6], Taylor J. Shingler[1], Michael A. Shook[1], Kenneth L. Thornhill[1,4], Elizabeth B. Wiggins[1], Edward L. Winstead[1,4], Armin Wisthaler[7,8], Luke D. Ziemba[1], and Richard H. Moore[1]

10 [1]NASA Langley Research Center, Hampton, VA
[2]NASA Postdoctoral Program, Oak Ridge Associated Universities, Oak Ridge, TN
[3]Bay Area Environmental Research Institute, Moffett Field, CA, USA
[4]Science Systems and Applications, Inc., Hampton, VA
[5]National Institute of Aerospace, Hampton, VA
15 [6]Scripps Institution of Oceanography, San Diego, CA
[7]Institute for Ion Physics and Applied Physics, University of Innsbruck, Technikerstrasse 25, 6020 Innsbruck, Austria
[8]Department of Chemistry, University of Oslo, P.O. 1033 – Blindern, 0315 Oslo, Norway

20 *Correspondence to*: Richard H. Moore (richard.h.moore@nasa.gov), Francesca Gallo (francesca.gallo@nasa.gov)

SI.1. Comparison between marine boundary layer and free troposphere aerosol properties for NAAMES-1, 2, and 3

Figures below show MBL (green bars) and FT (blue bars) mean values of aerosol properties for each C-130 spirals during NAAMES-1, -2, and -3. The red circles denote the ratio between MBL and FT mean values for each parameter considered.

5   **Figures SI.1.a.** Mean values of CO in the MBL and FT, and MBL/FT ratio
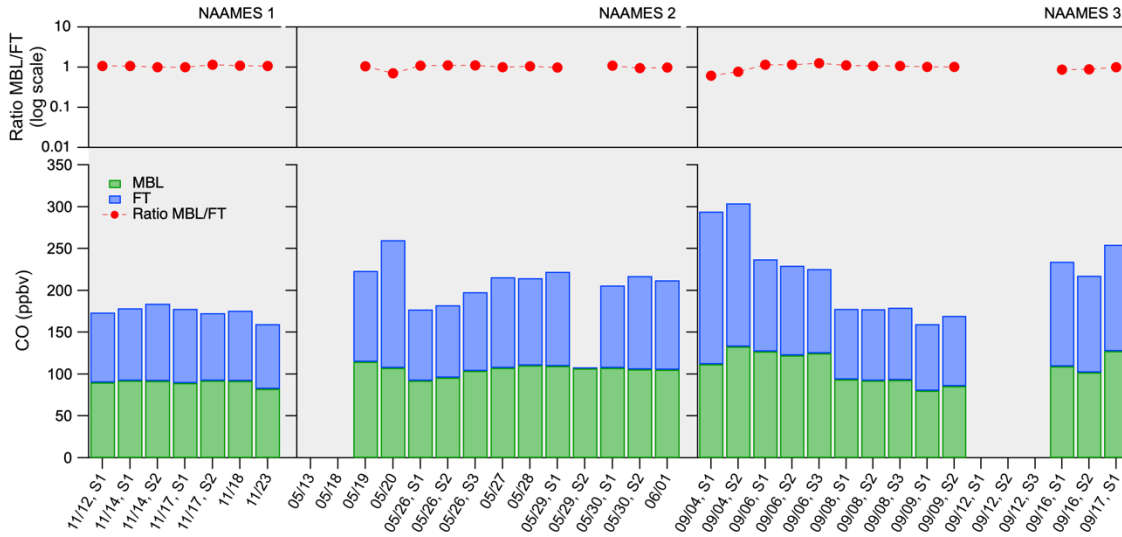
Figures SI.1.b. Mean values of organic in the MBL and FT, and MBL/FT ratio
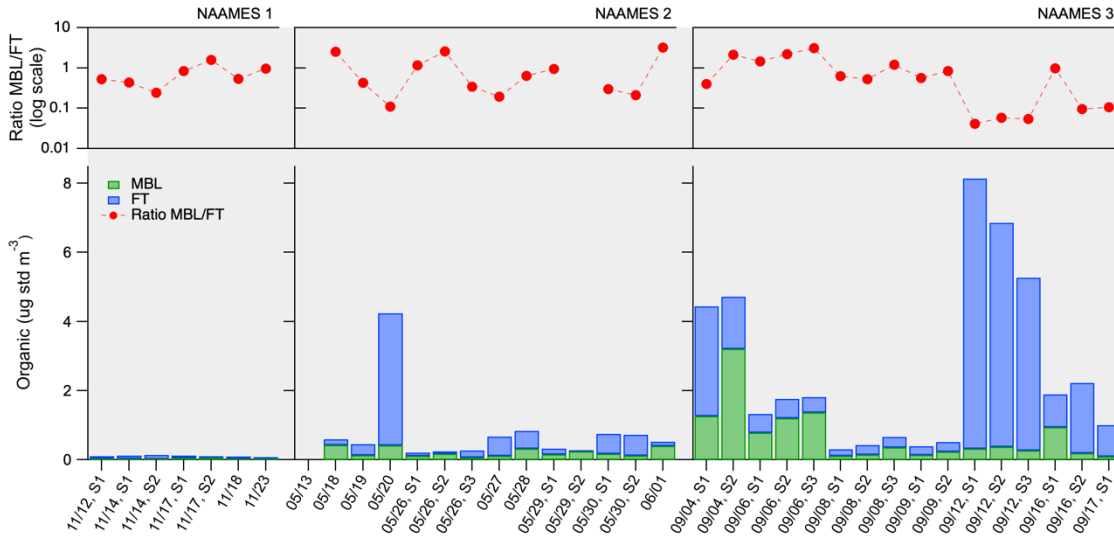
Figures SI.1.c. Mean values of total particle concentration in the MBL and FT, and MBL/FT ratio
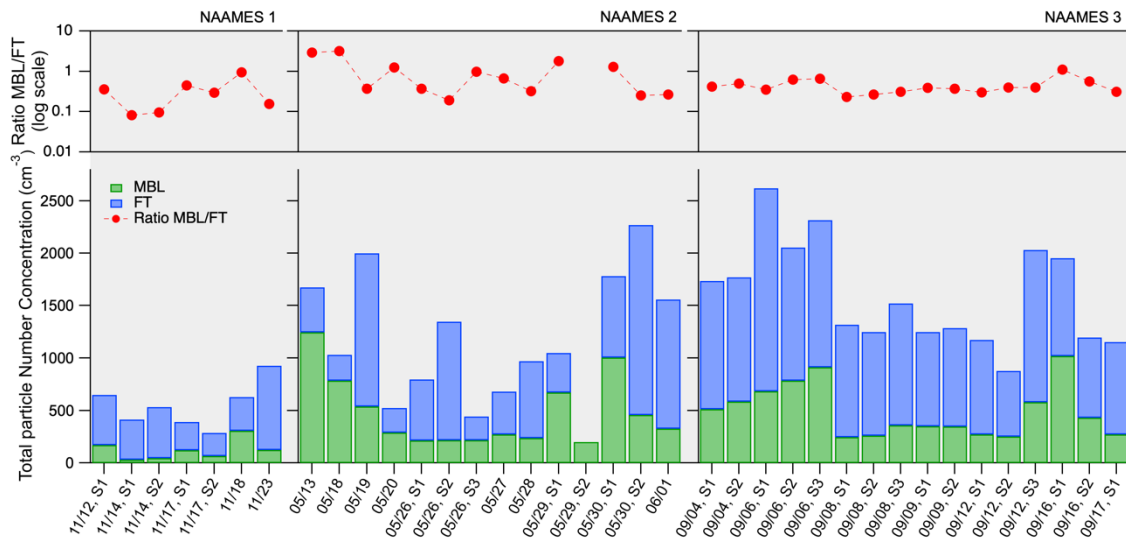
Figures SI.1.d. Mean values of cloud condensation nuclei in the MBL and FT, and MBL/FT ratio
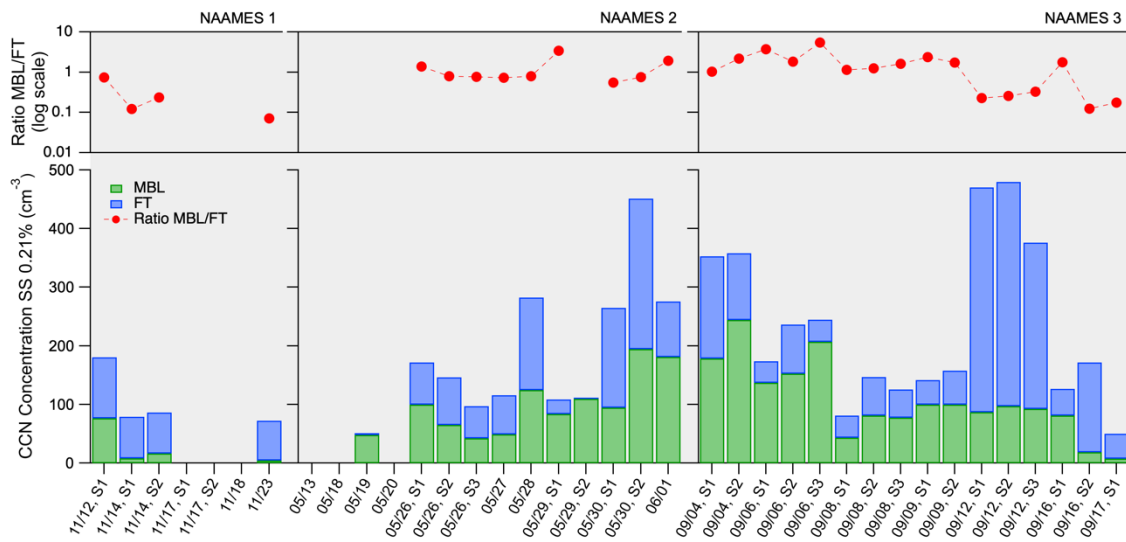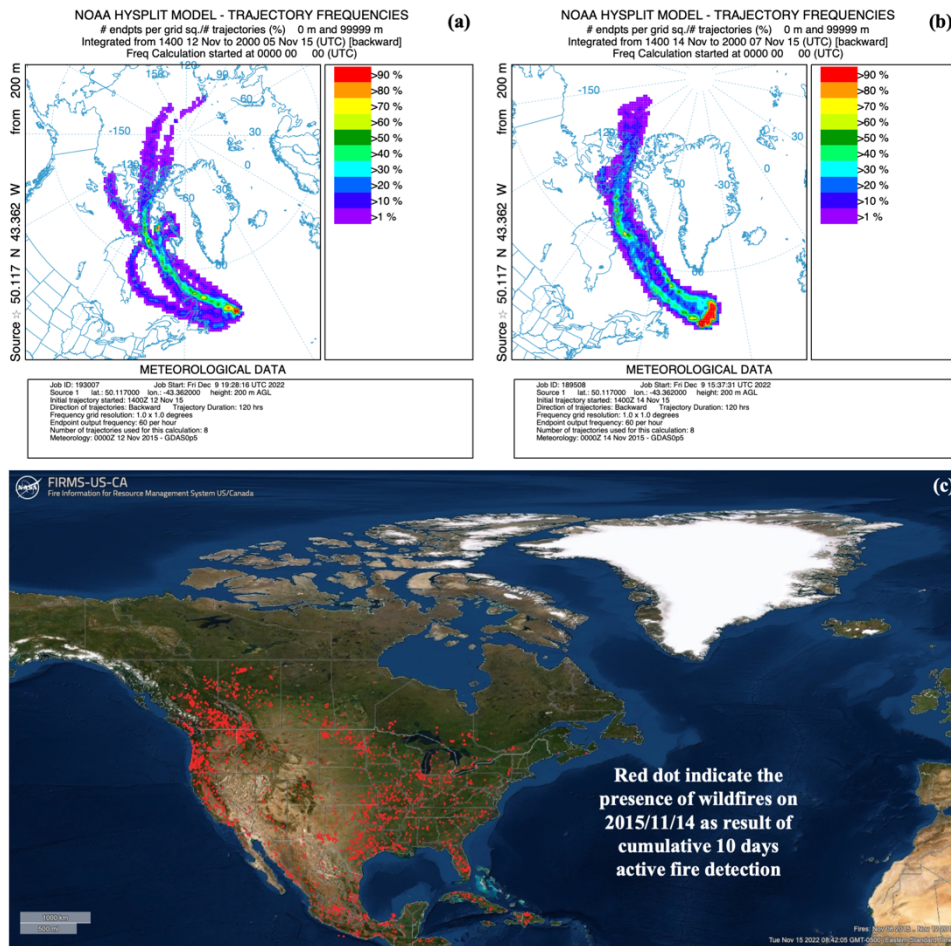
SI.~~2~~3. Vertical profiles of meteorological parameters and aerosol properties for NAAMES-1, 2, and 3

Figures below show vertical profiles for each C-130 spirals, the circle and square markers represent respectively 100-meters altitude mean and geometric mean values. The first panel on the left (a) shows the thermodynamic profiles of potential temperature (red), relative humidity (green), and H_2O mixing ratio (blue), and vertical profiles of cloud droplet number concentration (light blue). Blue, red, and black traces and markers in Panel (b) denote respectively CO mixing ratio, DMS mixing ratio and refractory black carbon particle (BC) mass. Panel (c) shows the vertical profiles of the mass concentrations of non-refractory organic (green), sulfate (red), nitrate (blue), and ammonium (yellow). Number concentrations of submicron particle (black) and cloud condensation nuclei (blue) are shown in Panel (d). The rightmost panel (e) shows the number concentration of particles in the NP (blue), At (red), and Ac (black) modes Aerosol measurements collected at the ocean surface aboard the *R/V Atlantis* are shown in the grey box.

Figures SI.~~2~~3.a. Vertical profiles of meteorological parameters and aerosol properties for NAAMES-1 spirals

1) 12 Nov. 2015 - Spiral 1, 13:00 - 13:21 UTC, C-130 Lat. 50.12 Long. -43.36, *R/V Atlantis* Lat. 51.04 Long. -43.62
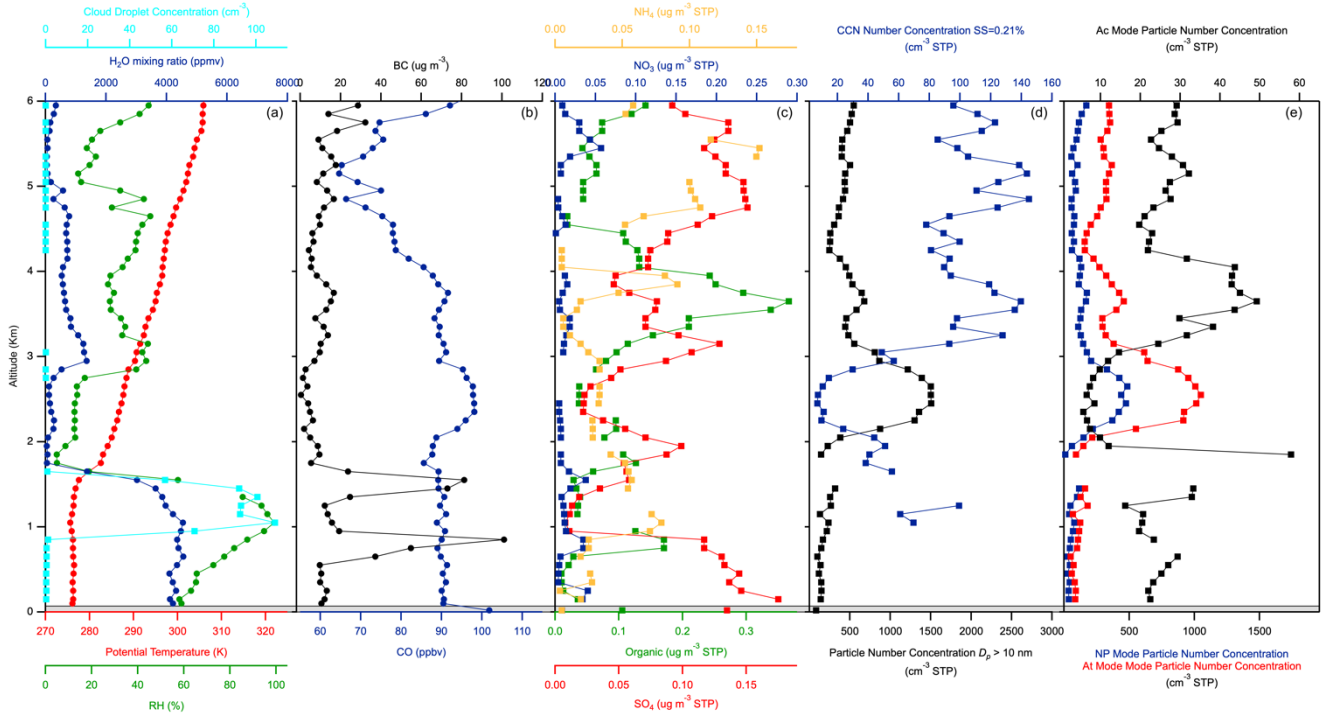
2) 14 Nov. 2015 - Spiral 1, 13:24 - 13:41 UTC, C-130 Lat. 54.04 Long. -38.35, *R/V Atlantis* Lat. 54.11 Long. -40.18
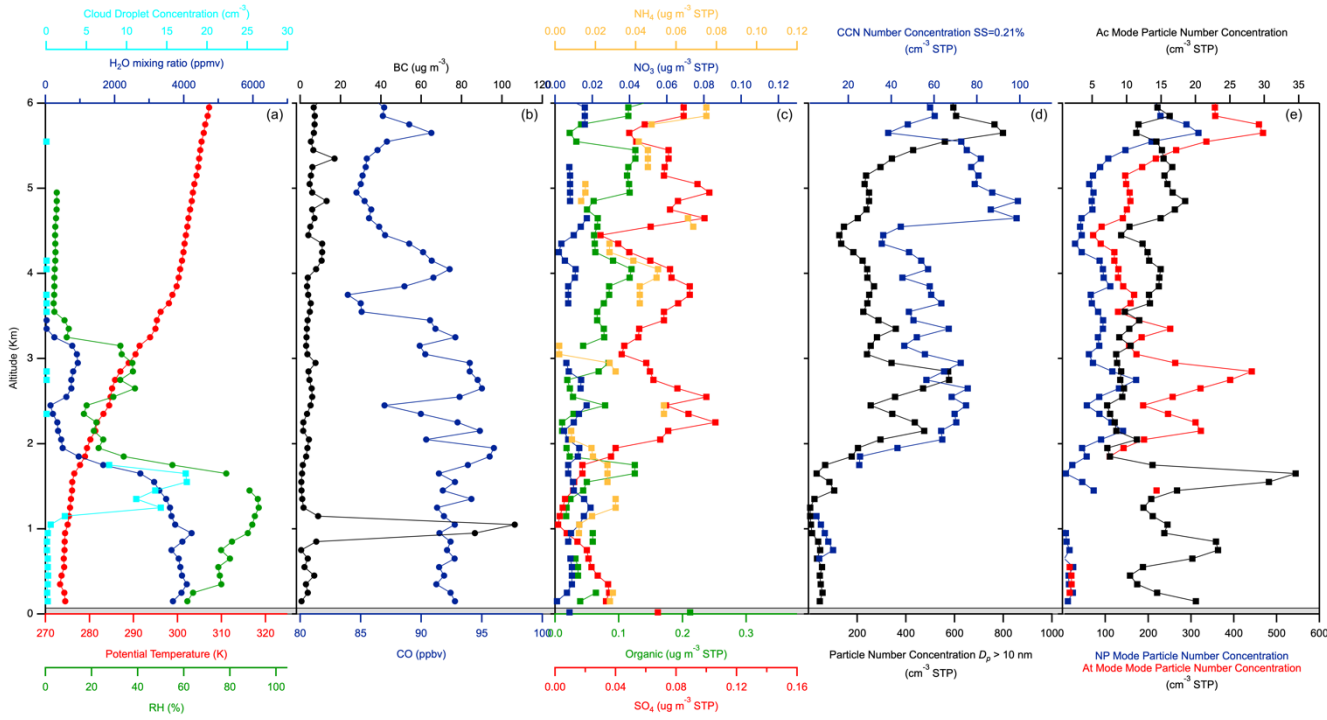
3) 14 Nov. 2015 - Spiral 2, 15:01 - 15:23 UTC, C-130 Lat. 54.16 Long. -41.51, *R/V Atlantis* Lat. 54.11 Long. -40.18
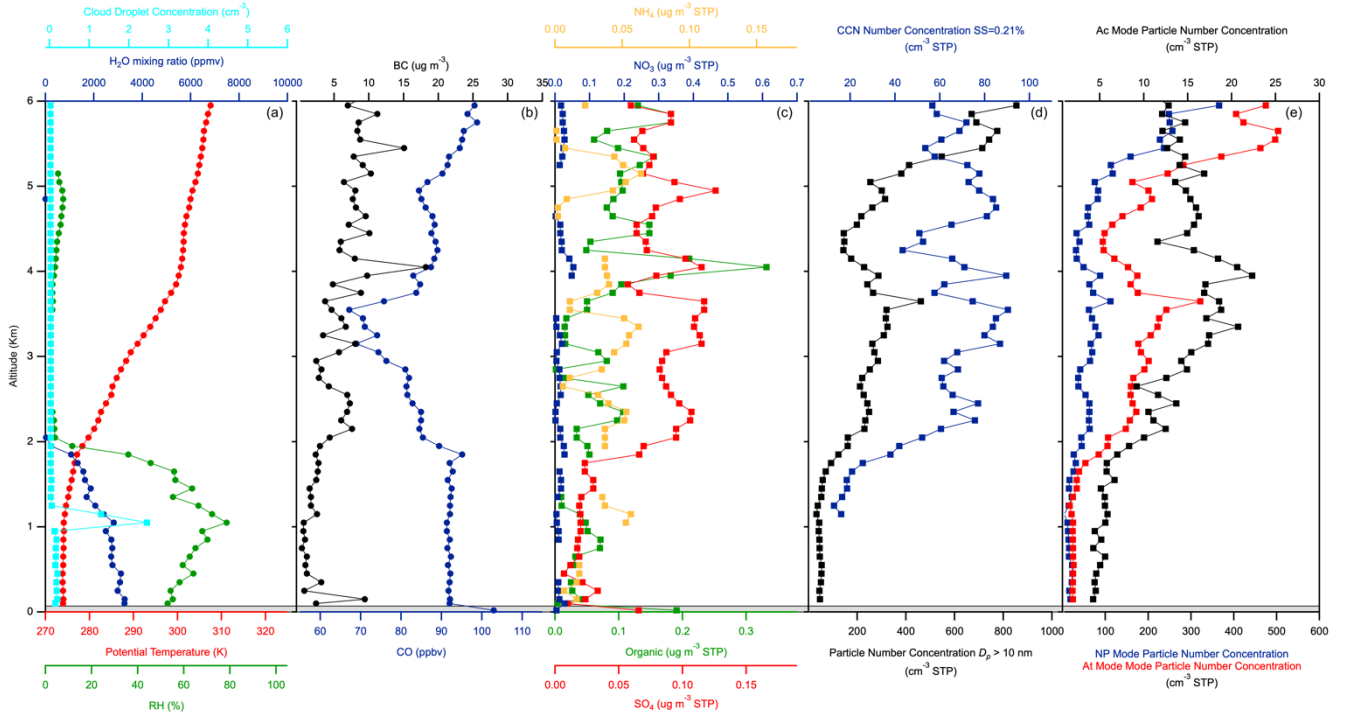
4) 17 Nov. 2015 - Spiral 1, 14:40 - 14:59 UTC, C-130 Lat. 50.75 Long. -39.65, *R/V Atlantis* Lat. 48.06 Long. -38.72
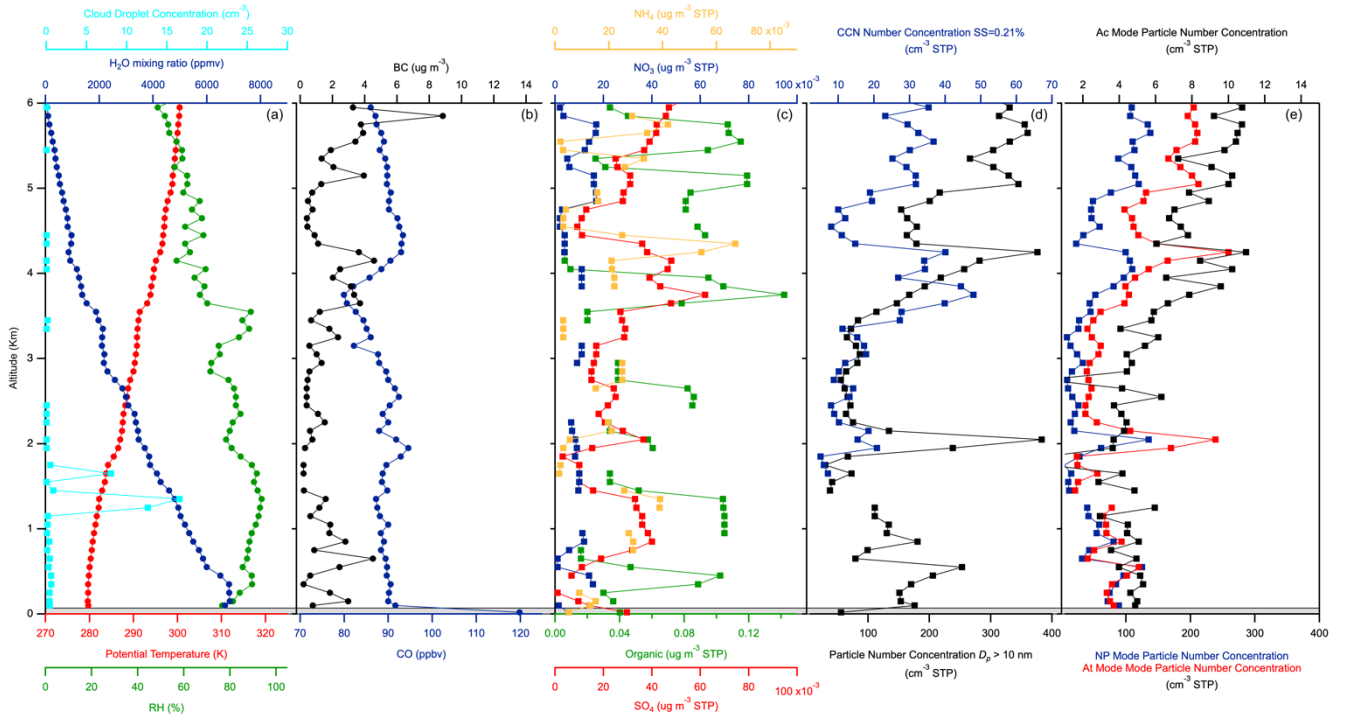
5) 17 Nov. 2015 - Spiral 2, 16:07 - 16:22 UTC, C-130 Lat. 49.80 Long. -39.72, *R/V Atlantis* Lat. 47.93 Long. -38.67
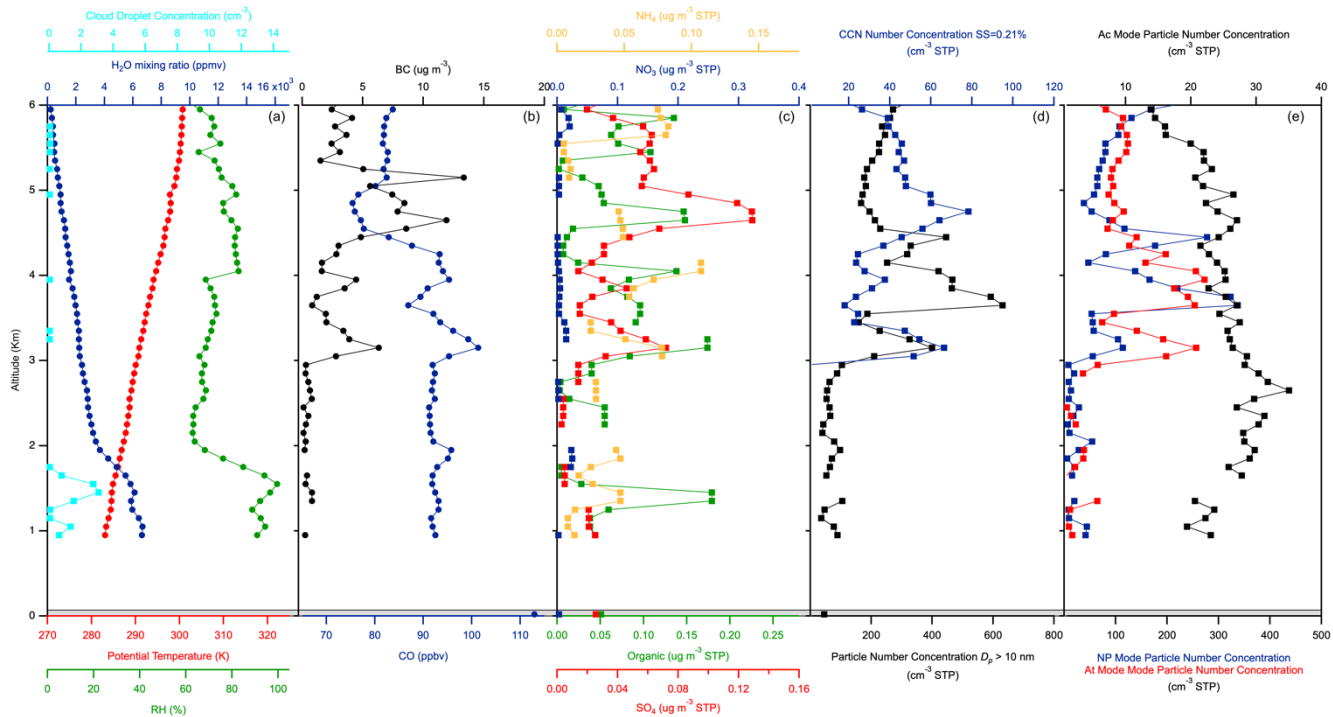
6) 18 Nov. 2015 - Spiral 1, 14:45 - 15:02 UTC, C-130 Lat. 46.46 Long. -36.69, *R/V Atlantis* Lat. 46.20 Long. -37.87
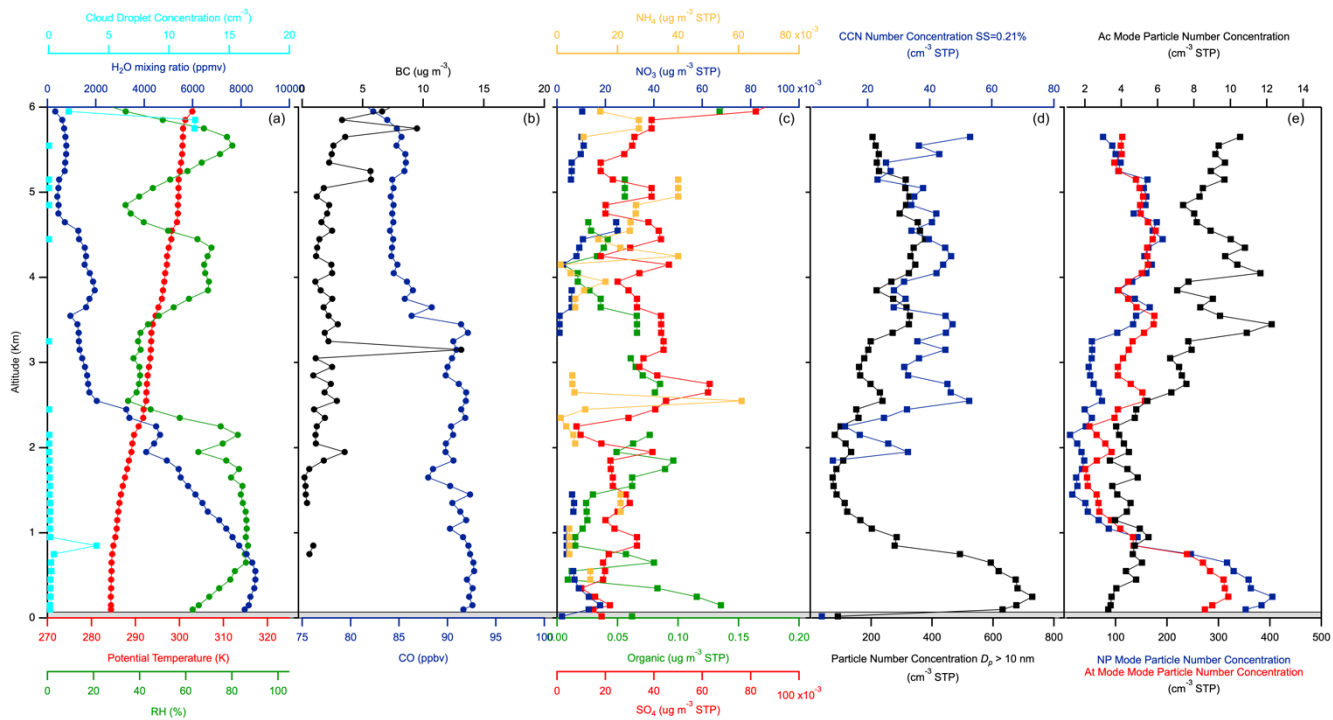
7) 23 Nov. 2015 - Spiral 1, 12:25 - 12:46 UTC, C-130 Lat. 42.50 Long. -39.80, *R/V Atlantis* Lat. 42.98 Long. -40.20
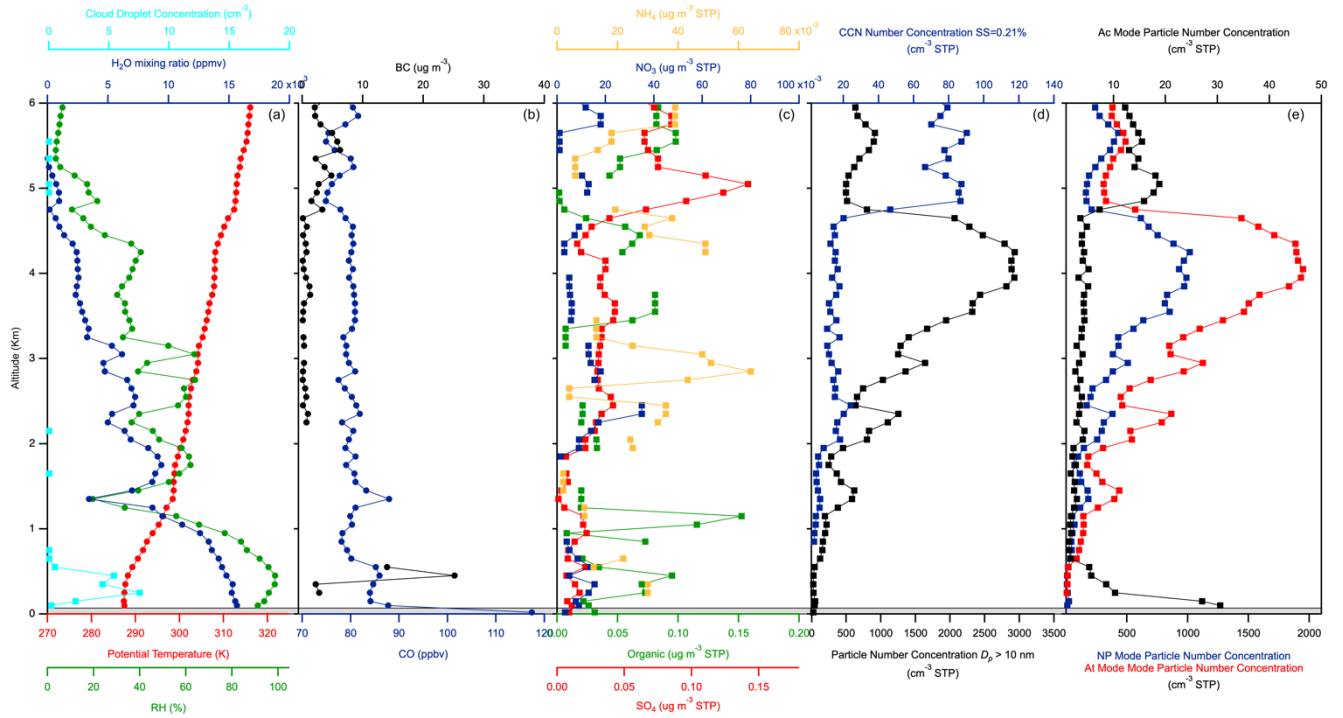
Figures SI.~~2~~3.b. Vertical profiles of meteorological parameters and aerosol properties for NAAMES-2 spirals

8) 13 May 2016 - Spiral 1, 21:09 - 21:30 UTC, C-130 Lat. 43.91 Long. -59.98, *R/V Atlantis* Lat. 42.72 Long. -61.57
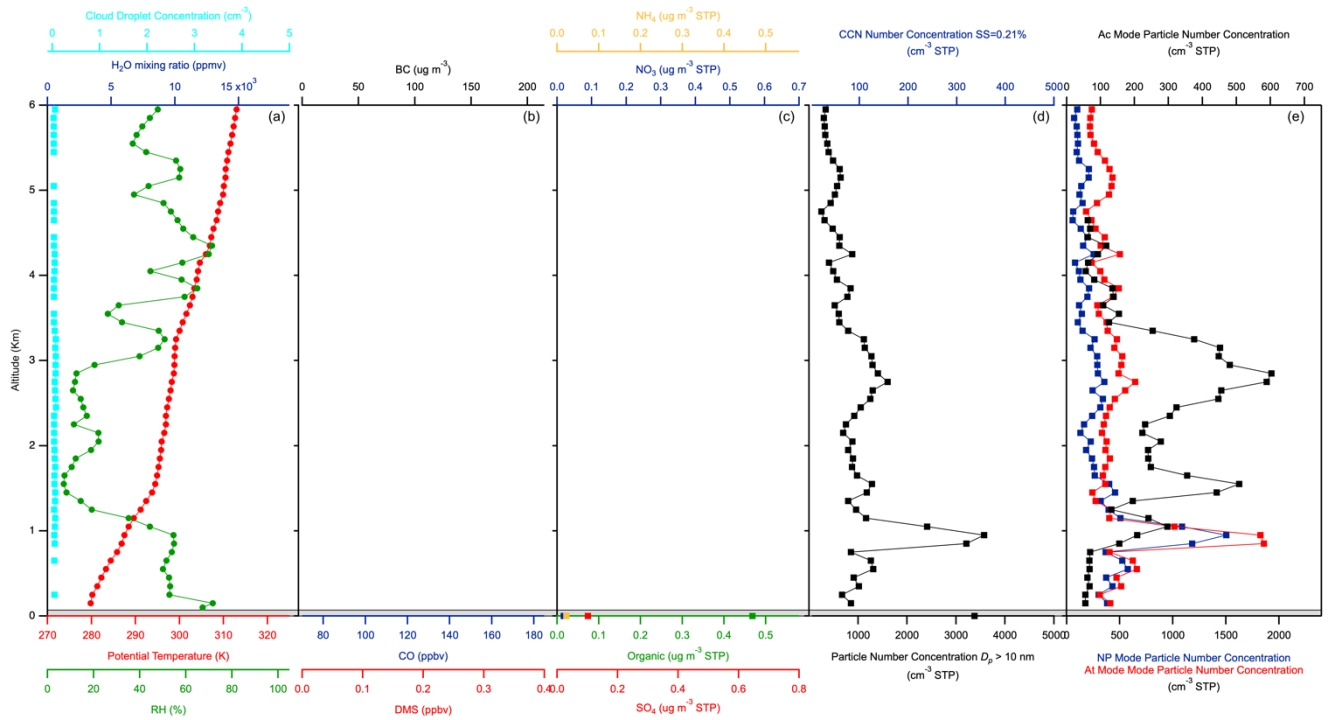
9) 18 May 2016 - Spiral 1, 11:19 - 11:40 UTC, C-130 Lat. 56.63 Long. -44.48, *R/V Atlantis* Lat. 56.33 Long. -46.06
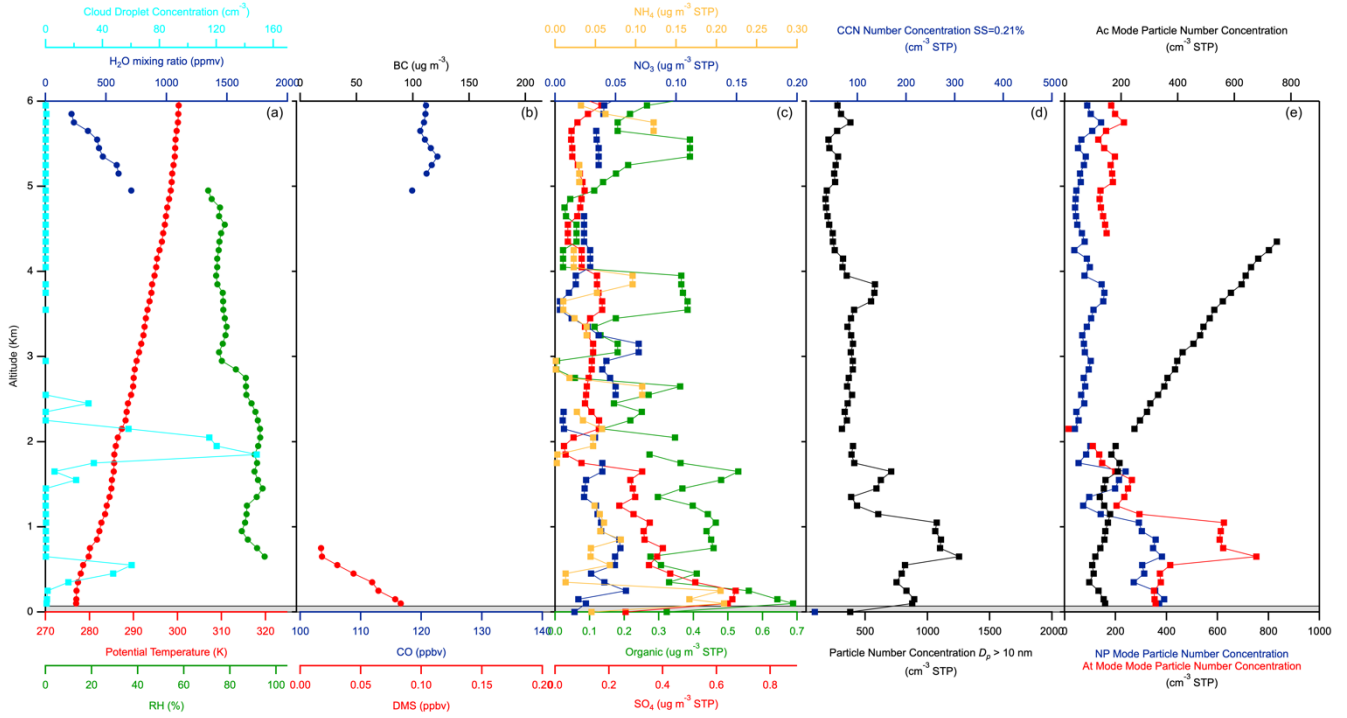
10) 19 May 2016 - Spiral 1, 13:54 - 14:15 UTC, C-130 Lat. 53.53 Long. -42.95, *R/V Atlantis* Lat. 56.33 Long. -46.05
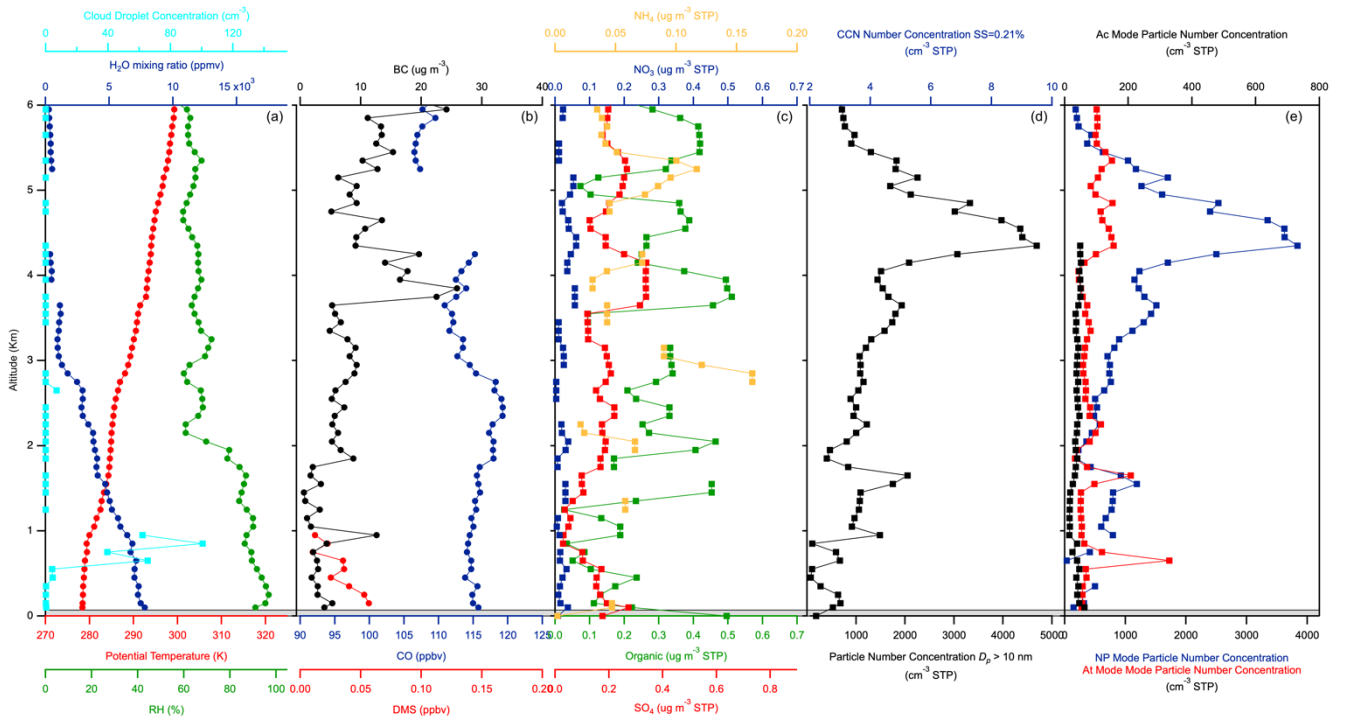
11) 20 May 2016 - Spiral 1, 14:58 - 15:15 UTC, C-130 Lat. 53.55 Long. -42.25, *R/V Atlantis* Lat. 53.53 Long. -42.24
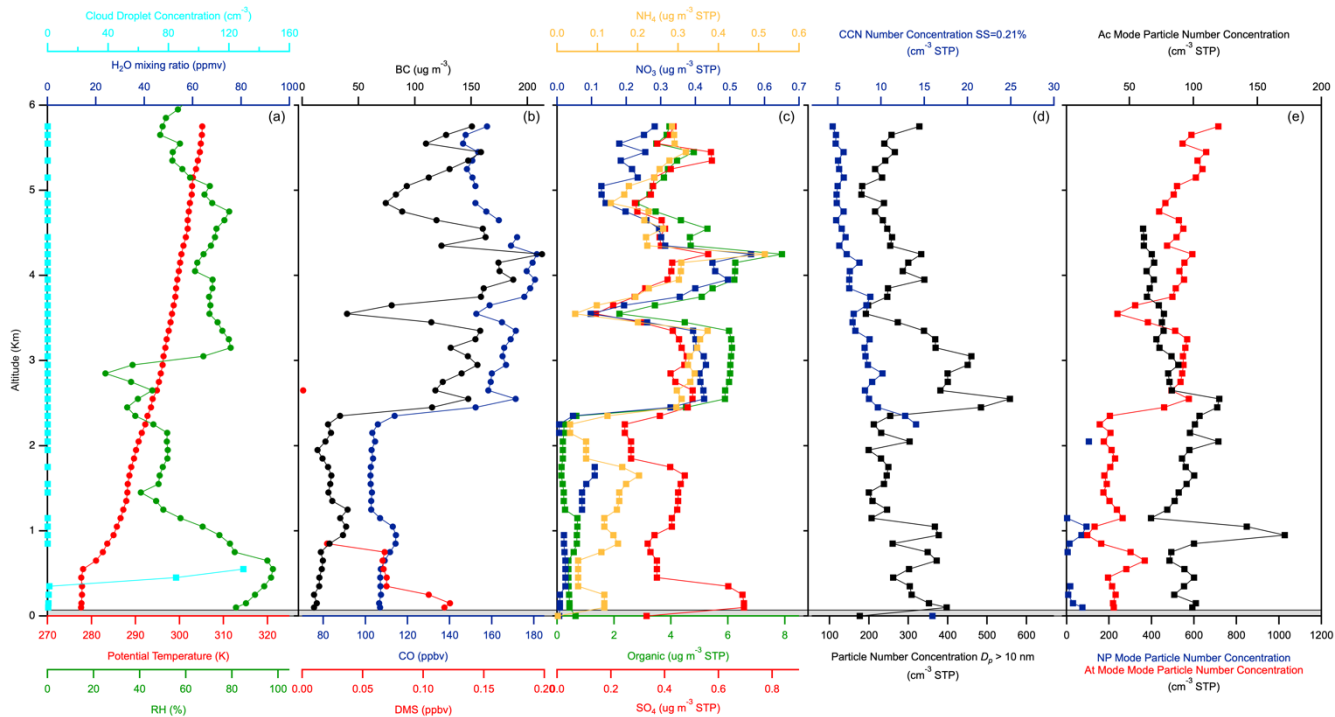
12) 26 May 2016 - Spiral 1, 14:17 - 14:41 UTC, C-130 Lat. 48.20 Long. -38.59, *R/V Atlantis* Lat. 47.39 Long. -38.64
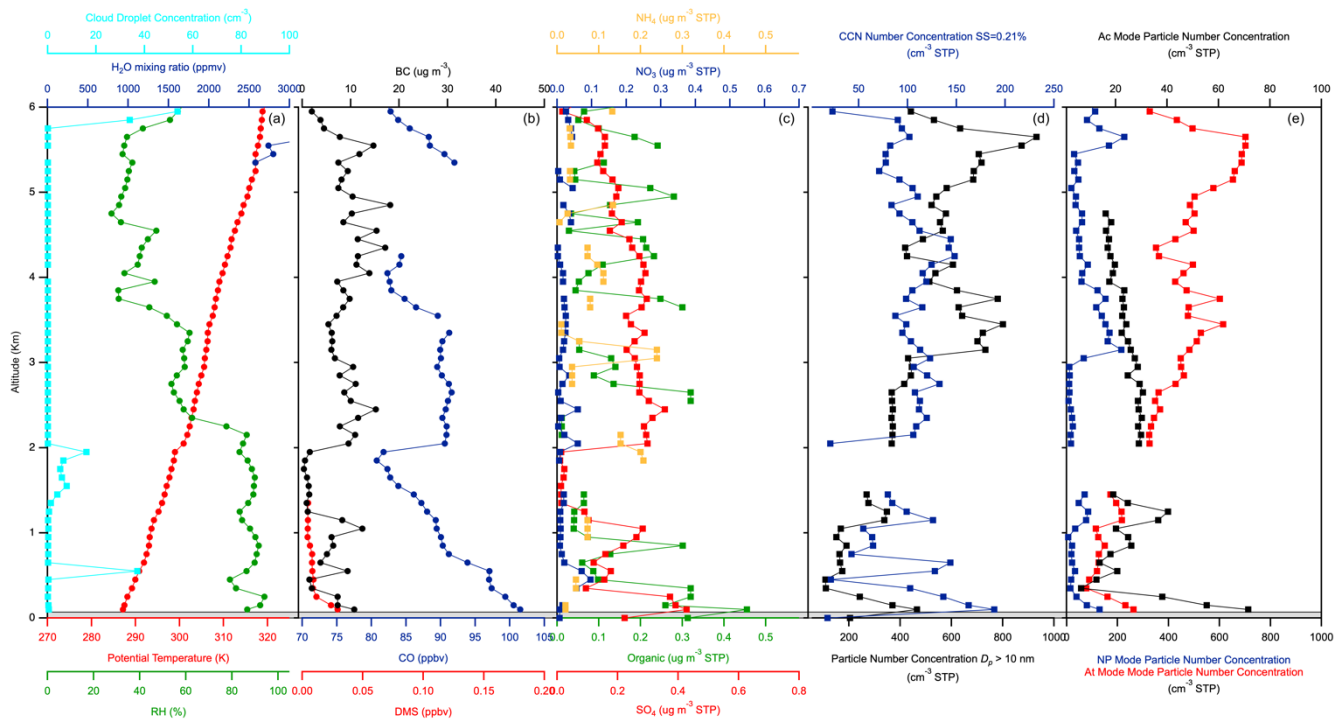
13) 26 May 2016 - Spiral 2, 15:44 - 16:08 UTC, C-130 Lat. 46.58 Long. -38.77, *R/V Atlantis* Lat. 47.38 Long. -38.60
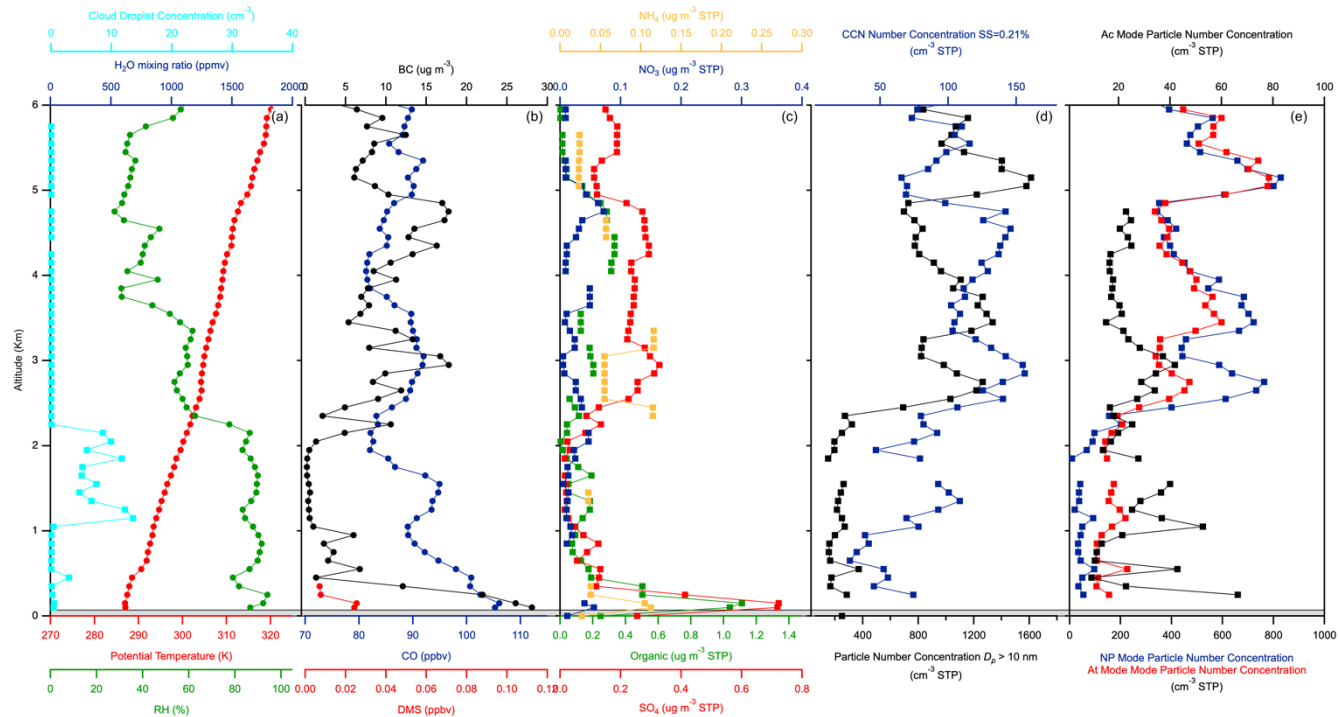
14) 26 May 2016 - Spiral 3, 18:24 - 18:39 UTC, C-130 Lat. 49.17 Long. -45.32, *R/V Atlantis* Lat. 47.33 Long. -38.53
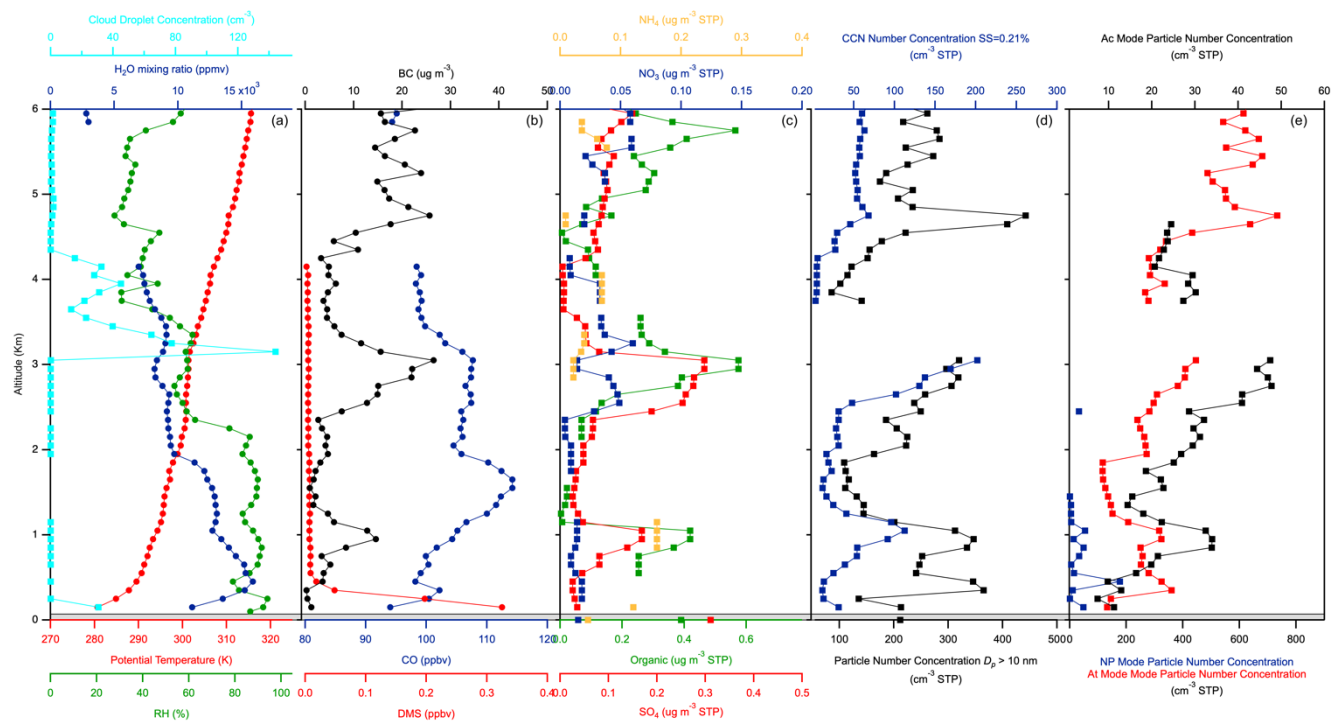
none
15) 27 May 2016 - Spiral 1, 13:00 - 13:21 UTC, C-130 Lat. 56.68 Long. -45.65, _R/V Atlantis_ Lat. 47.22 Long.   -38.21
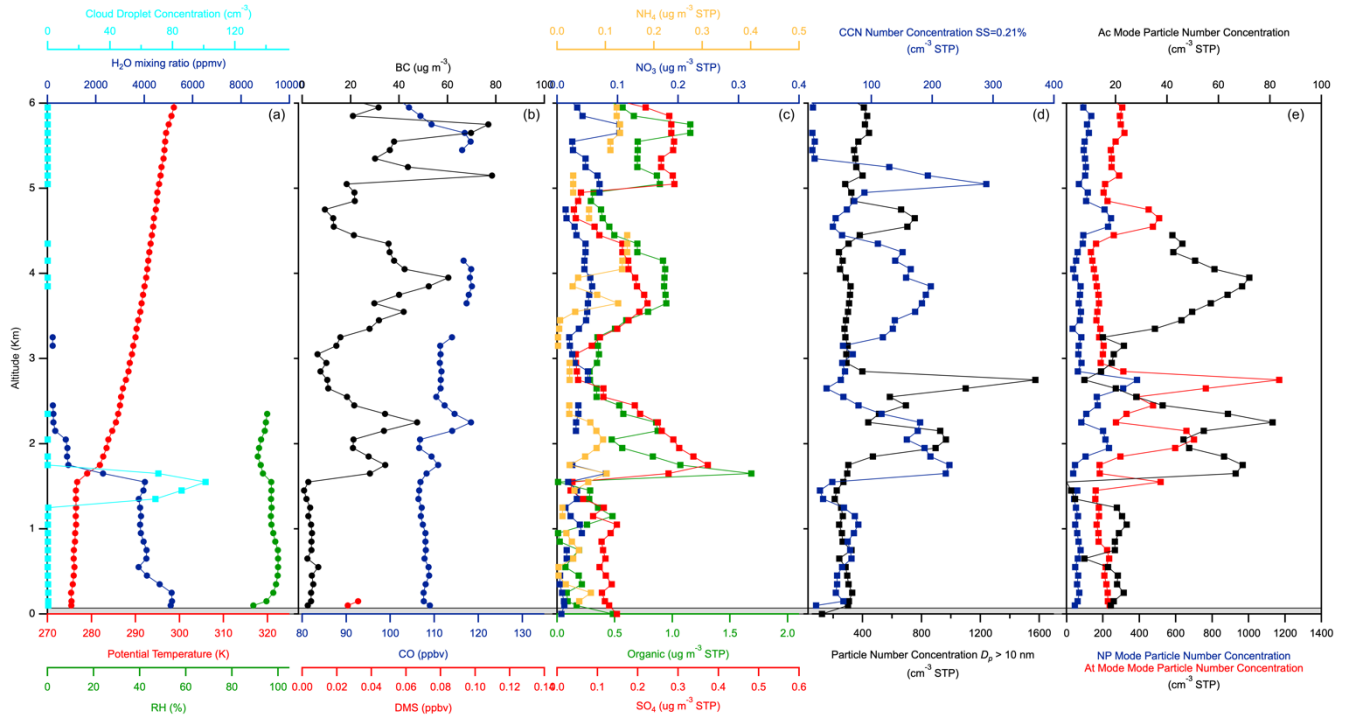
16) 28 May 2016 - Spiral 1, 13:24 - 13:41 UTC, C-130 Lat. 50.00 Long. -44.49, _R/V Atlantis_ Lat. 45.37 Long. -41.53
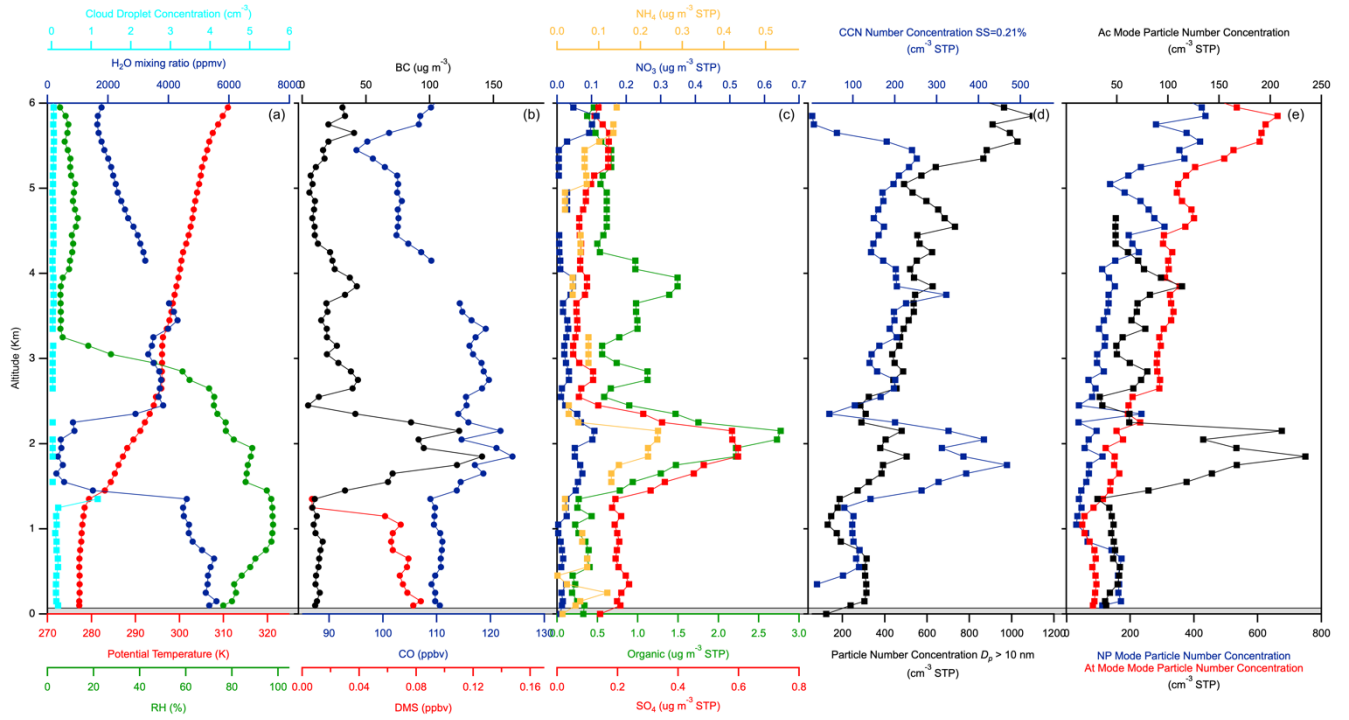
17) 29 May 2016 - Spiral 1, 12:28 - 12:52 UTC, C-130 Lat. 50.03 Long. -44.49, *R/V Atlantis* Lat. 44.19 Long. -43.58
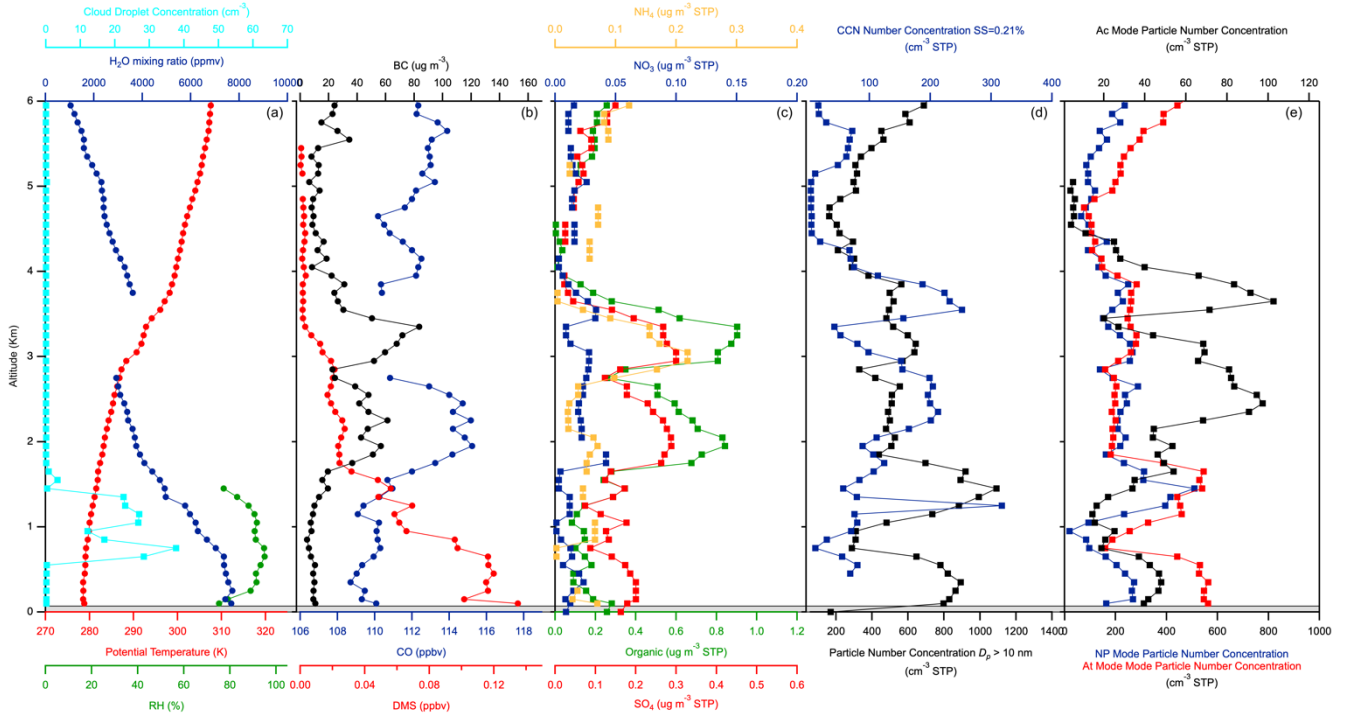
18) 29 May 2016 - Spiral 2, 13:44 - 13:56 UTC, C-130 Lat. 53.12 Long. -40.71, *R/V Atlantis* Lat. 44.20 Long. -43.53
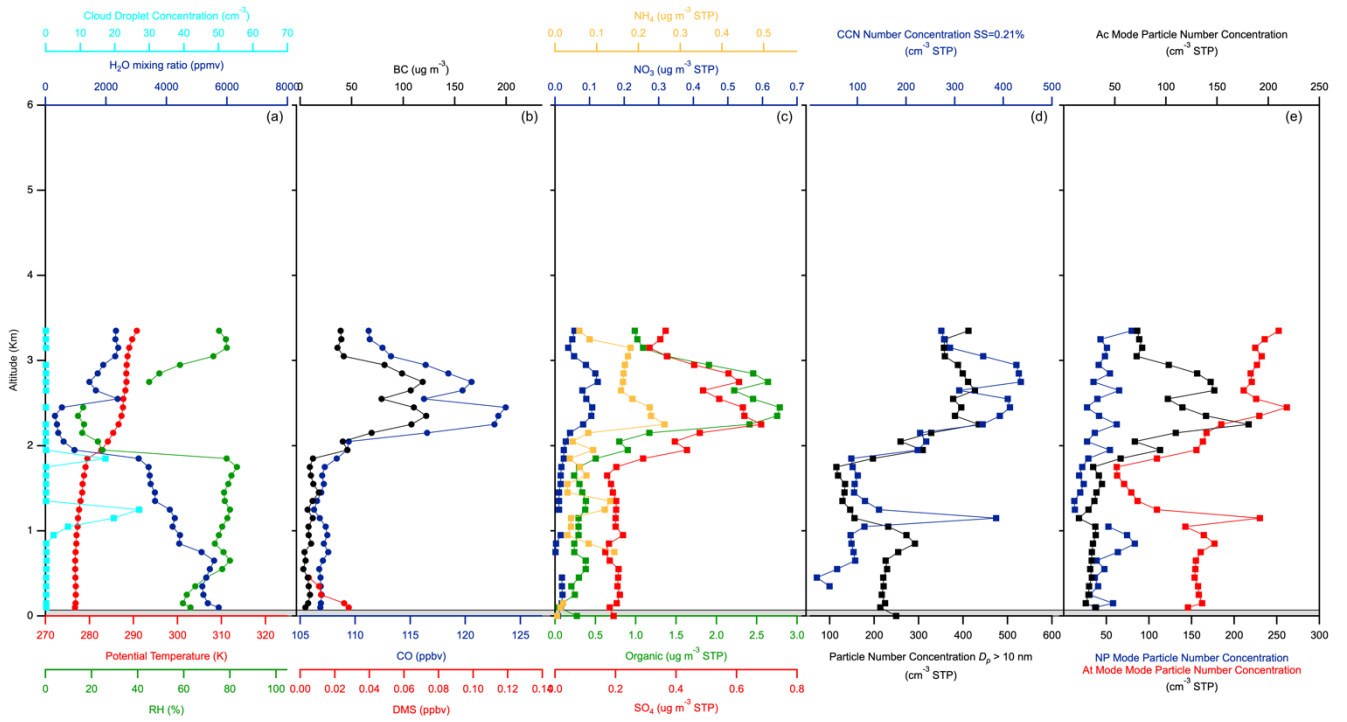
19) 30 May 2016 - Spiral 1, 14:46 - 15:07 UTC, C-130 Lat. 43.54 Long. -44.68, *R/V Atlantis* Lat. 44.62 Long. -43.11
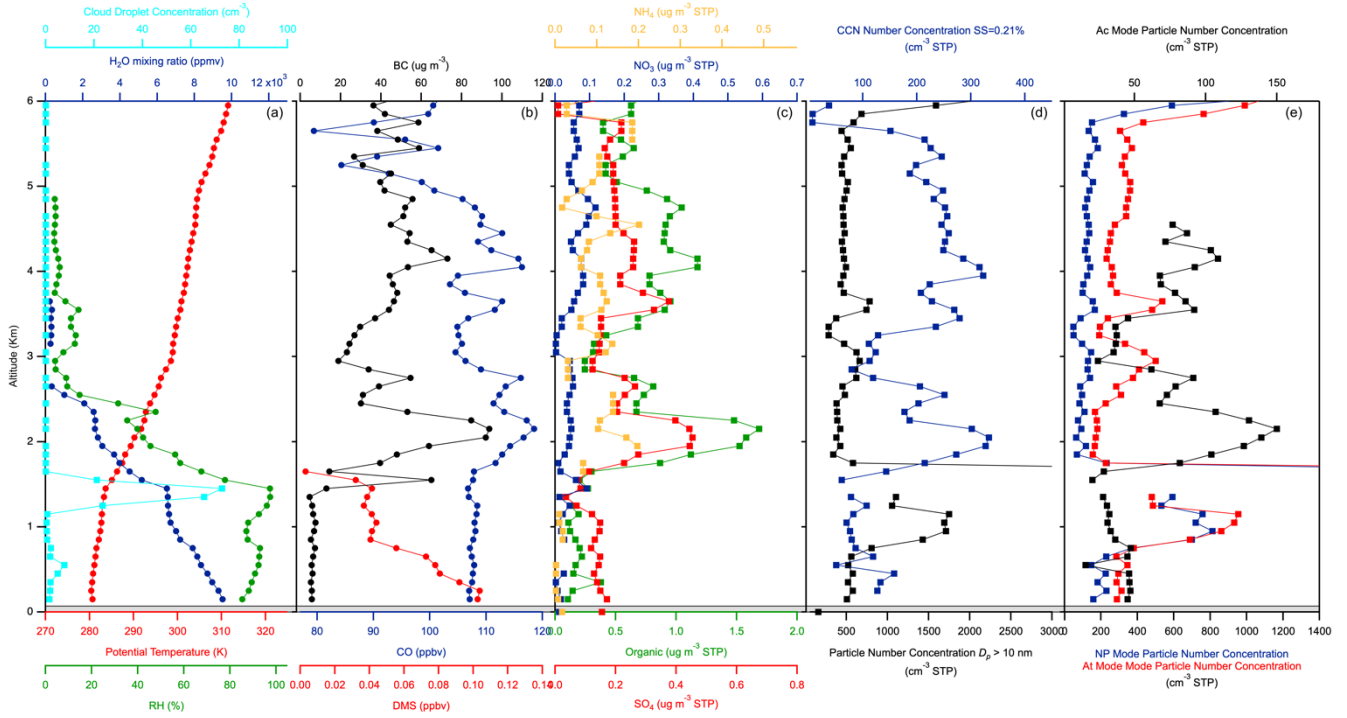
20) 30 May 2016 - Spiral 2, 17:39 - 17:58 UTC, C-130 Lat. 44.67 Long. -43.08, *R/V Atlantis* Lat. 44.70 Long. -43.03
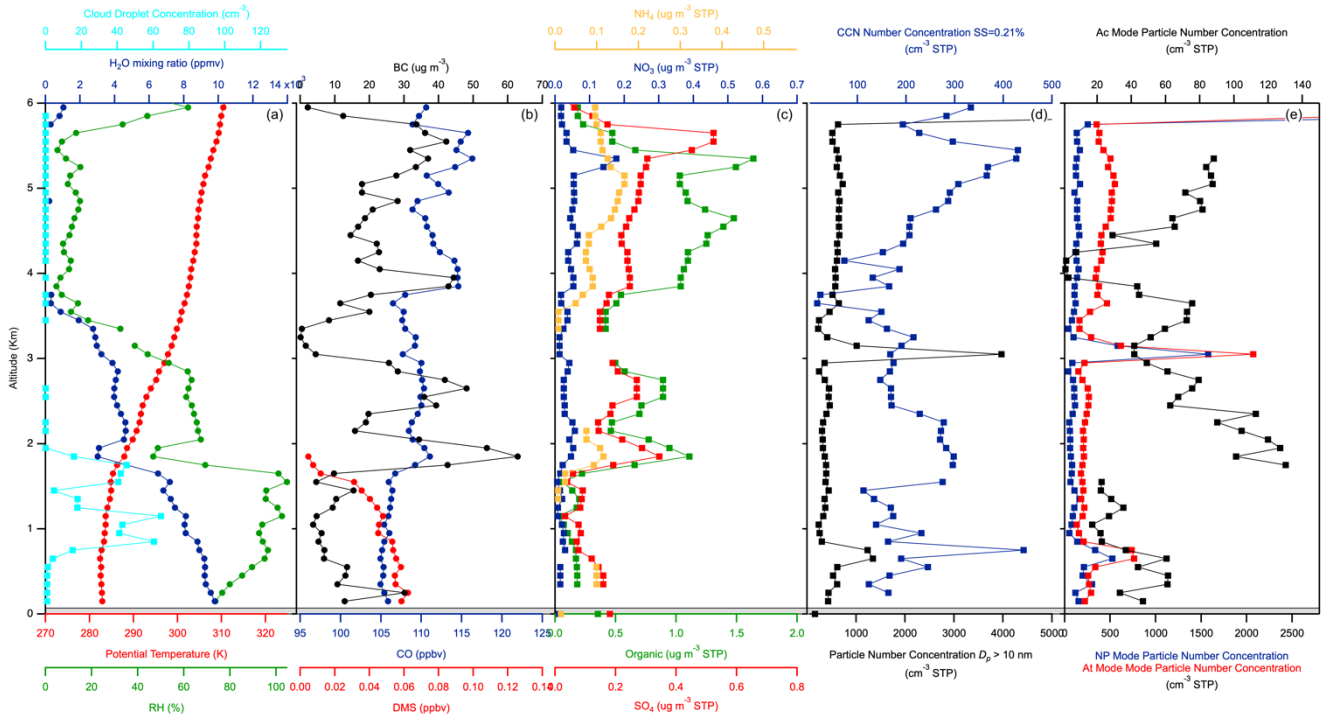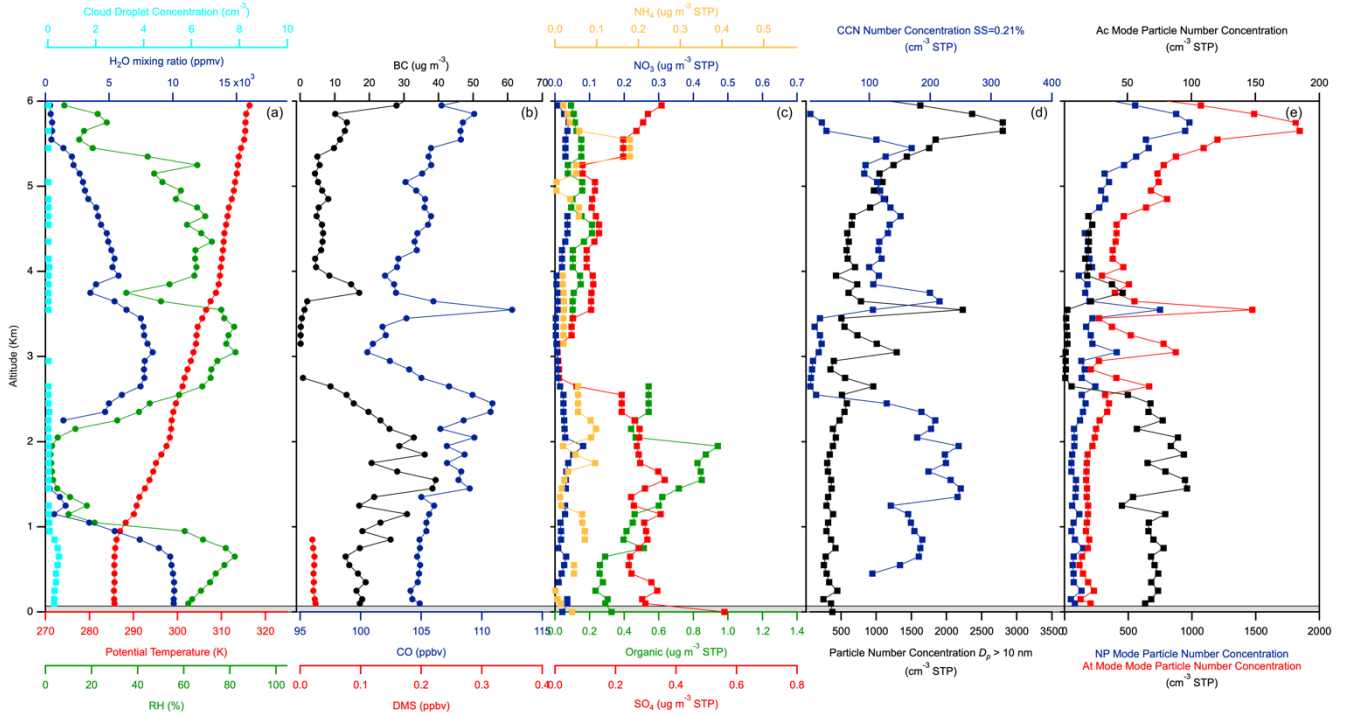
Figures SI.~~2~~3.c. Vertical profiles of meteorological parameters and aerosol properties for NAAMES-3 spirals

22) 4 Sept. 2017 - Spiral 1, 13:36 - 13:56 UTC, C-130 Lat. 43.06 Long. -43.74, *R/V Atlantis* Lat. 42.39 Long. -42.97
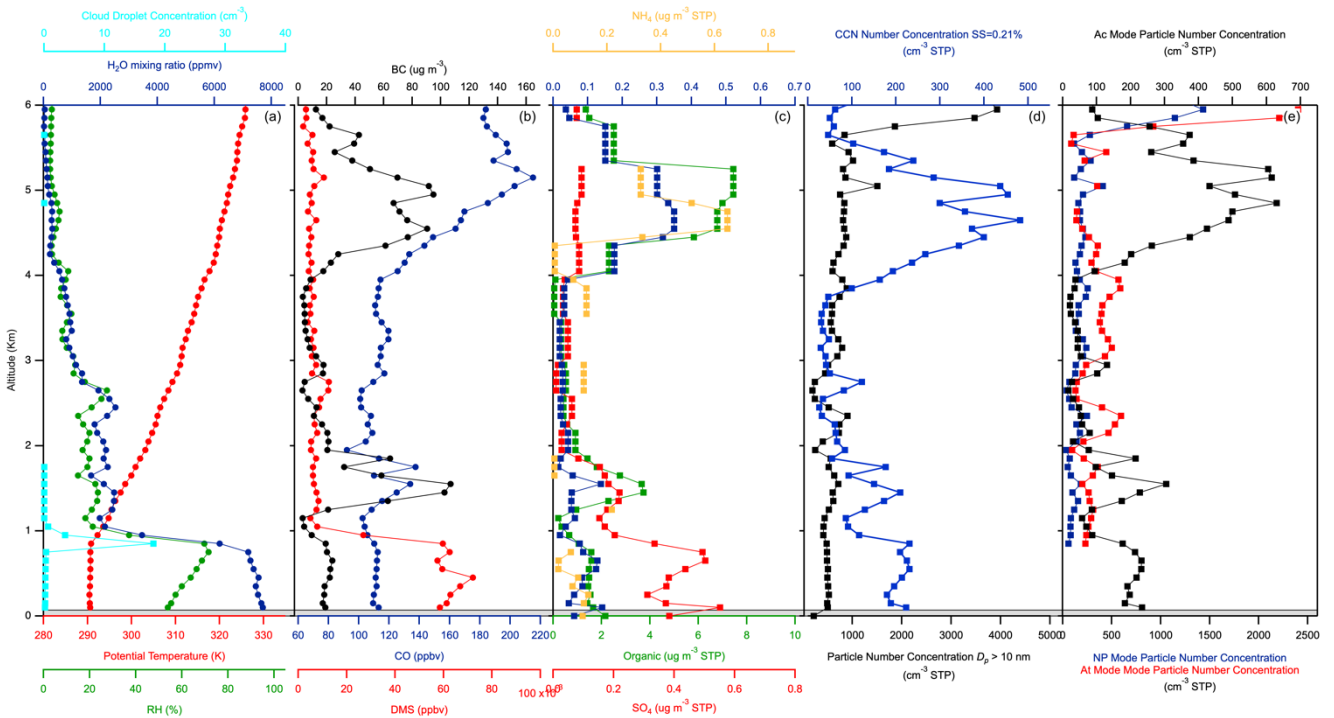
23) 4 Sept. 2017 - Spiral 2, 16:07 - 16:21 UTC, C-130 Lat. 42.02 Long. -42.41, *R/V Atlantis* Lat. 42.39 Long. -42.95
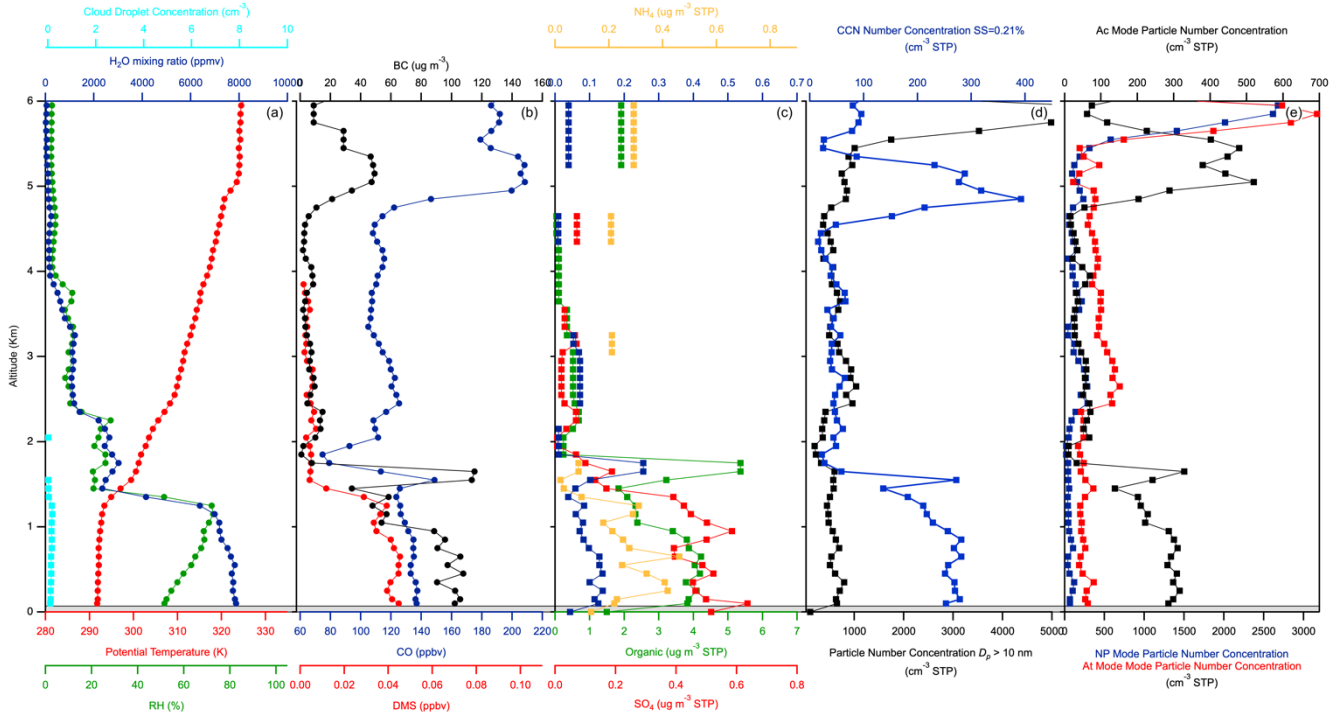
24) 6 Sept. 2017 - Spiral 1, 11:35 - 11:58 UTC, C-130 Lat. 44.16 Long. -41.78, *R/V Atlantis* Lat. 44.37 Long. -43.38
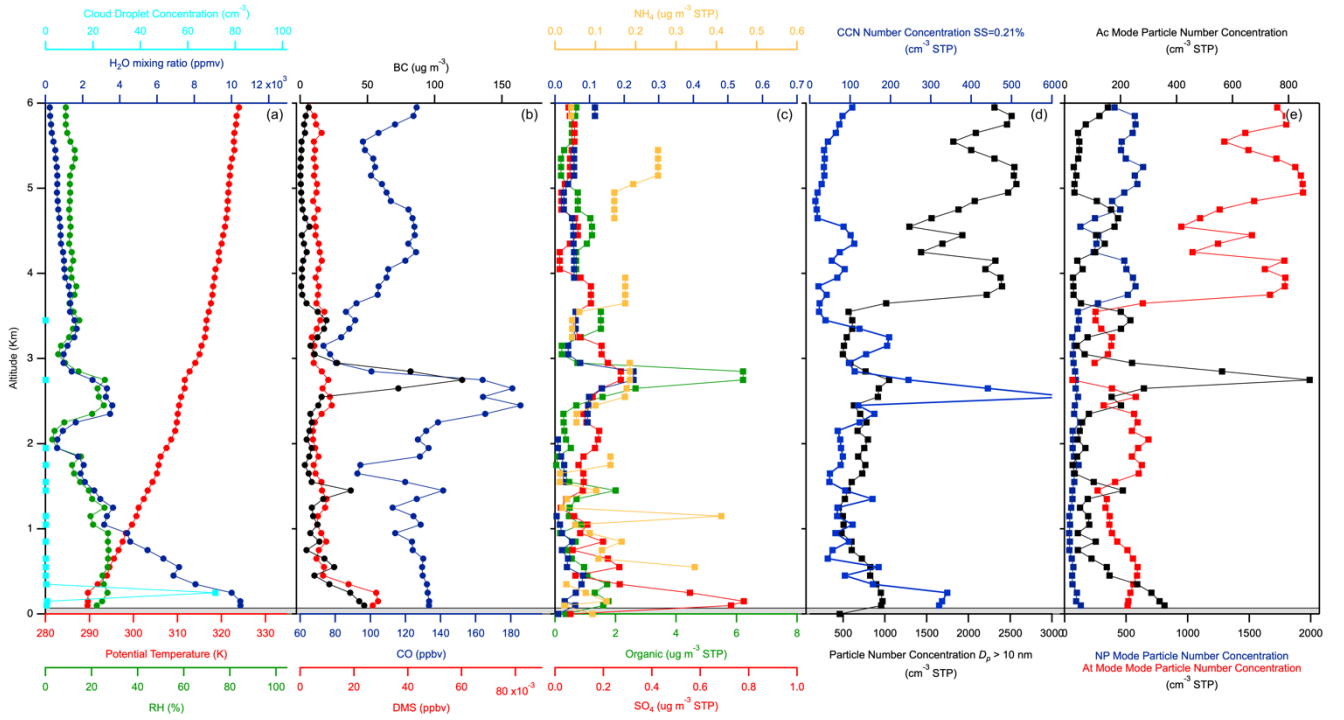
25) 6 Sept. 2017 - Spiral 2, 13:59 - 14:28 UTC, C-130 Lat. 44.36 Long. -43.36, *R/V Atlantis* Lat. 44.36 Long. -43.36
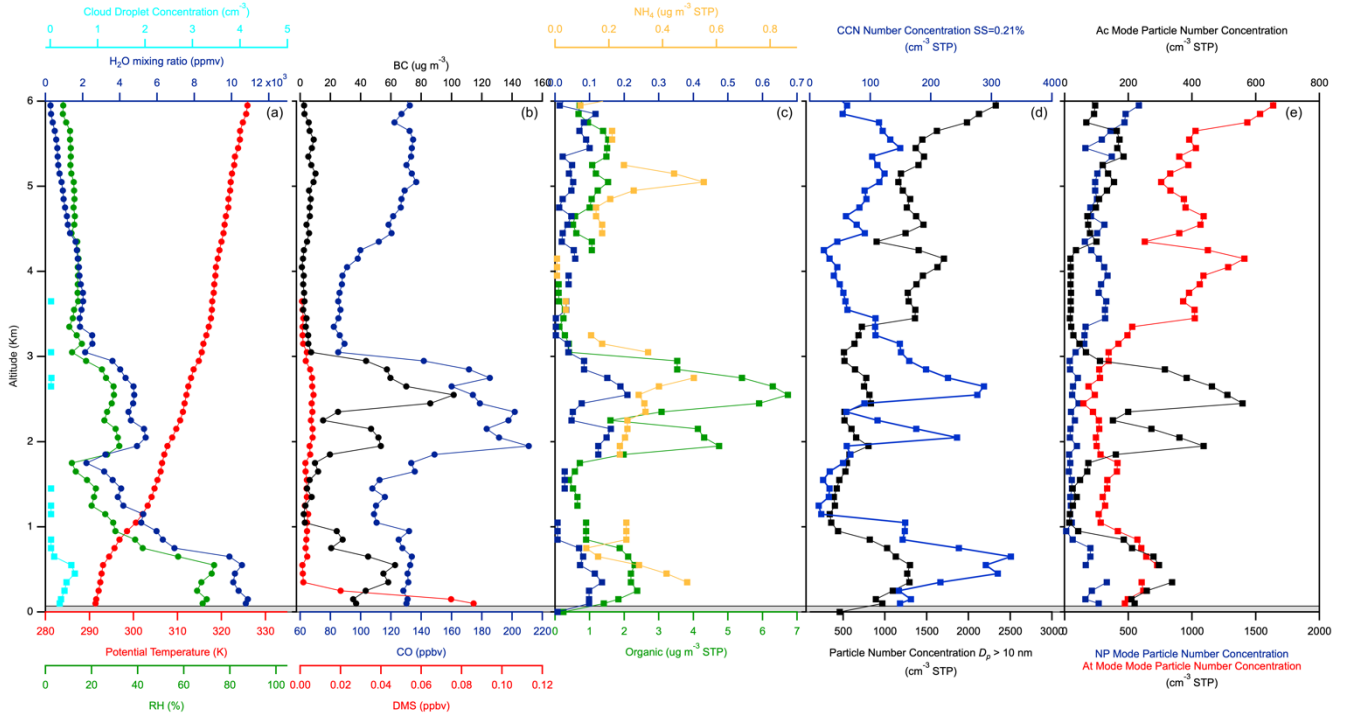
26) 6 Sept. 2017 - Spiral 3, 14:57 - 15:11 UTC, C-130 Lat. 44.38 Long. -43.74, *R/V Atlantis* Lat. 44.36   Long. -43.37
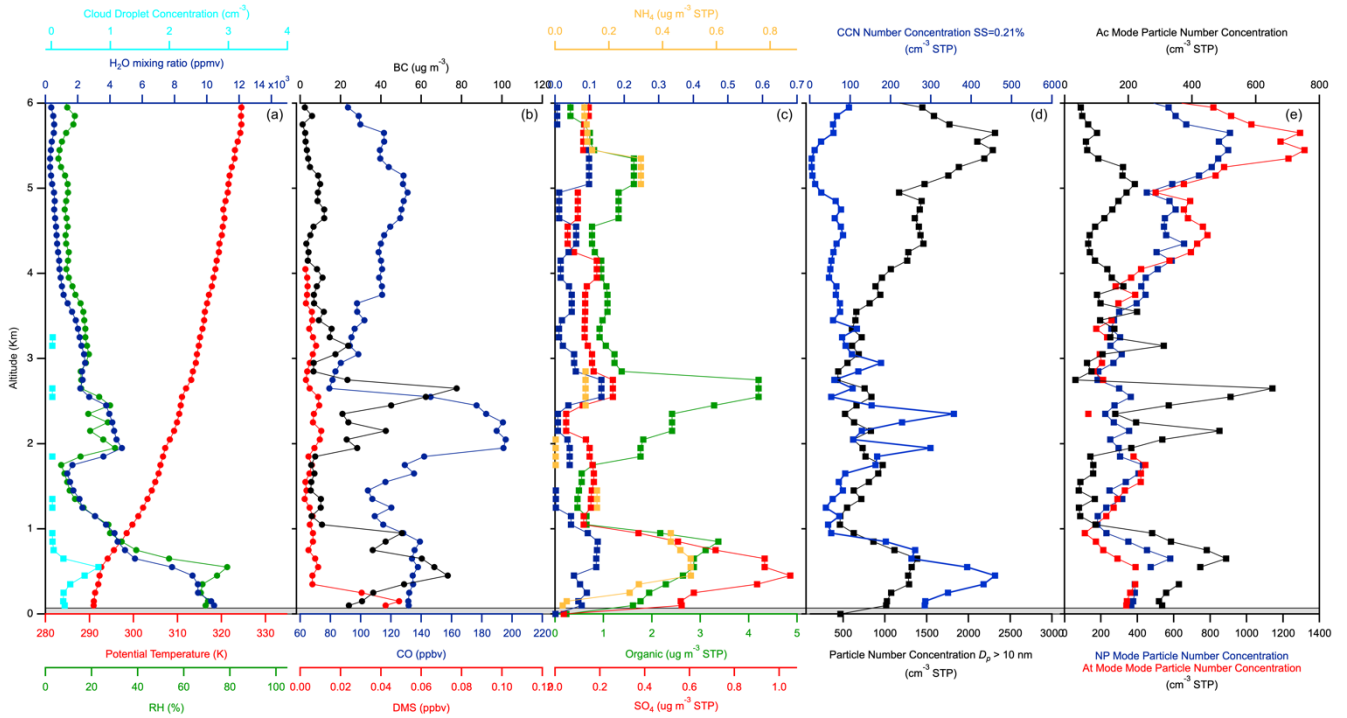
27) 8 Sept. 2017 - Spiral 1, 12:34 - 12:54 UTC, C-130 Lat. 47.66 Long. -40.58, *R/V Atlantis* Lat. 46.98 Long. -40.11
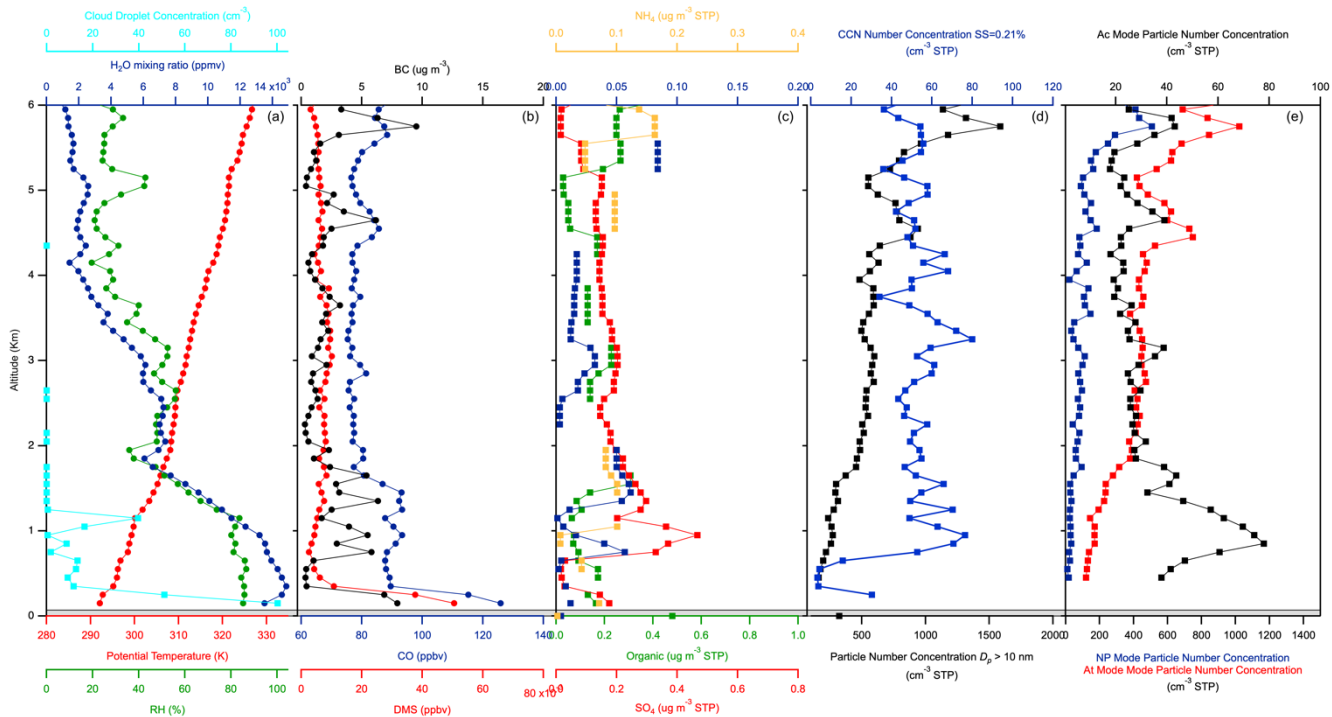
28) 8 Sept. 2017 - Spiral 2, 14:43 - 15:04 UTC, C-130 Lat. 47.24 Long. -40.27, *R/V Atlantis* Lat. 46.97 Long. -40.16
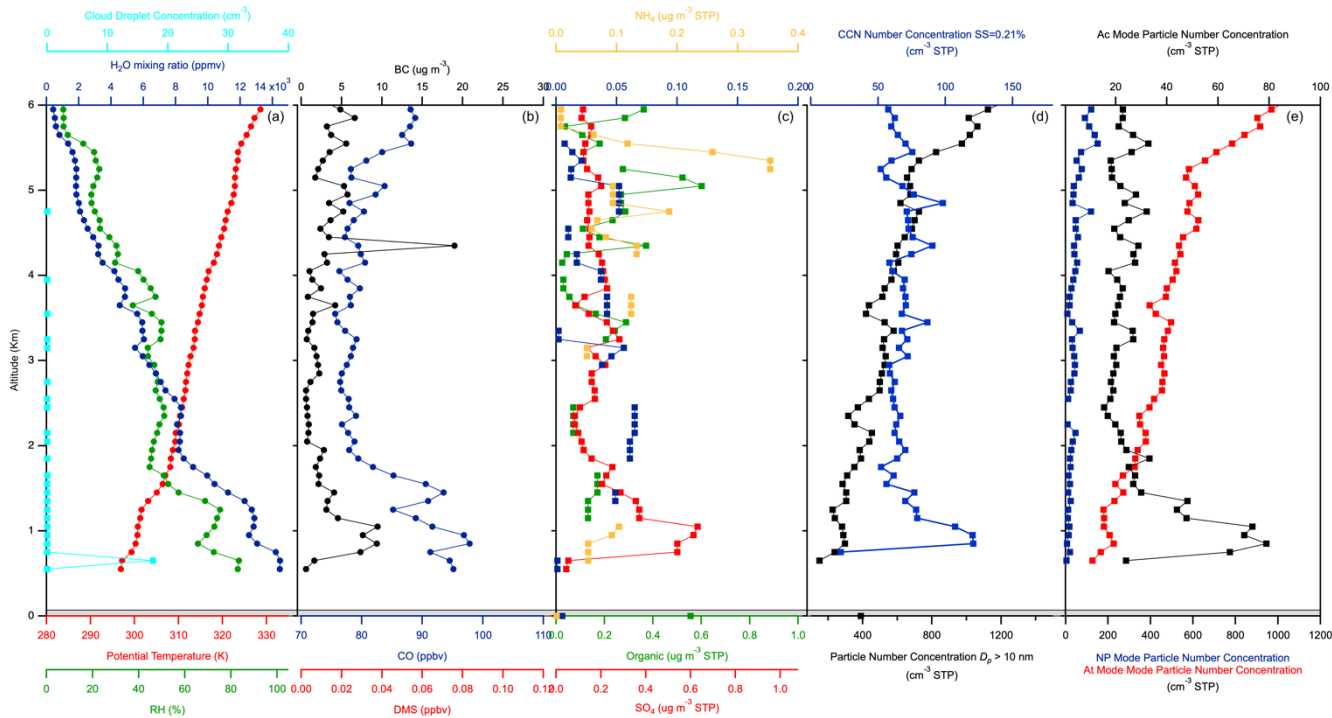
29) 8 Sept. 2017 - Spiral 3, 15:32 - 15:45 UTC, C-130 Lat. 47.45 Long. -39.19, *R/V Atlantis* Lat. 46.99 Long. -40.16
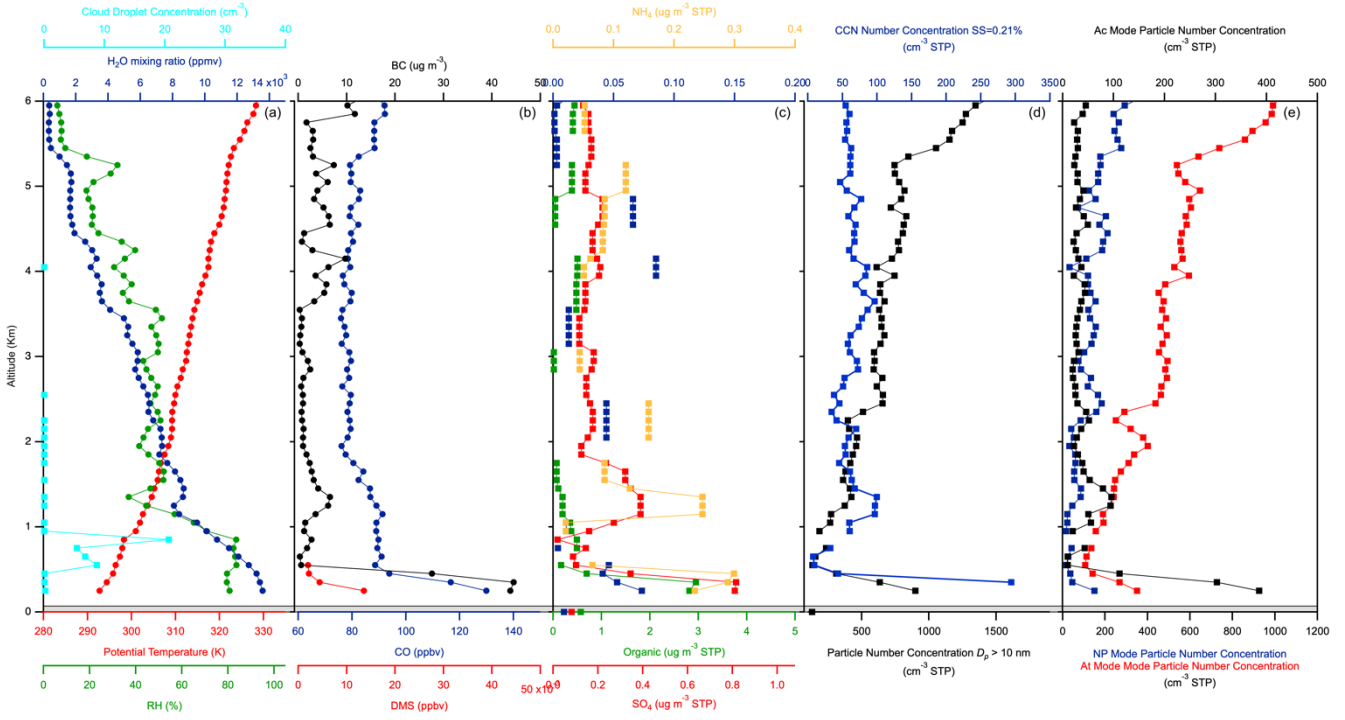
30) 9 Sept. 2017 - Spiral 1, 12:25 - 12:41 UTC, C-130 Lat. 48.45 Long. -36.35, *R/V Atlantis* Lat. 48.17 Long. -39.14
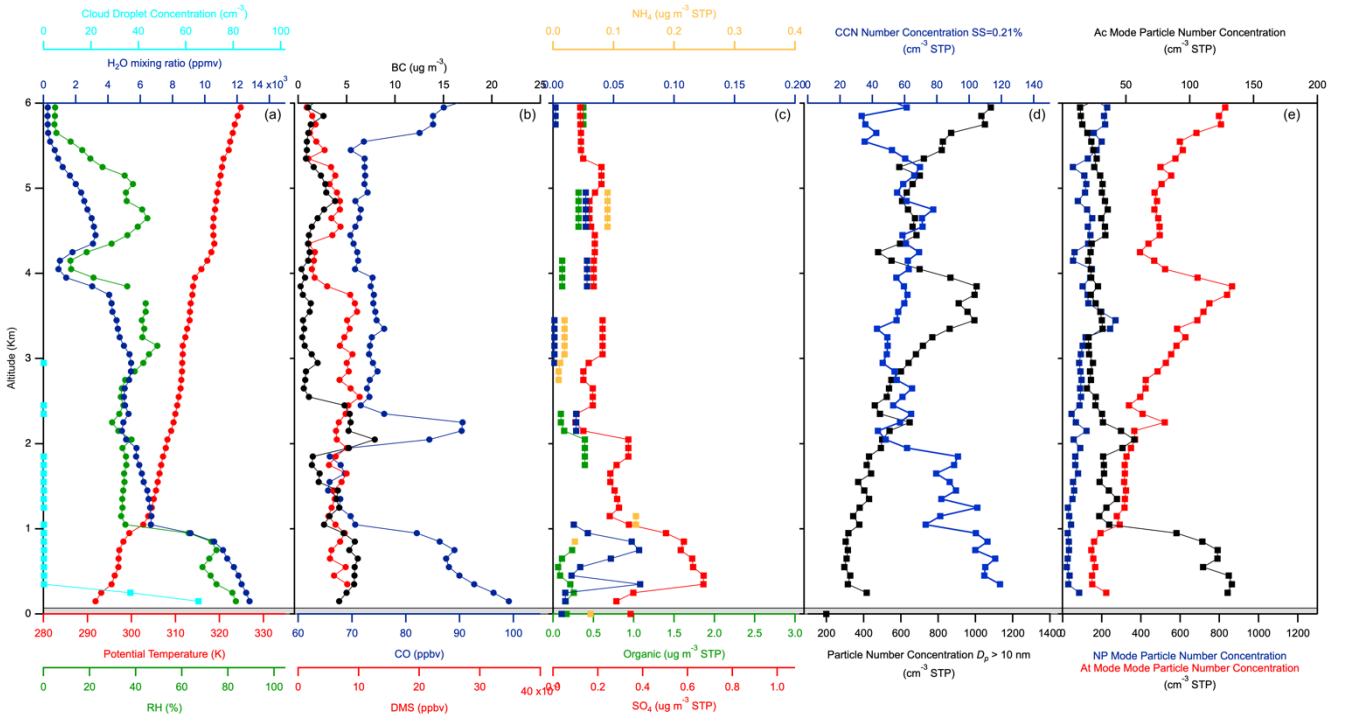
31) 9 Sept. 2017 - Spiral 2, 14:27 - 14:47 UTC, C-130 Lat. 48.48 Long. -38.95, *R/V Atlantis* Lat. 48.50 Long. -38.97
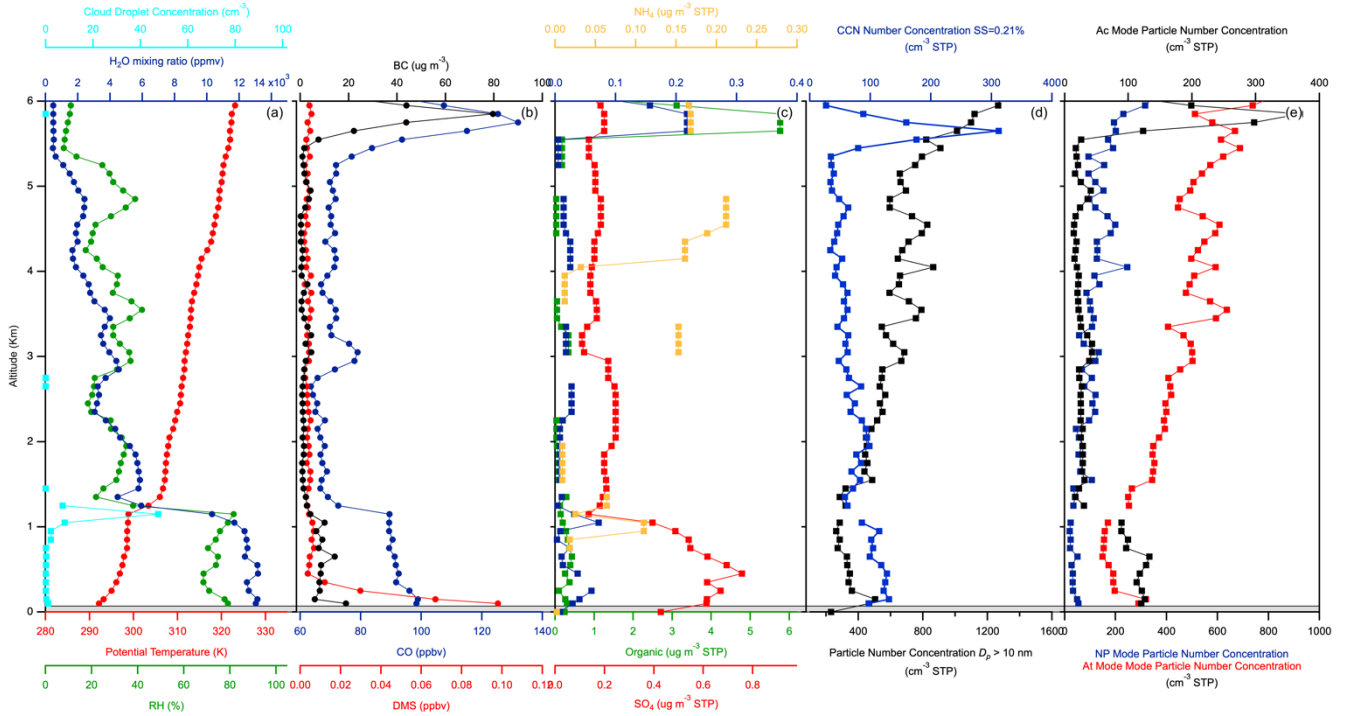
32) 12 Sept. 2017 - Spiral 1, 17:57 - 18:14 UTC, C-130 Lat. 51.83 Long. -40.58, *R/V Atlantis* Lat. 51.72 Long. -39.57
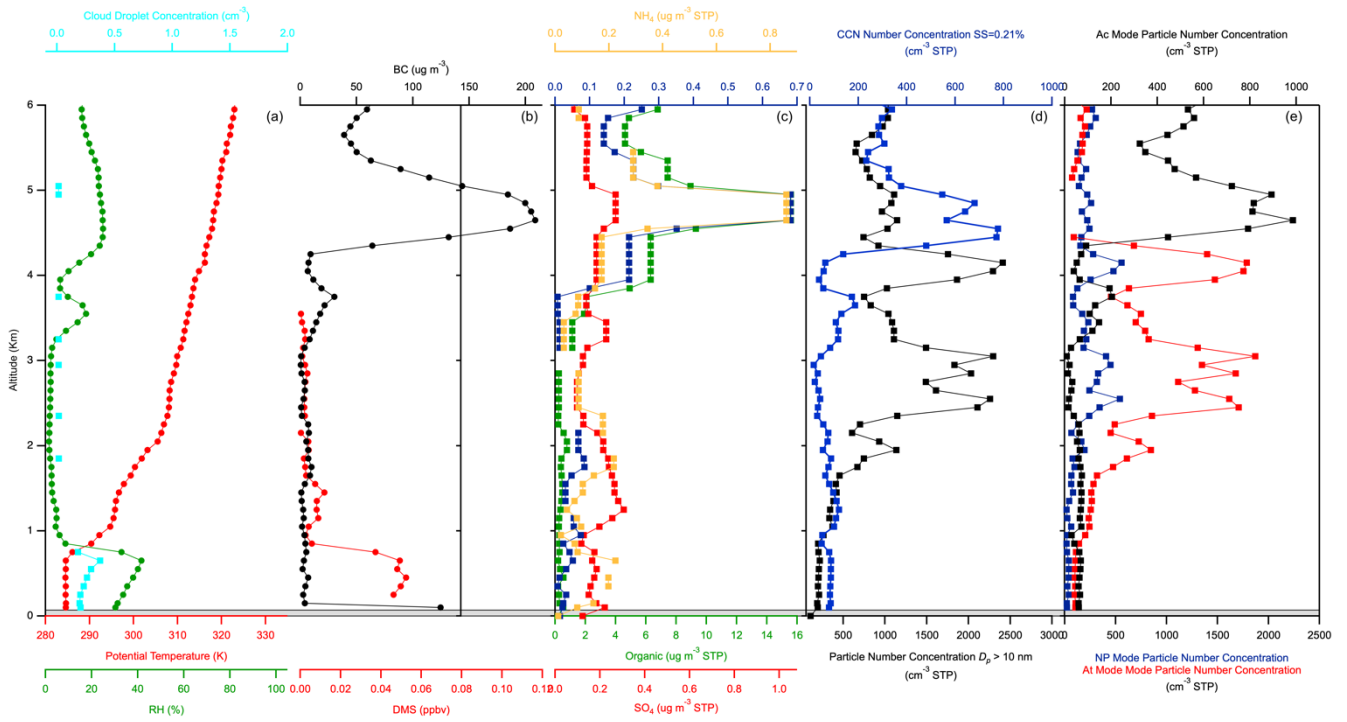
33) 12 Sept. 2017 - Spiral 2, 18:44 - 19:03 UTC, C-130 Lat. 51.72 Long. -39.57, *R/V Atlantis* Lat. 51.72 Long. -39.58
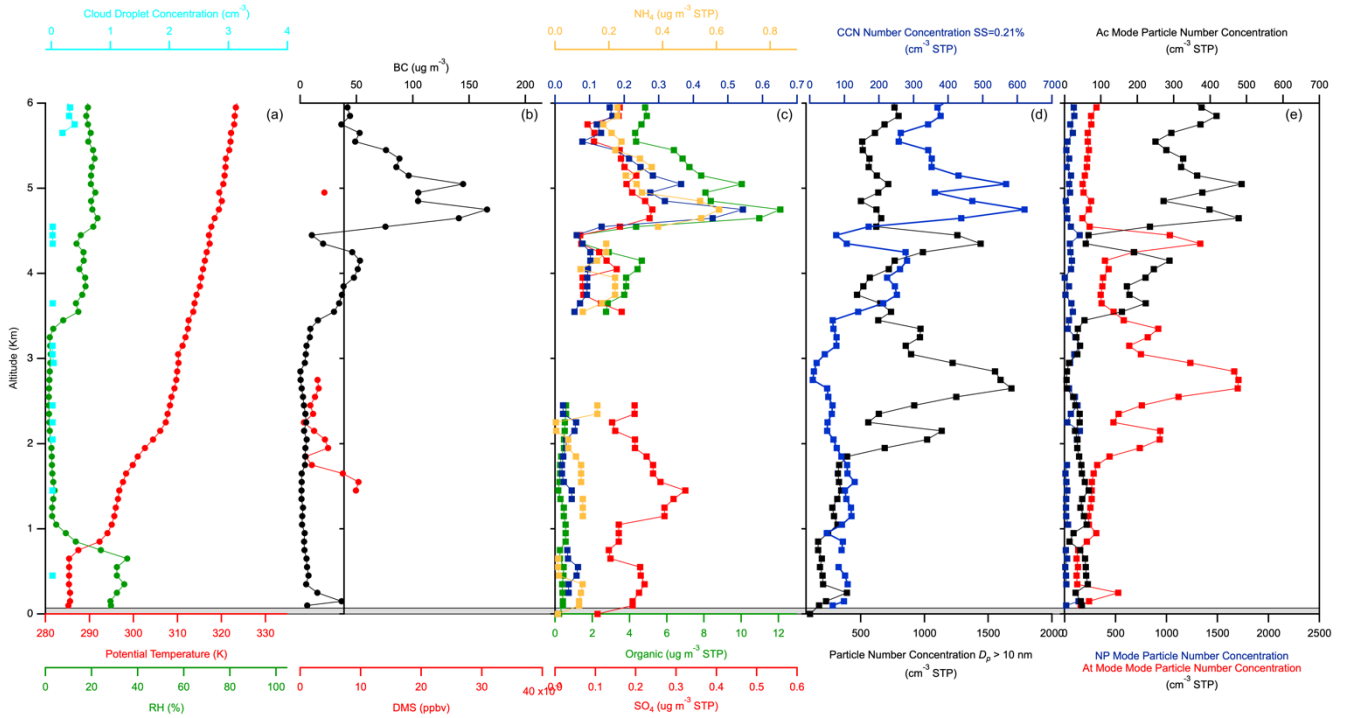
34) 12 Sept. 2017 - Spiral 3, 19:29 - 19:45 UTC, C-130 Lat. 51.45 Long. -38.35, *R/V Atlantis* Lat. 51.72 Long. -39.58
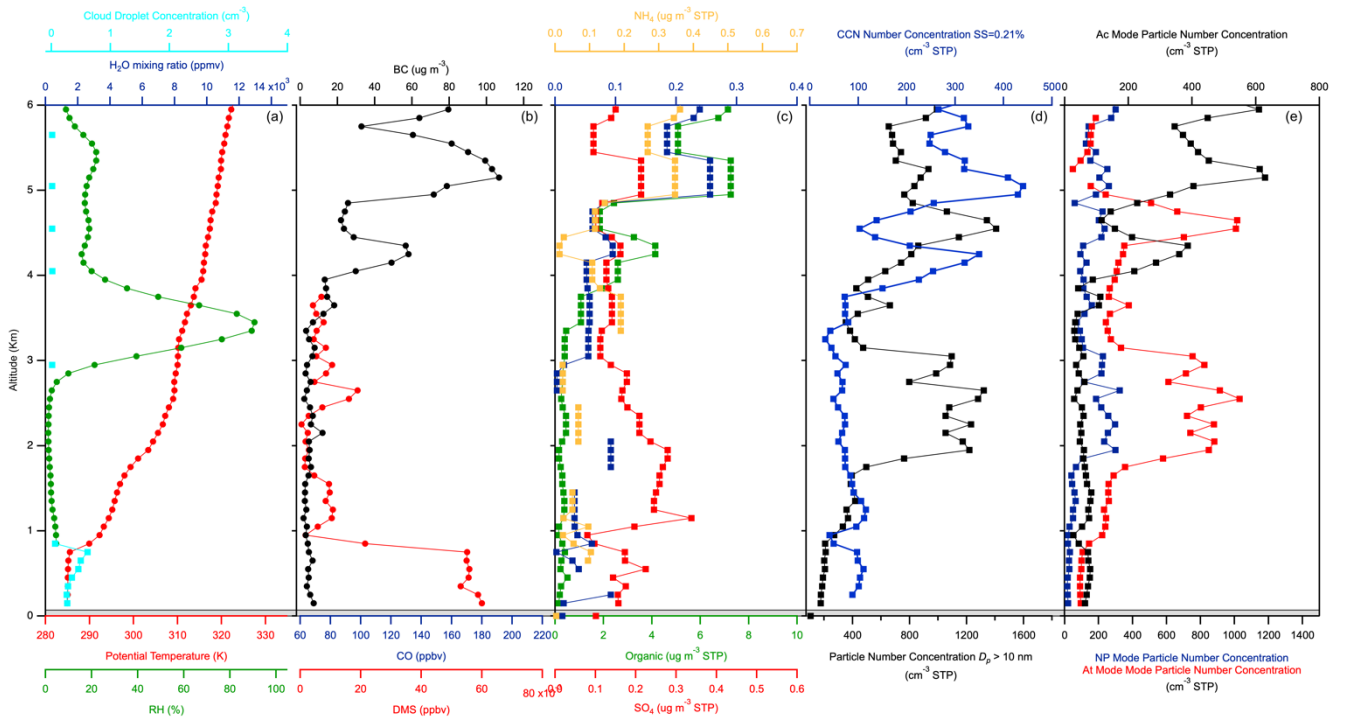
35) 16 Sept. 2017 - Spiral 1, 11:57 - 12:12 UTC, C-130 Lat. 54.03 Long. -38.95, *R/V Atlantis* Lat. 53.40 Long. -39.63
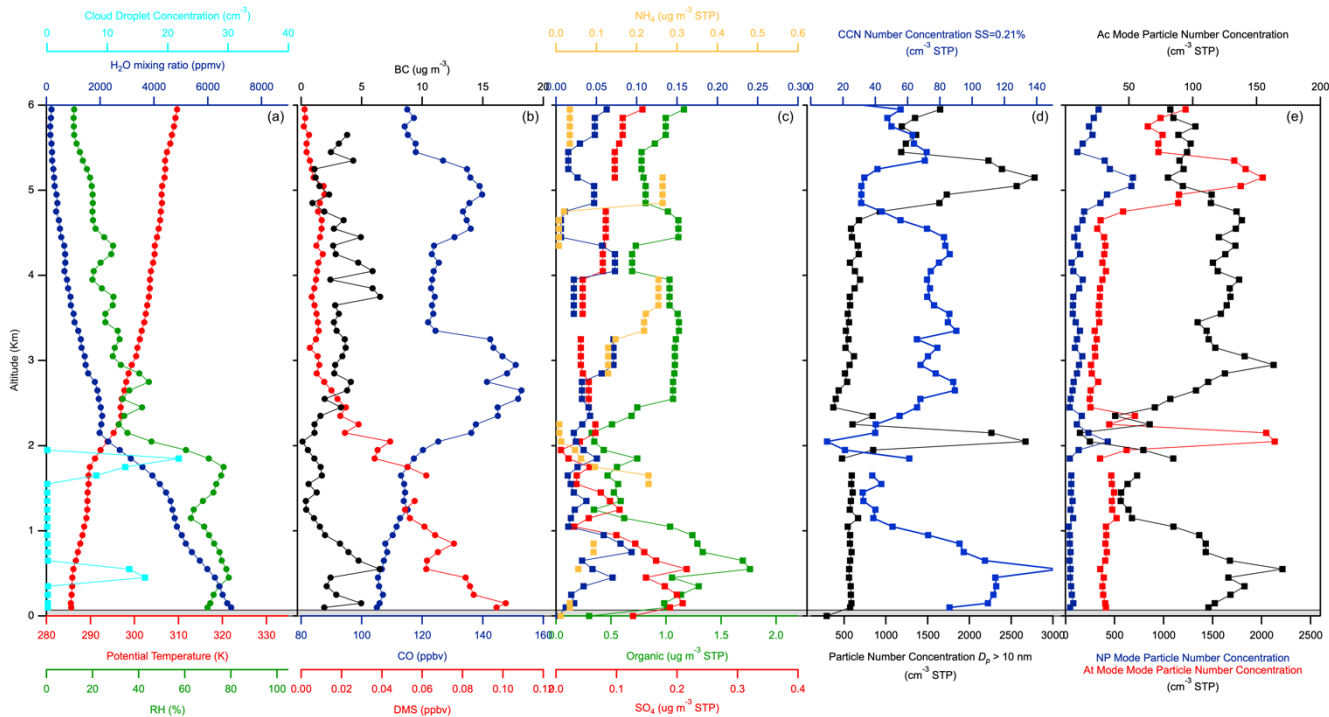
37) 17 Sept. 2017 - Spiral 1, 12:29 - 12:44 UTC, C-130 Lat. 53.38 Long. -39.43, *R/V Atlantis* Lat. 53.42 Long. -39.61